Scuola di Dottorato
Università degli studi di Milano-Bicocca

Department of Biotechnology and Biosciences

Converging Technology for Biomolecular Systems (TeCSBi)

Cycle XXXVI

The interplays between Rif2, Ku and Tel1 in the repair of DNA double-strand break

Pizzul Paolo
Matr. 804489

Tutor: Prof. Longhese Maria Pia

Supervisor: Prof. Bonetti Diego

Coordinator: Prof. Branduardi Paola

Academic Year 2022-2023

INDEX

ABSTRACT

Genome instability stands as a prominent hallmark of cancer cells, often deriving from deficiencies in DNA repair processes. Among the different types of DNA damage, double-strand breaks (DSBs) emerge as particularly hazardous lesions, known for their high cytotoxicity. To maintain genome stability and prevent cell death, it becomes fundamental that DSBs are recognized and repaired accurately. In eukaryotic cells, the response to DSBs involves the activation of the DNA damage response (DDR), a comprehensive system of pathways dedicated to the repair of DNA breaks. The repair of DNA DSBs involves two major pathways: homologous recombination (HR) and non-homologous end-joining (NHEJ). In NHEJ pathway the broken DNA ends are directly ligated and in this mechanism are involved components like the Ku70-Ku80 heterodimer, which plays a critical role by binding to the damaged DNA. The HR process uses sister chromatids or homologous chromosomes as a template to repair the DNA break. HR is initiated by nucleolytic degradation (resection) of the 5'-terminated strands at both DSB ends. The Mre11-Rad50-Xrs2 (MRX) complex initiates resection of DNA DSBs via the Mre11 endonuclease activity and recruits Tel1/ATM kinase. The yeast Rif2 protein inhibits Mre11 endonuclease activity and Tel1/ATM activation through a short motif, called MIN, which is known to bind the Rad50 subunit and to stimulate its ATPase activity.

In this thesis, I contributed to clarify the mechanism by which Rif2 restrains Tel1 activation and the consequences of this inhibition at DNA DSBs. By using AlphaFold Multimer modeling we pinpointed and validated the interaction surface between Rif2 MIN motif and Rad50. Furthermore, we engineered the *rif2-S6E* mutation that amplifies the inhibitory properties of

Rif2 by increasing Rif2-Rad50 interaction. Rif2^{S6E} diminishes the binding of Tel1 to DNA DSBs while leaving MRX association with DSBs unaffected. The reduced Tel1 association with DSBs in *rif2-S6E* cells results in impaired DSB end-tethering and together with the suppression of this defect by a hyperactivated variant of Tel1, suggest a direct role of Tel1 in maintaining the DSB ends close to each other. Finally, Rif2^{S6E} stimulates Rad50 ATPase and impairs Tel1-MRX interaction more efficiently than wild-type Rif2, indicating that Rif2-bound Rad50 is not competent for Tel1 binding.

A crucial challenge within NHEJ pathway lies in ensuring that the ends of DSBs are kept in close proximity to facilitate their accurate and effective rejoining. This essential function of end-tethering requires the coordinated actions of both the MRX/MRN complex and the Sae2/CtIP protein. In the second part of the thesis, I investigated if the Ku complex could have a role in the control of the mechanism of end-tethering. The characterization of *ku70-C85Y* mutation, which increases Ku affinity for DNA, has allowed us to show that the Ku complex promotes DSB end-tethering and the C85Y mutation enhances this bridging function by increasing Ku retention very close to the DSB ends. We also demonstrated that Tel1 antagonizes the Ku function double-strand in supporting end-tethering by promoting nucleosome removal and possibly Ku sliding inwards. As the presence of Ku at the DSB ends prevents the access of resection nucleases, the Tel1-mediated regulation of Ku association with the DSB ends provides an important layer of control in the choice between NHEJ and HR, suggesting a new function of Tel1 in the DNA damage response.

Taken together, the findings reported in this thesis unveil a complex and dynamic modulation of DNA DSB repair and Tel1/ATM activation. Ku complex together with MRX complex and Sae2 contributes to the essential process of DSB end-tethering, while Rif2 regulatory function acts limiting MRX-mediated Tel1 activation. Understanding these regulatory mechanisms is crucial for gaining insights into the molecular events that safeguard genome stability and orchestrate the sophisticated response of DNA repair pathways.

PUBLICATIONS

LIST OF PUBLICATIONS

(November 2020 – present)

Pizzul P., Casari E., Rinaldi C., Gnugnoli M., Mangiagalli M., Tisi R. and Longhese M. P. (2023). Rif2 interaction with Rad50 counteracts Tel1 functions in checkpoint signalling and DNA tethering by releasing Tel1 from MRX binding. *Nucleic acids research.* Accepted on 15th Dec 2023

Casari E., **Pizzul P.**, Rinaldi C., Gnugnoli M., Clerici M. and Longhese M. P. (2023). The PP2A phosphatase counteracts the functions of the 9-1-1 axis in checkpoint activation. *Cell Reports.* 2023, 42(11):113360.

Pizzul P.*, Rinaldi C.* and Bonetti D. (2023) The multistep path to replicative senescence onset: zooming on triggering and inhibitory events at telomeric DNA. *Frontiers in Cell and Developmental Biology*. 2023, 11:1250264.

Rinaldi C., **Pizzul P.**, Casari E., Mangiagalli M., Tisi R., & Longhese M. P. (2023). The Ku complex promotes DNA end-bridging and this function is antagonized by Tel1/ATM kinase. *Nucleic acids research*, 2023, 51(4), 1783–1802.

Casari E., Gnugnoli M., Rinaldi C., **Pizzul P.**, Colombo C.V., Bonetti D., Longhese M.P. (2022). To fix or not to fix: maintenance of chromosome ends versus repair of DNA double-strand breaks. *Cells*, 2022, 11, 3224 3.

Pizzul P.*, Casari E.*, Gnugnoli M., Rinaldi C., Corallo F., Longhese M.P. (2022). The DNA damage checkpoint: a tale from budding yeast. *Frontiers in Genetics*, 2022, 13, 995163

Rinaldi C., **Pizzul P.**, Longhese M.P., Bonetti D. (2021). Sensing R-loop-associated DNA damage to safeguard genome stability. *Frontiers in Cell and Developmental Biology*, 2021, 8, 618157

* These authors have contributed equally to the work

INTRODUCTION

Cancer and genome instability

Cancer is the second most common cause of death globally, accounting for an estimated 9.6 million deaths in 2018 (World Cancer Report, 2020). Understanding the mechanisms by which normal cells transform into cancerous ones can provide valuable insights into cancer prevention strategies. Cancer may develop after exposure to carcinogens, including hazardous chemicals, radiation, or infectious organisms, or cancer can be categorized as sporadic, for which no such exposure is evident. Cancer development after exposure includes the induction of carcinogen-related mutations, but critical mutations may also occur spontaneously. In this context, DNA repair may be protective to prevent mutations. Knowledge of such biological processes has contributed to reducing cancer incidence and mortality.

Hanahan and Weinberg have provided a logical framework for comprehending the multistep process of human tumor pathogenesis - (Hanahan & Weinberg, 2000). The hallmarks of the neoplastic phenotype include sustaining proliferative signaling, evading growth suppression, avoiding immune destruction, enabling replicative immortality, resisting apoptosis, deregulating cellular energetics, inducing angiogenesis, and activating invasion and metastasis (Figure 1).

In 2011, the same authors added four new characteristics to cancer cells (Hanahan & Weinberg, 2011) (Figure 1). Among them, genomic instability was defined as an enabling characteristic. In fact, while all the hallmarks are acquired during a multi-step transformation process, genome instability promotes tumor progression.

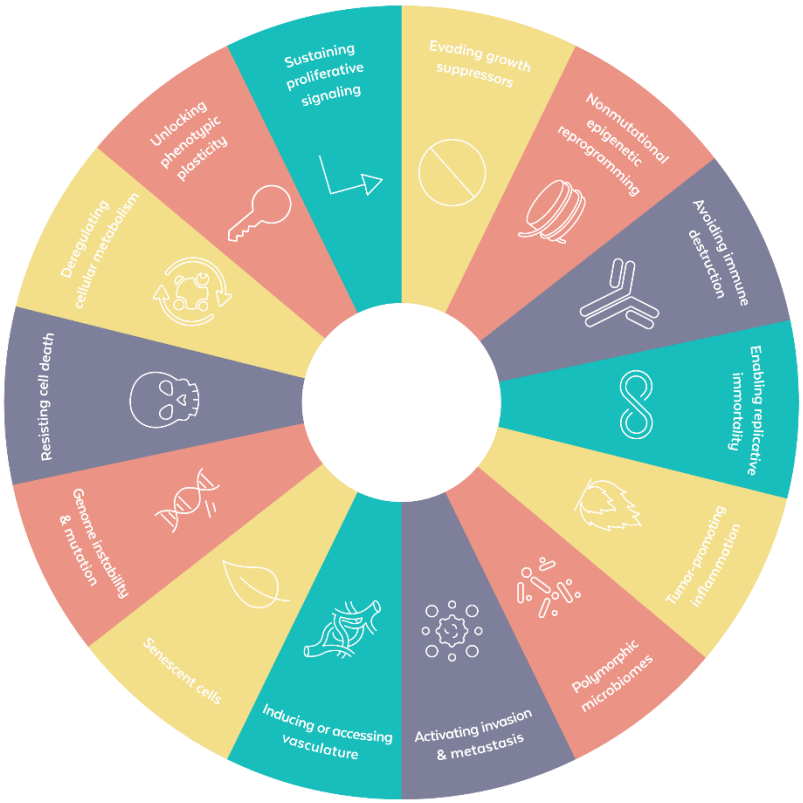

Figure 1. Hallmarks of cancer. These hallmarks outline a set of criteria that explain how normal cells can develop into malignant tumors by identifying specific characteristics and describing how they interact with one another. These characteristics include sustained proliferative signaling, evasion of growth suppressors, resistance to cell death, limitless replicative potential, angiogenesis, and genomic instability. Together, these hallmarks allow cancer cells to evade the normal controls that regulate cell growth and division, enabling them to continue to divide and proliferate (adapted from Negrini et al., 2010).

There are various forms of genomic instability (Negrini et al., 2010). Most cancers present chromosomal instability (CIN), which refers to the high rate by which chromosome structure and number change over time in cancer cells compared with normal cells. Although CIN is the major form of genomic instability in human cancers, other forms of genomic instability have also been described. These include microsatellite instability, a form of genomic instability that is characterized by the expansion or contraction of the number of oligonucleotide repeats present in microsatellite sequences (Fishel et al., 1993; Leach et al., 1993), and forms of genomic instability that are characterized by increased frequencies of base-pair mutations (Al-Tassan et al., 2002). These instabilities mostly arise as consequences of damaged DNA left unrepaired or repaired in the wrong way. A large number of agents could damage DNA and the source of these agents can originate from both cellular or extracellular environments (Roos et al., 2016).

Endogenous DNA damage arises from internal metabolic processes and encompasses damage caused by reactive oxygen species (ROS) and reactive nitrogen species (RNS). These products are generated during oxidative stress, metabolic activities, and the inflammatory response (Helena et al., 2018). Endogenous DNA damage also involves depurination and depyrimidination at specific foci. This occurs when N-glycosidic bonds between nitrogenous bases and deoxyribose residues are hydrolyzed, resulting in the formation of apurinic and apyrimidinic sites. Additionally, the spontaneous hydrolytic deamination of cytosine bases can modify DNA, leading to the presence of non-native uracil bases (Helena et al., 2018). In addition, spontaneous DNA alterations can occur during other cellular processes such as defective meiosis, DNA replication errors, uncontrolled recombination, off-target mutation,

inaccurate V(D)J recombination, collisions of replication/transcription and telomere shortening. On the other hand, DNA can be damaged by exogenous agents, originating from external environmental processes, including ionizing and solar ultraviolet radiation. Ionizing radiation generates a wide variety of DNA lesions. Exogenous DNA damage also includes environmental pollutants present in air, water, harmful chemicals, and food.

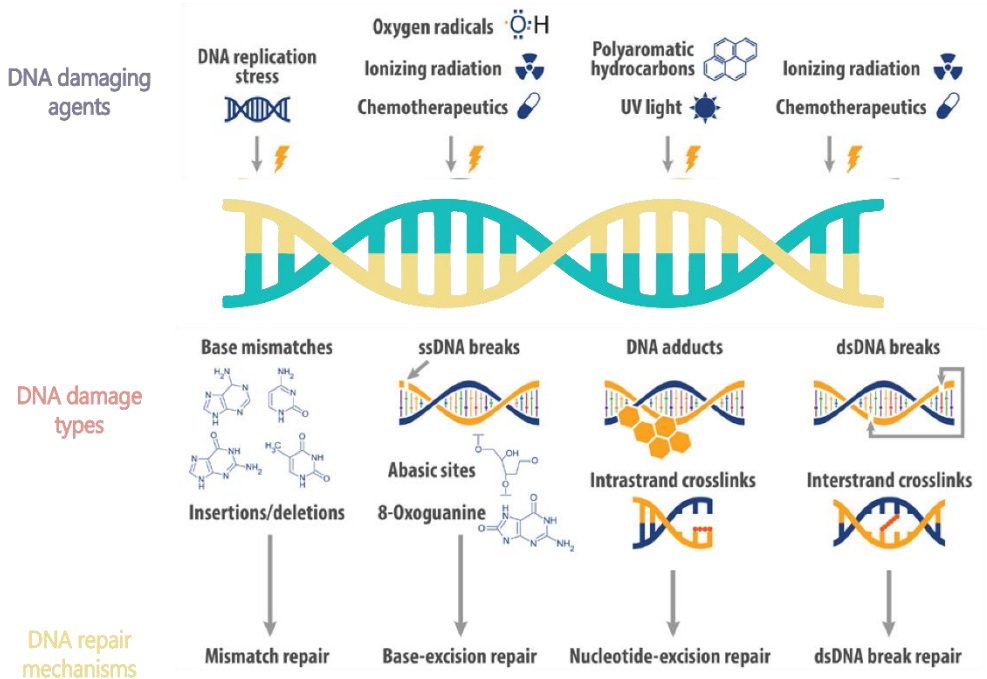

Figure 2. Endogenous and exogenous DNA lesions and possible DNA repair mechanisms. Depending on DNA damaging agents, DNA can be lesioned in different modes. According to the type of lesions, specific DNA repair mechanisms are involved in their fixing (adapted from Helena et al., 2018)

DNA damaging agents can induce different types of DNA lesions such as Single-Strand Breaks (SSBs), Double-Strand Breaks (DSBs), DNA crosslinks, base modifications or depletions, stalled replication forks or mismatches (Figure 2). To contrast genomic instability, cells have a process known as DNA damage response (DDR), in which DNA repair proteins act in complex pathways to remove or tolerate DNA lesions (Finn et al., 2012).

Generation of a DNA double strand break

A double strand break is generated when the sugar phosphate backbones on both DNA strands are broken in or near the same location to allow the physical dissociation of the DNA double helix into two molecules (Aparicio et al., 2014). Since the break occurs in both DNA strands, DSBs are one of the most deleterious DNA lesions, as they can cause mutations and chromosomal rearrangements. DSBs can arise as a consequence of both endogenous and exogenous insults (Aguilera & García-Muse, 2013; Mehta & Haber, 2014; So et al., 2017).

Several studies have indicated that the occurrence rate of spontaneous DSB is approximately 1 per 10^8 base pairs (bp) in both yeast and mammalian cells (Mehta & Haber, 2014). The replication process itself can induce DSBs formation, in particular in the presence of replication stress. Indeed, any situation that leads to the stalling of the replication fork has the potential to cause DSBs (Aguilera & García-Muse, 2013). Moreover, commonly used chemotherapeutic drugs like camptothecin (CPT) or etoposide, which are topoisomerase inhibitors, can cause the irreversible binding of the topoisomerase enzyme on DNA. This causes the block of the replication forks and the creation of replication intermediates whose resolution can induce DSBs (Mehta & Haber, 2014). Additionally, CPT-inhibition of topoisomerase activity can create nicks in the DNA, which, in turn, can be converted into DSBs during the passage of the replication complex (Aguilera & Gómez-González, 2008). Moreover, exogenous agents such as hydroxyurea (HU) or aphidicolin can impair fork progression by depleting nucleotide pools or inhibiting DNA polymerase, respectively (Mehta & Haber, 2014). Other

agents that can induce DSB include: base alkylating agents, such as methyl methanesulfonate (MMS), that stall replication forks and inhibit transcription; cross-linking agents, such as cisplatin and psoralens, that covalently crosslink bases belonging to the same strand (intra-strand) or to complementary strands (inter-strand); ionizing radiation (IR) and radiomimetic agents, such as phleomycin (phleo) or bleomycin (bleo), that introduce DSBs around the genome by mimicking the action of IR.

DSBs are also generated as a result of regular cellular metabolism. The reactive oxygen species (ROS) produced during cellular processes can oxidize bases and cause both single and double strand breaks. Moreover, DNA replication, meiotic recombination, and programmed rearrangements in lymphoid cell development contribute to the formation of endogenous DSBs. Among these, DNA replication is considered the primary cause of DSBs in proliferating cells due to the fragility of DNA intermediates at the replication forks. Importantly, breaks can occur in presence of stalled DNA polymerase, resulting in the formation of persistent single-strand DNA (ssDNA) intermediates. These broken or collapsed replication forks containing ssDNA share similarities with DSBs at various stages of processing and can contribute to genomic instability if not adequately repaired (Aparicio et al., 2014).

Response to a DNA double-strand break: the DNA damage checkpoint

Failure to respond to DNA damage can have severe consequences, and can result in mutations, gross chromosomal rearrangements and/or aneuploidy, which lead to disease, loss of fitness and death. In eukaryotes, cellular responses to most types of DNA damage involve a signaling transduction pathway, which is responsible for sensing DNA damage and coordinating DNA repair transactions with the cell cycle and other key cellular processes to prevent the inheritance of unrepaired and broken chromosomes (Waterman et al., 2020a). In the presence of DNA damage, the DDR is activated by sensor proteins that recognize the lesion and activate a phosphorylation cascade named DNA damage checkpoint (Ciccia & Elledge, 2010). The DNA damage checkpoint in turn induces cell-cycle arrest, activation of specific transcriptional programs, support and control of the repair processes and, if the damage persists, activation of specific cellular responses that lead to the activation of apoptotic or senescence programs (Ciccia & Elledge, 2010; Finn et al., 2012).

In *S. cerevisiae*, there are three distinct DNA damage checkpoints throughout the cell cycle. Firstly, the G1/S checkpoint hinders the G1/S transition (Gerald et al., 2002) by delaying bud emergence, spindle pole body duplication, and entry into the S-phase. This delay allows the repair of lesions before DNA replication begins (Gerald et al., 2002). Secondly, the intra-S phase checkpoint regulates origin firing and ensures the stability of the replisome on damaged DNA. Its role is to promote the efficient recovery of DNA replication once the lesions have been repaired. Lastly, the G2/M checkpoint slows down the

metaphase to anaphase transition, preventing the segregation of damaged sister chromatids. These three DNA damage checkpoints are conserved from yeast to humans and share common components: sensors that identify DNA lesions and initiate the signal transduction; transducers, typically protein kinases, that transmit and amplify the damage signal by phosphorylating other kinases and/or downstream target proteins; and effectors, which include downstream targets of the transducer protein kinases (Nyberg et al., 2002) (Figure 3).

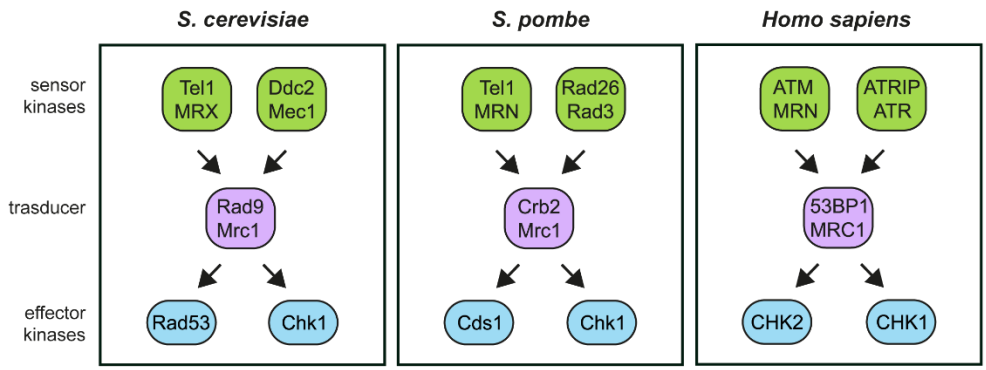

Figure 3. DNA damage checkpoint architecture in *S. cerevisiae*, *S. pombe* and *H. sapiens*. (Adapted from Pizzul et al., 2022)

The main players of these signal transduction cascades are the apical protein kinases that in yeast are represented by Tel1 and Mec1. These proteins are part of the phosphatidylinositol-3-kinase-related kinase (PIKKs) family and play a crucial role in activating the checkpoints when recruited to damaged DNA. Tel1, specifically, has been identified as the ortholog of the human ATM (ataxia-telangiectasia mutated) gene, mutations of which lead to the autosomal

recessive disorder known as ataxia-telangiectasia (Greenwell et al., 1995; Morrow et al., 1995; Savitsky et al., 1995). On the other hand, Mec1 corresponds to the ortholog of the human ATR (ATM and Rad3-related) gene, mutations of which are responsible for causing the Seckel syndrome (O'Driscoll et al., 2003).

These two DNA damage sensors respond to different types of DNA lesions. In particular, Tel1/ATM responds primarily to DSBs, while Mec1/ATR is activated by a wider range of genotoxic lesions whose processing generates ssDNA intermediates (Ciccia & Elledge, 2010). As part of the PIKK family, Tel1/ATM and Mec1/ATR are large proteins of 270-450 kDa, and present N-terminal HEAT repeat domains followed by kinase domains in C-terminus (Bosotti et al., 2000; Lempiäinen & Halazonetis, 2009).

The recruitment of Tel1/ATM to DSBs is mediated by the highly conserved MRX/MRN complex (Mre11-Rad50-Xrs2, in yeast, MRE11- RAD50-NBS1, in mammals), that is one of the first protein complex recruited to a DNA break. In addition, Tel1/ATM activation also relies on the MRX/MRN complex. In fact, cells defective in any MRX/MRN component present defects in Tel1/ATM activation, even if only the interaction with the C-terminal domain of Xrs2/NBS1 is crucial for recruiting Tel1/ATM at DSBs (J. H. Lee & Paull, 2005; Nakada et al., 2003). Tel1/ATM binding to DNA ends plays a structural role by stabilizing the interaction between MRX/MRN and DNA ends. This stabilization is crucial for allowing the proper binding of MRX/MRN to DNA, which is essential for supporting the repair of DSBs (Cassani et al., 2016).

The other key sensor of DNA damage response is Mec1/ATR that recognizes and is activated by ssDNA traits that are coated by the Replication Protein A (RPA) complex (Zou & Elledge, 2003). The recognition of ssDNA by Mec1/ATR relies on its interactor Ddc2/ATRIP, as loss of Ddc2/ATRIP causes the same phenotypes as loss of Mec1/ATR, indicating that Ddc2/ATRIP is required for full Mec1/ATR activity (Gobbini et al., 2013). Mec1/ATR activation during S-phase requires higher levels of RPA-coated ssDNA than those necessary to activate the checkpoint in G1 or in G2, guaranteeing that the ssDNA normally generated at functional replication forks, is not enough to induce a checkpoint response (Shimada et al., 2002; Tercero et al., 2003). Following Mec1 recruitment to double-strand breaks (DSBs), various pathways exist for the complete catalytic activation of Mec1/ATR (Saldivar et al., 2017; Wanrooij & Burgers, 2015). First, Mec1/ATR can be activated by the Dpb11/TOPBP1 scaffold, which is recruited to DNA lesions at ssDNA/dsDNA junctions created by the nucleolytic processing (resection) of the DNA. Dpb11 is recruited to DNA lesions by the 9-1-1 complex, which is a heterotrimer with a ring-shaped structure composed of Ddc1, Mec3, and Rad17 proteins (RAD9-RAD1-HUS1 in humans) (Waterman et al., 2020). The 9-1-1 complex is recruited to DNA in a Mec1-Ddc2-independent manner by the Replication factor C (RFC)-like clamp loader Rad24-Rfc2-Rfc5 (RAD17-RFC2-RFC5 in humans) (Kondo et al., 2001; Majka et al., 2006; Melo et al., 2001; Navadgi-Patil & Burgers, 2009). In *S. cerevisiae*, both Dpb11 and the 9-1-1 component Ddc1 have Mec1-activating domains, whereas in mammals an ATR-activating domain is present in TOPBP1 but absent in the 9-1-1 complex. A second mode of Mec1/ATR activation involves the ATP-dependent

helicase/nuclease Dna2 (yeast) and ETAA1 (mammals) (Bass et al., 2016; Haahr et al., 2016; Kumar & Burgers, 2013; Y.-C. Lee et al., 2016). Interestingly, in contrast to TOPBP1, which relies on a single-strand DNA/double-strand DNA junction for recruitment via 9-1-1 loading, ETAA1, through its interaction with RPA, has been proposed to facilitate ATR activation specifically at extended regions of RPA-coated single-stranded DNA. Lastly, in budding yeast, Ddc1 by itself stimulates Mec1 activation, but this function is probably not present in both *S. pombe* and humans (Navadgi-Patil & Burgers, 2009). These activators show partial redundancy in promoting Mec1 kinase activity during the cell cycle. In fact, Ddc1 appears to mediate Mec1 activation when DNA damage occurs in G1, whereas checkpoint activation in G2 involves both Dpb11 and 9-1–1 (Navadgi-Patil & Burgers, 2009, 2011). Dna2, Dpb11, and Ddc1 all contribute to activate Mec1 during S-phase (Kumar & Burgers, 2013). Beyond the activation of Mec1 catalytic activity, all these activators can act as scaffolds to keep proteins close to each other and facilitate phosphorylation events (Berens & Toczyski, 2012) (Figure 3).

Once activated, Tel1/ATM and Mec1/ATR phosphorylate different substrates in order to support the propagation of the checkpoint signal. The main effector of the apical kinases Tel1/ATM and Mec1/ATR are the checkpoint kinases Rad53 (human CHK2) and Chk1 (human CHK1). These checkpoint kinases govern two separate pathways of the checkpoint phosphorylation process. While Rad53 is the primary effector kinase responsible for initiating the checkpoint response to DNA damage across all phases of the cell cycle, Chk1 specifically contributes to activating the G2/M

checkpoint (Sanchez et al., 1999). When activated, Rad53 and Chk1 phosphorylate numerous downstream targets that are involved in cell cycle progression and transcriptional regulation. In the activation mechanism of Rad53 and Chk1 are involved the mediator protein Rad9/53BP1 and Mrc1/Claspin. Rad9 plays a crucial role in promoting Rad53 phosphorylation and the activation of the DNA damage checkpoint in both the G1 and G2 phases, whereas Mrc1, a component of the replisome, promotes Rad53 activation during S-phase (Bacal et al., 2018). The recruitment of Rad9 has two significant effects on Rad53 activation. Firstly, it enables Mec1 and Tel1 to phosphorylate Rad53 in its SCD (Serine Cluster Domain), leading to the activation of the kinase. Secondly, it facilitates the recruitment of other Rad53 molecules through interactions with Rad9 or other Rad53 molecules. This increased local concentration of Rad53 promotes in-trans autophosphorylation of Rad53. Once Rad53 is hyperphosphorylated, it becomes fully active and is released from Rad9 in an ATP-dependent manner (Gilbert et al., 2001).

Rad9 is recruited to chromatin through different mechanisms. In the absence of DNA damage, the Rad9 Tudor domains can recognize histone H3 methylated on lysine 79, a modification catalyzed by the histone methyltransferase Dot1 (Giannattasio et al., 2005; Grenon et al., 2007; Toh et al., 2006; Wysocki et al., 2005). When DNA damage occurs, Rad9 is recruited to the damaged sites by interacting with histone H2A (human H2AX) that has been phosphorylated at serine 129 (γH2A/γH2AX) by Mec1 and Tel1 (Downs et al., 2000; Hammet et al., 2007; Shroff et al., 2004). Additionally, Rad9 recruitment to DNA lesions relies on the presence of Dpb11, which acts as a

scaffold that brings Rad9, 9-1-1 and Mec1-Ddc2 molecules close together to facilitate Rad9 phosphorylation by Mec1. The interaction between Dpb11 and Rad9 requires Rad9 phosphorylation by the Cdk1-Clb complexes (Granata et al., 2010; Pfander & Diffley, 2011) (Figure 4).

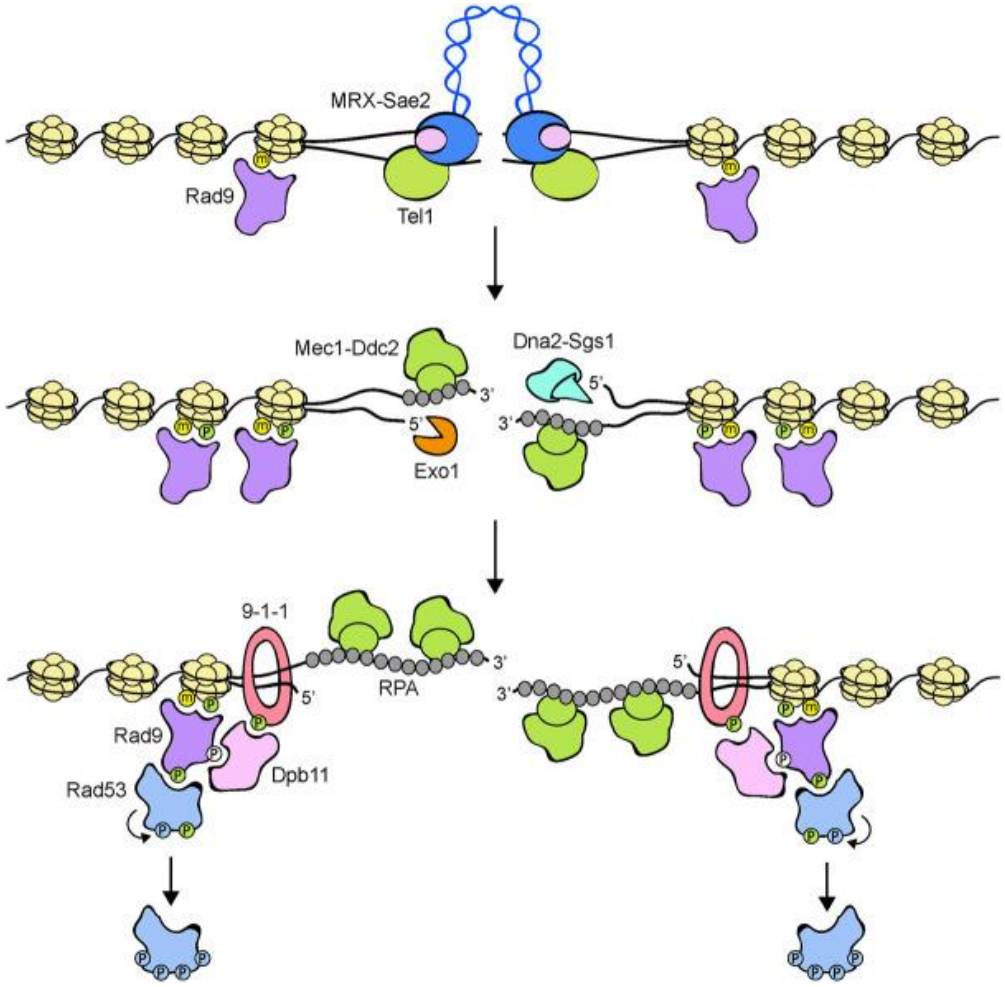

Figure 4. Model for Rad53 activation in response to DNA DSBs. The MRX-Sae2 complex is rapidly recruited to DNA ends. Rad9 is already bound to chromatin via interaction with methylated histone H3 (yellow dots). MRX bound to DNA ends recruits and activates Tel1, which in turn phosphorylates histone H2A on S129 (green dots), an event that leads to a further enrichment of Rad9 at DSBs. DSB end processing by Exo1 and Dna2-Sgs1 nucleases generates ssDNA that is coated by RPA. RPA-coated ssDNA allows the recruitment of Mec1-Ddc2 and a switch from Tel1 to Mec1 signaling. The 9-1-1 clamp loader recruits the 9-1-1 complex at the 5' recessed end of the ssDNA-dsDNA junction. Mec1 in turn phosphorylates the Ddc1 subunit of the 9-1-1 complex (green dots), thus creating a docking site for Dpb11 binding. Rad9, once phosphorylated by Cdk1 (white dots), can also bind to Dpb11 that acts as a scaffold to promote Rad9-Mec1 interaction and therefore Rad9 phosphorylation by Mec1. Phosphorylated Rad9 first acts as an adaptor to bring Rad53 into proximity to Mec1 to allow Mec1-dependent Rad53 phosphorylation. Then, Rad9 promotes Rad53 in trans-autophosphorylation (light blue dots) by increasing the local concentration of Rad53 molecules. Fully activated Rad53 molecules are then released from the Rad9 complex (Pizzul et al., 2022).

Repair of a DNA double-strand break

To maintain the integrity of DNA during cell divisions, eukaryotic cells have developed sophisticated repair mechanisms capable of facing various forms of DNA damage. Among these, DNA double-strand breaks (DSBs) are particularly crucial, as they can lead to genetic alterations such as insertions, deletions, or chromosomal rearrangements, which are often implicated in the development of cancers. DSBs are mainly repaired by two highly conserved mechanisms: Homologous Recombination (HR), that utilizes extensive homology from a sister chromatid or homologous sequence elsewhere in the genome, and Non-Homologous End Joining (NHEJ), that relies on minimal or no homology (Wright et al., 2018). Regardless of the mechanism, successful repair of DSBs involves crucial steps, including end processing by nucleases, the involvement of DNA polymerases, and a final ligation step to complete repair of the broken DNA. These two pathways are mutually exclusive, meaning that when a DSB undergoes HR repair, NHEJ is completely suppressed (Pannunzio et al., 2018; Wright et al., 2018) and *vice versa*. In human a key protein involved in the choice between HR and NHEJ is 53BP1. This protein prevents DNA end resection, thus promoting NHEJ together with other proteins and the complex shieldin. Therefore, 53BP1 recruitment to the DSB is tightly controlled, and sophisticated mechanisms (in general, through chromatin modifications) exist to control 53BP1 in the DSB vicinity (Rass et al., 2022).

Non-Homologous End Joining

The name NHEJ originally arose to distinguish it from repair that requires extensive DNA homology, such as Homologous Recombination. Most components of NHEJ have been conserved between yeast and mammalian cells, although it can introduce mutations at the repair junction (Critchlow et al., 1997; Lewis & Resnick, 2000; Lieber, 2010). In general, NHEJ process can be mainly divided into the three steps: DSB recognition, processing, and ligation (Figure 5). However, depending on the complexity of the DSB, additional processes and factors can be recruited during the process. In the case of simple DSB ends without complicated configurations, the DNA ends can be directly ligated through standard recognition and processing. For complex DSBs that contain substantial mismatched or covalently modified DNA ends, additional factors are required to facilitate modifications of the DSBs before the ligation. The recognition of DSBs is mediated by the complex Ku. Normally, Ku functions as a heterodimer consisting of Ku70 and Ku80 subunits which assemble into a preformed ring to anchor the double-stranded DNA sequences at the DSB end (Walker et al., 2001). When a DNA breakage occurs, Ku rapidly detects and maintains in close proximity the two DSB ends to form a Ku:DNA complex. Indeed, along with MRX complex, Ku maintains the DSB ends relatively close to one another to avoid further translocation (Downs & Jackson, 2004a). This mechanism, called end-tethering, inhibits DSB mobility and prevents DSBs from undergoing abnormal translocation and fusion. Importantly, the conformation of Ku is modified upon binding to DNA sequences (Hartlerode & Scully, 2009), thereby allowing it to serve as a scaffold to other NHEJ factors. Thus, Ku recruits NHEJ factors into a multi-

protein complex and facilitates DSB processing and ligation. One of the main proteins recruited is the DNA ligase IV, an ATP-dependent ligase that in yeast interacts with its cofactor Lif1 (XRCC4 in mammals) that stimulates the ligase activity (Grawunder et al., 1997). Lif1 association to DSBs requires the presence of the Nej1 protein (XLF in mammals) (Daley & Wilson, 2005; Hefferin & Tomkinson, 2005). In mammals, XLF has structural similarity to XRCC4 and XLF N-terminal head domain interacts with the N-terminal head domain of XRCC4 (Ahnesorg et al., 2006).

In mammals, NHEJ also involves the presence of the DNA-dependent protein kinase (DNAPKcs), which is a Ser/Thr kinase belonging to the phosphoinositide 3-kinase related protein kinase (PI3KK) family, along with mTOR, ATM, and ATR. DNA-PKcs consist of an N-terminal domain with a helical domain and distinct phosphorylation clusters, a FAT domain, and a catalytic domain (Sharif et al., 2017). Together with Ku, DNA-PKcs form a complex with the DNA and can phosphorylate both itself and other repair factors (Meek et al., 2008). Additionally, this complex plays a role in maintaining the broken ends together and in the recruitment to DSBs of downstream NHEJ components through phosphorylation events (J. M. Williams et al., 2014). Furthermore, the Ku complex in mammals has the ability to directly recruit specific DNA polymerases to address potential DNA loss at the repair junction during NHEJ. Two such DNA polymerases are the DNA polymerase μ (POLμ) and DNA polymerase λ (POLλ), which can incorporate either dNTPs or rNTPs in a template-dependent or a template-independent manner (Bertocci et al., 2006). They can also interact with Ku through their N-terminal domains (Chang et al., 2017). Similarly, Pol4 in yeast plays a similar role by interacting with DNA Ligase IV and gap-filling eventual

complex junctions (Dudášová et al., 2004; Tseng & Tomkinson, 2002). In mammals, Artemins is one of the most important proteins involved in the processing of the DNA ends to make them suitable to ligation. It possesses exo- and endo-nuclease activities and is activated in complex with DNA-PKcs (Goodarzi et al., 2006; Gu et al., 2010). This complex uses its endonucleolytic activity to remove 5' and 3' DNA overhangs, creating ends that can be rejoined by the XRCC4-DNA Ligase IV complex (Dudášová et al., 2004; Poinsignon et al., 2004). Other proteins, such as WRN helicase, FEN1 endonuclease, and EXO1 exonuclease have been involved in the processing of DSB ends during NHEJ (Pannunzio et al., 2018). In yeast, one of the most extensively studied nucleases is Rad27, which serves as the counterpart to mammalian FEN1. Rad27 is a structure-specific nuclease that possesses both flap endonuclease and 5' to 3' exonuclease activities (Harrington & Lieber, 1994).

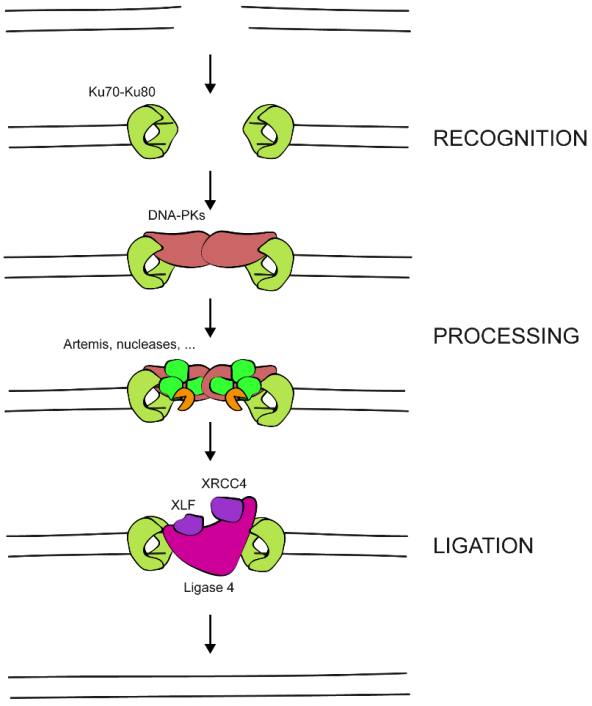

Figure 5. Schematic overview of NHEJ. After a DSB, the Ku complex can recognize the break where it protects DNA from degradation and acts as a scaffold to recruit NHEJ components like DNA-PKs, XRCC4, and XLF. The broken ends are kept together and DNA Ligase IV religates them. The DNA lesion is repaired but some mutations may be inserted at joined site.

Homologous Recombination

Homologous Recombination (HR) requires a homologous sequence as a repair template for DSBs, enabling the recombination machinery to accurately restore any missing genetic information in the proximity of the break site (Kowalczykowski, 2015). In most cases, in actively dividing cells, the sister chromatid serves as repair template. As a consequence, recombination is confined to specific cell cycle stages, namely the S and G2 phases, when the sister chromatid is available, and therefore requires a stringent regulatory mechanism. The choice between NHEJ and HR as repair pathways is primarily dictated by the initial processing of the DNA break (Cejka, 2015). NHEJ involves minimal DNA end processing, while HR is initiated by DNA resection at the break site, a process that exposes long stretches of ssDNA. This ssDNA is then employed to search for a homologous dsDNA sequence, often found in the sister chromatid, which serves as a template for the repair of the DSB by the recombination pathway. Simultaneously, extended DNA end resection renders the DSB generally not suitable for direct ligation and inhibits end-joining. Therefore, extensive DNA end resection commits DSB repair to the HR-mediated pathway (Chapman et al., 2012; Shibata, 2017; Symington & Gautier, 2011). Currently, different models of HR have been described: the Double Strand Break Repair model (DSBR), the Synthesis-Dependent strand Annealing (SDSA) and the Break Induced Replication (BIR) (Figure 6) (San Filippo et al., 2008). These three mechanisms differ in their outcomes but share the initial steps. The first common event is the extensive resection that leads the formation of 3'-tailed ssDNA coated by Replication Protein A (RPA). The primary role of RPA is to protect ssDNA

from the action of nucleases and prevent the formation of secondary structures that might arise by self-annealing of ssDNA (Wold, 1997). However, RPA-coated ssDNA itself cannot initiate the invasion of the intact donor DNA. In fact, the strand-invasion process is catalyzed the Rad51 recombinase. Rad51 presents a highly conserved structure among eukaryotes that resembles the bacterial RecA protein, in terms of residues that bind DNA and contribute to ATP hydrolysis (San Filippo et al., 2008). Similar to bacterial RecA, Rad51 forms a right-handed helical polymer on ssDNA or dsDNA, spanning thousands of base pairs. However, Rad51 alone is not able to displace RPA from ssDNA due to RPA higher affinity for ssDNA and its higher concentration compared to Rad51 (Symington, 2014). To facilitate the exchange between RPA and Rad51, additional proteins, called mediators are required in both yeast and mammals. In yeast, the key mediator is Rad52 (Krejci et al., 2012; San Filippo et al., 2008). Mechanistically, Rad52 forms a complex with Rad51 and delivers it to the RPA-ssDNA complex. Since Rad52 works as a multimers of 11 subunits, it can bridge at least eleven molecules of Rad51 in close proximity, increasing the probability of the exchange with RPA (San Filippo et al., 2008). Other mediators, such as Rad55 and Rad57, have also been identified in yeast and help to mitigate the inhibition of Rpa1 on Rad51. Furthermore, the Shu complex, conserved only in *S. pombe*, has been implicated in the positive regulation of the Rad51 filament formation (Krejci et al., 2012). In mammals, the most important mediator of HR is BRCA2, whose loss of function mutations are associated with ovarian and breast cancer (Holloman, 2011). Once the Rad51 filament has been assembled, the invasion takes place on the intact DNA molecule. In studies conducted in *E. coli*, it has been proposed that the homology search process occurs through random

collisions between the Rad51 filament and the donor DNA. When a stable interaction is established, a synaptic complex is formed. The invasion of the Rad51 filament induces the displacement of the same-polarity DNA strand, resulting in the formation of a specific structure called D-loop. In yeast, all the steps of pairing, homology searching, and D-loop formations are positively regulated by Rad54 (Symington, 2014). Rad54 belongs to the Swi2/Snf2 superfamily of proteins and possesses activities such as dsDNA-ATPase, DNA translocase, and chromatin remodeling. In addition to its positive regulatory role in promoting strand pairing, Rad54 also promotes strand separation, facilitating the pairing between the Rad51 filament and the donor DNA. Another important function of Rad54 is to negatively regulate the binding of Rad51 on dsDNA, preventing an incorrect use of Rad51 by the cell. Interestingly, once the synaptic complex is formed, Rad54 removes some Rad51 molecules from the 3'-OH end allowing the binding of the DNA polymerase complex (Symington, 2014). In particular, in the context of the D-loop structure the synthesis seems to be carried out by DNA Polδ, even if with a lower processivity than the one showed during S-phase. Moreover, in this mechanism the replicative proteins PCNA and Dpb11 are required (Symington, 2014). At this point, different ways to conclude the HR repair exist (Figure 6). The first model proposed was the Double Strand Break Repair model (DSBR). According to this model, the D-loop, formed through strand invasion, anneals with the other 3'-OH strand on the damaged molecule that was not involved in the strand invasion process. This initiates a second round of DNA replication, resulting in the formation of Holliday junctions (HJs), which are four-way intermediates DNA structure. To complete the repair process, different nucleases and helicases participate in the HJs resolution.

Different protein complexes are known to be responsible for HJs resolution: the Mus81-Mms4 and Slx1-Slx4 complexes (human SLX1-SLX4/MUS81-EME1 complex) and the STR complex composed by Sgs1, TopIII and Rmi1 (human BLM, TOP3α and RMI1/2) (Bizard & Hickson, 2014; Lilley, 2017). In the case of the Mus81-Mms4/Slx1-Slx4 complexes, HJs are resolved through an endonucleolytic cleavage. This mode of resolution generates both crossover (CO) and non-crossover products (NCO). On the other hand, the STR complex, consisting of Sgs1/BLM helicase and the topoisomerase activity of TOP3, produces only NCO products through its concerted action (Bizard & Hickson, 2014; Lilley, 2017).

An alternative HR model, called Synthesis Dependent Strand Annealing (SDSA), was proposed to explain the higher occurrence of NCO events compared to CO events. According to the SDSA model, the 3'-OH strand invades the homologous donor forming the D-loop that, after limited DNA synthesis, is displaced. If DNA synthesis has elongated enough to allow the invading strand to re-annealing with the damaged molecule, then the repair process is concluded by fill-in synthesis and ligation. As a result, only NCO products are generated. The SDSA mechanism is the predominantly active during mitosis, while the DSBR mechanism, which involves the resolution of Holliday junction, is more common in meiosis (Symington & Gautier, 2011). The last model of Homologous Recombination repair is the Break Induced Replication (BIR). BIR is a replication process that relies on recombination and results in nonreciprocal transfer of DNA from the donor to the recipient chromosome. During BIR only a single strand of one DSB end invades the homologous duplex and initiates replication. This triggers the migration of the

D-loop as far as the replication continues, using donor as template. BIR can occur through several rounds of strand invasion, DNA synthesis, and dissociation. It can lead to chromosome rearrangements when dissociation and reinvasion occur within repetitive inter-dispersed sequences (Symington, 2014).

There are alternative pathways for repairing DSBs that do not involve strand invasion and, therefore, do not require the involvement of Rad51. One of them is the Single-Strand Annealing (SSA), which occurs when the DSB is surrounded by two direct repeats. After DNA end resection, the repeats can anneal to each other, resulting in the deletion of the DNA portion between the direct repeats (Krejci et al., 2012). Additionally, DSBs can be repaired by Microhomology-Mediated End Joining (MMEJ), where micro homologous regions anneal to each other. The MMEJ model consists in five steps: resection of the DSB ends, annealing of micro homologous region, removal of heterologous flaps, fill-in synthesis and ligation by DNA ligase Lig3/Lig1 (DNA ligase III/I in humans) (Seol et al., 2018; H. Wang & Xu, 2017). MMEJ and HR may share the initial end resection step in DSB repair. However, while HR requires extensive end resection to recruit Rad51 recombinase, limited end resection is sufficient for exposing of micro homologous region and promoting MMEJ (McVey & Lee, 2008).

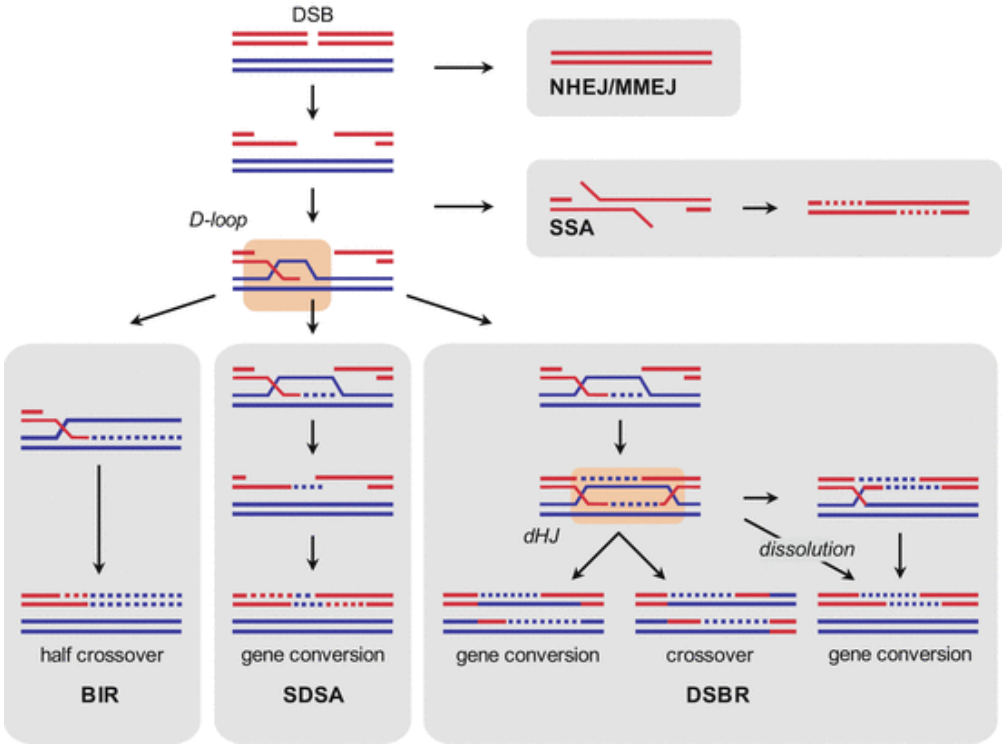

Figure 6. Model for repair of DNA double-strand breaks by homologous recombination. MMEJ and single-strand annealing (SSA) rely on different extents of homology between the two DSB ends for repair independent of a donor molecule. Homologous recombination proceeds using a homologous donor DNA. D-loops can be disrupted and subsequently repaired by SDSA. The result of the repair by SDSA is always a non-crossover outcome. SDSA occurs by disruption of the extended D-loop and annealing the newly synthesized DNA with the second end of the broken molecule. In DSBR the extended D-loop can also undergo second-end capture or invasion to form a double Holliday junction (HJs). This may either lead to a crossover or a non-crossover outcome. Invasion by the second break end makes HJs formation and hence crossover outcome more likely. HJs can be dissolved into non-crossovers by nuclease action (Sebesta & Krejci, 2016).

DNA end resection

DNA end resection involves the degradation of the 5'-terminated DNA strand in the 5' to 3' direction from the break site to generate a 3' ssDNA overhang. Generation of this 3'-terminated ssDNA is essential for the usage of homologous DNA sequences for repair (Ranjha et al., 2018). In contrast to NHEJ, extended DNA end resection is an obligate step that initiates all recombination pathways. DNA end resection of the 5'-terminated DNA strand occurs in two main steps (Mimitou & Symington, 2008; Z. Zhu et al., 2008). The first step is catalyzed by the MRX/MRN complex and Sae2/CtIP (Ogawa et al., 1995; Paull & Gellert, 1998; Sartori et al., 2007). The nucleolytic processing by these proteins is limited to the vicinity of the DNA end (generally up to 300 nucleotides in yeast) and is thus referred to as short-range DNA end resection (Z. Zhu et al., 2008). Resection is initiated by the endonucleolytic cleavage of the 5'-terminated DNA strand away from the DNA end, followed by 3'→5' exonuclease that proceeds back toward the DNA end. Both the exonuclease and the endonuclease activities during the first resection step are likely catalyzed by Mre11/MRE11 (Cannavo & Cejka, 2014; Garcia et al., 2011; Neale et al., 2005; Shibata et al., 2014). Mre11/MRE11 first endonucleolytically cleaves the 5'-terminated DNA in the vicinity of the DNA end. This endonucleolytic cleavage requires the ATPase activity of Rad50/RAD50 as well as Sae2/CtIP and NBS1 (but not strictly Xrs2 in yeast) as co-factors (Anand et al., 2016; Deshpande et al., 2016; Kim et al., 2007; Oh et al., 2016). Importantly, the capacity of Sae2 and CtIP to promote Mre11/MRE11 depends on phosphorylation of key residues on Sae2/CtIP, at least some of which are under cyclin-dependent kinase (CDK)

control (Cannavo & Cejka, 2014; Huertas et al., 2008; Huertas & Jackson, 2009). Cell-cycle-dependent phosphorylation of Sae2/CtIP represents one of the key control mechanisms that allow resection, and recombination to initiate only in S and G2 phases of the cell cycle, when a sister chromatid is available as a template for repair (Orthwein et al., 2015). Downstream of the endonuclease cut, Mre11/MRE11 subsequently uses its 3'→5' exonuclease activity to proceed back toward the DNA end, generating a 3' ssDNA overhang. The initial endonucleolytic cleavage away from the DNA end allows the resection machinery to bypass end-binding factors or noncanonical structures that may be present at the break end. This includes protein blocks, such as Spo11 in meiosis, stalled topoisomerases, or the Ku complex (Bonetti, Clerici, Manfrini, et al., 2010a; Chanut et al., 2016; Keeney et al., 1997; Keeney & Kleckner, 1995; Langerak et al., 2011; Mimitou & Symington, 2010; Neale et al., 2005). Indeed, the efficiency of 5' DNA end cleavage *in vitro* by MRX-Sae2 is stimulated by the presence of protein blocks at DNA ends. The initial endonucleolytic cleavage by Mre11/MRE11 creates entry sites for the long-range resection enzymes. These subsequently catalyze resection in the 5'→3' direction away from the DNA end to generate extended ssDNA overhangs (up to several kilobases in length) and represent the second step of the resection process. The 3'→5' exonucleolytic DNA degradation by MRX/MRN and the 5'→3' degradation by the long-range enzymes downstream of the endonucleolytic cut have been termed "bidirectional" resection. In addition to the nuclease function, the MRX/MRN complex has structural roles to recruit the long-range resection enzymes (Cejka et al., 2010; Nicolette et al., 2010; Nimonkar et al., 2011; Niu et al., 2010). The long-range resection factors include either of two nucleases, Exo1/EXO1 or

Dna2/DNA2, which are well conserved between yeast and human cells (Gravel et al., 2008; Mimitou & Symington, 2008; Z. Zhu et al., 2008). Exo1/EXO1 is a dsDNA-specific exonuclease (Tran et al., 2002), which specifically degrades the 5'-terminated DNA strand within dsDNA, generating 3' ssDNA overhangs. In contrast, Dna2/DNA2 is an ssDNA-specific 5'→3' nuclease that cannot process dsDNA on its own, and requires a RecQ family helicase partner (Bae et al., 1998; Levikova et al., 2013; Z. Zhu et al., 2008). This includes Sgs1 in yeast and either Bloom syndrome helicase (BLM) or WRN in human cells (Levikova et al., 2013; Pinto et al., 2016; Sturzenegger et al., 2014). Sgs1/BLM/WRN unwinds dsDNA to generate ssDNA, which becomes rapidly coated by replication protein A (RPA). RPA-coated ssDNA is subjected to degradation by Dna2/DNA2. Both human DNA2 and yeast Dna2, in addition to their essential nuclease activity, contain a helicase domain, which likely functions as an ssDNA translocase to facilitate the degradation of 5'-overhanged DNA by the Dna2/DNA2 nuclease (Levikova et al., 2017; Miller et al., 2017).

DSB resection is also negatively controlled to prevent excessive generation of ssDNA. In particular, the Ku complex, which forms a heterodimer ring structure that encircles the dsDNA with a particular high affinity, competes with MRX complex for DSB binding (Blier et al., 1993; Griffith et al., 1992; Mimori & Hardin, 1986; Walker et al., 2001; Yaneva et al., 1997). The association of Ku to the DSB ends restricts the formation of ssDNA by impairing the association and/or the activity of the Exo1 nuclease. Moreover, the long-range resection is inhibited by the checkpoint protein Rad9, which acts as a barrier for the nucleases Exo1 and Sgs1/Dna2 (Lazzaro et al., 2008;

S. E. Lee et al., 1998a). In turn, one way of the Rad9 recruitment to DSBs depends on its interaction with histone H2A phosphorylated on Ser129 (γH2A), showing a relation between the chromatin modifications and extension of DSB resection (Hammet et al., 2007; Javaheri et al., 2006; Shroff et al., 2004; Toh et al., 2006).

Resection could be also limited by a physical barrier formed by nucleosomes. Nucleosomes consist of about 146 base pairs of DNA wrapped approximately twice around two copies of a protein complex called histone core. The histone core is formed by H2A–H2B and H3–H4 assembled in tetramer (Frigerio et al., 2023). The presence of nucleosomes impedes the action of nucleases, in fact Exo1 is unable to resect a nucleosome-rich substrate *in vitro*, while Sgs1-Dna2 can process DNA wrapped around nucleosomes only when enough nucleosome-free DNA is present. Therefore, nucleosome removal or repositioning is important to allow efficient nuclease action (Adkins et al., 2013). Moreover, since nucleosomes are evicted near a DSB, their removal might occur after Mre11-dependent incision of the 5'-terminated strands, even if Mre11 preferentially cleaves nucleosome-free DNA (Mimitou et al., 2017; W. Wang et al., 2017). These data are consistent with a coexistence of both nucleosomes and MRX bound at DSB ends and the fact that MRX can diffuse along dsDNA even in the presence of nucleosomes (Myler et al., 2017). Even Ku complex is influenced by nucleosome presence. In fact, the Ku complex localizes to DNA ends that are locally depleted of nucleosomes and Ku diffusion is inefficient on nucleosome-associated DNA ends (Roberts & Ramsden, 2007). Lastly, histones can undergo to post translational modification, such as phosphorylation, methylation, ubiquitylation, and

acetylation. These modifications participate in the DSB response by affecting chromatin structure in histone-histone, histone-DNA interactions, or by providing binding sites for other factors (Frigerio et al., 2023).

MRX complex: structure, function, and regulation

The *MRE11*, *RAD50*, and *XRS2* genes were initially discovered due to their role in the repair of ionizing radiation (IR) induced DNA damage and in meiotic recombination in *S. cerevisiae* (Krogh & Symington, 2004). While Mre11 and Rad50 are conserved in prokaryotes, archaea, and eukaryotes, Xrs2/NBS1 is found only in eukaryotes (Sharples & Leach, 1995; Stracker & Petrini, 2011). These three proteins interact to form a heterohexameric DNA binding complex, consisting of dimers of each subunit (Kinoshita et al., 2009; G. J. Williams et al., 2010). This complex is tightly regulated by different interactors and by its ability to bind and hydrolyze ATP.

Mre11 is part of the lambda phosphatase family of phosphoesterases and presents manganese-dependent nuclease activities *in vitro*, including 3→5' dsDNA exonuclease activity and a ssDNA endonuclease activity that targets ssDNA/dsDNA transitions and hairpin loops. The nuclease activity of Mre11 is enhanced by both Rad50 and Xrs2/NBS1 *in vitro* (Paull & Gellert, 1998, 1999; Trujillo et al., 1998). The C-terminal region of Mre11 has two DNA binding sites, the most C-terminal of which is required for meiotic DSB formation is *S. cerevisiae*, and the other one presents a Rad50 interaction site (Furuse et al., 1998; Usui et al., 1998; G. J. Williams et al., 2011). Rad50 is a SMC-protein and it contains Walker A and B nucleotide (NTP)-binding motifs at amino- and carboxy-terminal ends, respectively (Kinoshita et al., 2009). In particular, these regions are separated by anti-parallel coiled-coil domains that form large proteinaceous rings or rods, which are joined by a Cys-X-X-Cys motif that mediates interactions with another Rad50 molecule via tetrahedral coordination of a zinc ion (K. P. Hopfner et al., 2001; K.-P. Hopfner et al.,

2002; Park et al., 2017). This multimerization of Rad50 is required for DNA end-thetering of the MRX complex (Wiltzius et al., 2005). Moreover, Rad50 exhibits ATPase activity *in vitro*, which is required for DNA repair and meiosis (Alani et al., 1990; K.-P. Hopfner et al., 2000). The ATPase activity of the Rad50 subunit drives conformational changes of the complex, which regulate MRX functions in DNA binding, DSB end tethering, Tel1/ATM activation and resection (Syed & Tainer, 2018). In the presence of a non-hydrolysable ATP analogue, Rad50 dimer possesses a rigid high affinity DNA-binding conformation, in which the head domains interact with each other and form a groove that can accommodate dsDNA (Lammens et al., 2011; Lim et al., 2011; G. J. Williams et al., 2011; R. S. Williams et al., 2008). In this ATP-bound conformation (MR-ATP resting-state), Mre11 cannot access dsDNA and therefore is unable to exert its nuclease activity (Deshpande et al., 2014; Liu et al., 2016; Möckel et al., 2012; Seifert et al., 2016). On the other hand, ATP hydrolysis results in a large conformational change to an open structure exposing the Mre11 nuclease active site (Lammens et al., 2011; Lim et al., 2011; G. J. Williams et al., 2011).

Xrs2/NBS1 is the least conserved component of the MRX/MRN complex and probably acts as a regulatory and protein recruitment module (Stracker & Petrini, 2011). In humans, NBS1 contains FHA (forkhead associated) and BRCT (BRCA1 C-terminus) domains in the N-terminal region, which are separated from the MRE11 and ATM DNA binding domains by a flexible tether (Lloyd et al., 2009; R. S. Williams et al., 2009). The BRCT domains of NBS1 interact with the checkpoint adaptor MDC1, which in turn binds to phosphorylated H2AX to amplify and/or maintain the DNA damage checkpoint (Stracker & Petrini, 2011).

In *S. cerevisiae*, it has been shown that activation of Mre11 endonuclease activity requires the Sae2 protein (CtIP in mammals), which stimulates Mre11 endonuclease activity within the context of the MRX complex (Cannavo & Cejka, 2014). This function depends on the interaction between Rad50 and Sae2, which is facilitated by Sae2 phosphorylation by cyclin-dependent kinases (Anand et al., 2016; Cannavo et al., 2018). Although Sae2 does not affect the overall ATP hydrolysis rate by Rad50, stimulation of Mre11 endonuclease by Sae2 requires ATP hydrolysis by Rad50 (Cannavo et al., 2019), indicating that Sae2 plays a crucial role in coupling ATP hydrolysis with activation of the Mre11 endonuclease. The conserved residues with human of Sae2 are restricted to the C-terminal region and to the dimerization domain near its N-terminus (Limbo et al., 2007; McKee & Kleckner, 1997; Prinz et al., 1997; Sartori et al., 2007). In *E. coli*, the Mre11-Rad50 nucleolytically active subcomplex includes an interface that involves an outer β sheet of Rad50 nucletide binding domain (NBD) and a loop in Mre11, defined as "fastener" (Käshammer et al., 2019). Mutations affecting Mre11-Rad50 binding reduce Mre11 nuclease activity, suggesting that this interface is important to stabilize the Mre11-Rad50 cutting conformation (Käshammer et al., 2019). The fastener loop is not conserved in eukaryotes but some studies have suggested that a cutting configuration also exists in eukaryotic MR complexes as well. Instead of the fastener loop, Sae2 binding to the Rad50-Mre11 interface is required to stabilize this nucleolytically active conformation and promote Mre11 endonuclease activity (Cannavo et al., 2018). In addition, Sae2 not only stimulates the endonuclease activity of the MRX complex, but also controls its turnover at DSBs. In the absence of Sae2, MRX and therefore Tel1 accumulation at the DSB ends increases, leading to a persistent Rad53-

mediated cell cycle arrest that increases the DNA damage sensitivity of *sae2*Δ cells (H. Chen et al., 2015; Clerici et al., 2006; Gobbini et al., 2015; Puddu et al., 2015; Usui et al., 2001; Yu et al., 2018). The lack of Mre11 nuclease activity also causes persistent MRX and Tel1 association at DSB ends, indicating that timely removal of the MRX complex from DSBs requires the Mre11 endonuclease activity (Clerici et al., 2006; Lisby et al., 2004). MRX is crucial for recruiting and activating Tel1/ATM to both DSBs and telomeres. In *S. cerevisiae*, Tel1/ATM, once it is loaded on the DSB, promotes/stabilizes MRX complex association in a positive feedback loop (Cassani et al., 2016a; Hirano et al., 2009; Martina et al., 2012).

Protecting chromosome ends: telomeres

The natural ends of chromosomes must be distinguished from intrachromosomal DNA DSBs, which activate the DNA damage response. Chromosome ends are safeguarded through a protective structure called telomere with a process called capping (de Lange, 2018; Wellinger & Zakian, 2012). Various proteins bind to the telomeric DNA and protect it from fusion, degradation, and recognition as a DSB that would otherwise lead to chromosome instability and cell death (Gobbini et al., 2014). In most eukaryotes, the telomeric DNA at the ends of chromosomes is characterized by high repetition of short nucleotide sequences that are rich in TG. Specifically, these sequences are oriented in the 5' to 3' direction towards the chromosome end. In addition to double-stranded telomeric DNA, the 3' end (G-strand) extends beyond its complementary strand (C-strand) to form a single-stranded overhang called the G-tail (Wellinger & Zakian, 2012). In *S. cerevisiae*, these short tandem DNA repeats are long approximately 300 +/-75 basepairs with $C_{1\text{-}3}A/TG_{1\text{-}3}$ repeats. Adjacent to the telomeric regions there are sub-telomeric regions containing repeated elements called X and Y', which are closer to the centromere. Most telomeric DNA is replicated by standard semiconservative DNA replication. Since DNA polymerases can only replicate DNA in the 5' to 3' direction and require a primer to initiate DNA synthesis, the removal of the terminal RNA primer at the 5' ends of newly replicated strands leaves a gap that cannot be filled in by the canonical DNA replication machinery. As a result, telomeric DNA sequences become progressively shorter with each round of DNA replication. However, in most eukaryotes, this loss of telomeric DNA is counteracted by a ribonucleoprotein enzyme

called telomerase. Telomerase uses its RNA component as a template to add telomere repeats at the telomeric 3' overhang in a reverse transcriptase reaction (Greider & Blackburn, 1985). In mammalian cells, the minimal catalytic core of telomerase consists of the telomerase reverse transcriptase (TERT) and the telomerase RNA (TERC). In *Saccharomyces cerevisiae*, telomerase is composed of the reverse transcriptase Est2, the template RNA TLC1, and two accessory proteins Est1 and Est3 (Jain & Cooper, 2010). The checkpoint kinase Tel1/ATM is involved in the maintainance of the length of telomeres, and its recruitment to telomere depends on the MRX/MRN complex with a positive feedback-loop (Keener et al., 2019; Ritchie & Petes, 2000).

Protein complexes are responsible for distinguishing telomeric DNA from intrachromosomal DNA DSBs. These complexes are recruited to telomeres and prevent DDR activation, degradation, fusions, and recombination events. In budding yeast, the proteins involved in this process include CST, Ku, and the Rap1-Rif1-Rif2 complexes. The CST complex, which consists of Cdc13, Stn1, and Ten1 subunits, is also present in mammalian cells and comprises the CTC1, STN1, and TEN1 subunits (Y. C. Chen et al., 2009; Miyake et al., 2009; Wu et al., 2012) (Figure 7). This complex binds the telomeric 3' G-tail and is fundamental for chromosome capping and telomere replication (Churikov et al., 2013; Nugent et al., 1996). The Ku complex plays a crucial role in telomere protection by encircling the telomeric dsDNA. It specifically inhibits Exo1-mediated nucleolytic degradation, similarly at DSBs (Bonetti et al., 2010a). Additionally, Ku contributes to the maintenance of telomere length by interacting with the telomerase subunits Est1 and Est2, as well as with the telomerase RNA TLC1 (Chan et al., 2008; Fisher & Zakian, 2005; Peterson et

al., 2001). The association of Ku complex with TLC1 is required for TLC1 nuclear retention, suggesting an involvement of Ku in the nuclear-cytoplasmic trafficking of telomerase. However, Ku recruitment at telomeres is independent of TLC1 and occurs throughout the cell cycle (Fisher et al., 2004; Gallardo et al., 2008, 2011; Peterson et al., 2001; Stellwagen et al., 2003).

Another complex that possesses a capping function in yeast is composed by Rap1, Rif1, and Rif2 proteins. This complex is the functional counterpart of the human shelterin complex, which consists of TRF1, TRF2, RAP1, TIN2, TPP1, and POT1 subunits (de Lange, 2018). The complex made by Rap1, Rif2, and Rif1 represses telomere-telomere fusions by NHEJ, telomere degradation, and checkpoint activation (Bonetti, et al., 2010; Marcand et al., 2008; Vodenicharov et al., 2010). As DNA binding protein, Rap1 is also able to bind telomeres, where it exerts various functions: negatively regulates telomere length, suppresses transcription, and inhibits telomeric fusions via NHEJ (Azad & Tomar, 2016; Y. Chen et al., 2011; Conrad et al., 1990; Kabir et al., 2010; Kurtz & Shore, 1991; Kyrion et al., 1992; Lustig et al., 1990; Moretti & Shore, 2001; Pardo & Marcand, 2005; Sussel & Shore, 1991). The DNA binding modes of Rap1 through its Myb-domains influence its functional properties (Bonetti et al., 2020).

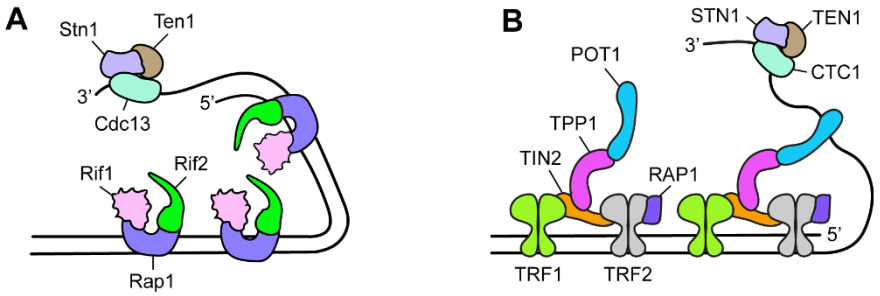

Figure 7. Telomeric structure and capping proteins in yeast and humans. (A) Schematic representation of the yeast Rap1-Rif1-Rif2 and CST complexes. CST in yeast is composed of Cdc13, Stn1, and Ten1 proteins. (B) Schematic representation of the mammalian shelterin complex, composed by TRF1, TRF2, TIN2, RAP1, TPP1, and POT1 subunits, and the CST complex, composed of CTC1, STN1 and TEN1 subunits (Casari et al., 2022).

The protein Rif2

The protein Rif2 is a 46 kDa globular protein that belongs to the ATPase associated with diverse cellular activities (AAA+) protein family. The Rif2^{AAA+} domain consists of the ASCE motif, an α bundle, and an N-terminal domain called Rif2^{RBM} (Shi et al., 2013). Rif2 physically interacts with Rap1, through a direct interaction with the C-terminal region of Rap1 (Rap1^{RCT}). In the Rif2-Rap1 complex structure, each Rif2 molecule binds to two distinct Rap1^{RCT} molecules through two independent interfaces: the Rif2^{AAA+} domain and the Rif2^{RBM}. Thus, a single Rap1 molecule, through its RCT domain, simultaneously binds two Rif2 molecules in a non-overlapping manner (Shi et al., 2013). *RIF2* has paralog *ORC4* that arose from the whole genome duplication. Rif2 negatively regulates telomere elongation and counteracts Tel1 activation, nucleolytic degradation, and NHEJ at telomeres (Bonetti, Clerici, Manfrini, et al., 2010b; Hardy et al., 1992; Marcand et al., 2008; Ritchie & Petes, 2000). These activities are probably mediated through inhibition of the MRX complex at telomeres. Rif2 was initially proposed to counteract Tel1-mediated stabilization of MRX association at DNA ends by competing with Tel1 for Xrs2 binding. However, Rif2 can inhibit Tel1 kinase activity *in vitro* independently of Xrs2. Additionally, Rif2 interacts with Rad50 and stimulates its ATPase activity independently of Xrs2 (Cassani et al., 2016a; Hailemariam et al., 2019), suggesting that Rif2 regulates MRX and Tel1 functions at DNA ends through the direct interaction with Rad50. Specifically, a small region from residues 1 to 36, called MIN (MRN-INhibitor), mediates the inhibitory effects of Rif2 on NHEJ, resection and MRX association to DNA ends (Khayat et al., 2021; Roisné-Hamelin et al., 2021). The MIN motif interacts

with Rad50 and is necessary for Rif2 to stimulate Rad50 ATPase. Since ATP binding by Rad50 supports the MRX capacity to bind DNA and to promote Tel1 activation and NHEJ, these findings suggest that Rif2 inhibits these MRX functions through the MIN motif by triggering ATP hydrolysis by Rad50 and therefore by discharging the MRX ATP-bound state (Deshpande et al., 2014; Hailemariam et al., 2019; Lammens et al., 2011; Liu et al., 2016; Seifert et al., 2016). The Rad50 residues that interact with Rif2-MIN domain are located on the outer β sheet of Rad50 NBD. Interestingly, mutations in this region fail to interact with Sae2 (Cannavo et al., 2018), suggesting that Rif2 and Sae2 binding sites may partially overlap on Rad50 and that Rif2 and Sae2 may compete for binding to Rad50. (Khayat et al., 2021; Marsella et al., 2021; Roisné-Hamelin et al., 2021).

However, how Rif2 inhibits MRX and Tel1 activity remains unclear. One mechanism could involve Rif2 stimulating the ATPase activity of Rad50, which then affects MRX binding to DNA and Tel1 activation. Alternatively, Rif2 may directly inhibit the interaction between Tel1 and Rad50, preventing Tel1 from associating with DNA ends. These different inhibitory mechanisms suggest that Rif2 plays a complex role in regulating MRX and Tel1 activity.

RESULTS

Chapter 1

Nucleic Acids Research
accepted on 15th Dec 2023

Nucleic Acids Research

Rif2 interaction with Rad50 counteracts Tel1 functions in checkpoint signalling and DNA tethering by releasing Tel1 from MRX binding

Paolo Pizzul[1], Erika Casari[1], Carlo Rinaldi[1], Marco Gnugnoli[1], Marco Mangiagalli[1], Renata Tisi[1] and Maria Pia Longhese[1*]

[*] Corresponding Author

[1] Dipartimento di Biotecnologie e Bioscienze, Università degli Studi di Milano-Bicocca, Milano, 20126, Italy

DNA double-strand breaks (DSBs) are cytotoxic lesions that can lead to cell death, gross chromosomal rearrangements, or loss of genetic information. Cells have evolved two major pathways to repair DNA DSBs: non-homologous end-joining (NHEJ) and homologous recombination (HR). In NHEJ, the DSBs are directly ligated with no or limited processing at their ends (Stinson & Loparo, 2021), while in HR the broken DNA ends are nucleolytically degraded to generate 3' single-stranded DNA (ssDNA) overhangs that pair with intact homologous DNA templates (Mehta & Haber, 2014). The generation of DNA DSBs also elicits a checkpoint response, whose key players are the apical protein kinases Tel1 and Mec1, as well as their mammalian orthologs ATM and ATR, respectively (Pizzul et al., 2022). Upon DSB recognition, Tel1 and Mec1 transduce the checkpoint signals to the downstream effector kinases Rad53 and Chk1 (CHK2 and CHK1 in mammals, respectively), whose activation requires the protein Rad9 (53BP1 in mammals).

The highly conserved Mre11-Rad50-Xrs2/NBS1 (MRX in *Saccharomyces cerevisiae* and MRN in mammals) complex acts as a main sensor of DNA DSBs (Syed & Tainer, 2018; Tisi et al., 2020). At the molecular level, the core Mre11-Rad50 subcomplex exists as a hetero-tetrameric assembly, in which two Mre11 subunits interact with two Rad50 nucleotide-binding domains to form a globular head from which two long Rad50 coiled coils protrude (de Jager et al., 2001; Hopfner et al., 2001; Lammens et al., 2011; Lim et al., 2011; Williams et al., 2008). MRX/MRN is required to maintain the DSB ends tethered to each other (Kaye et al., 2004; Lobachev et al., 2004; Nakai et al., 2011; Lee et al., 2008), an activity that has been attributed to the ability of Rad50 coiled

coils to form intermolecular complexes that bridge the DNA ends (Hohl et al., 2015; Park et al., 2017; Tatebe et al., 2020; Rotheneder et al., 2023). In addition, MRX/MRN is necessary to initiate resection of DNA DSBs that possess various secondary DNA structures and protein blocks at their ends (Lobachev et al., 2002; Neale et al., 2005; Reginato et al., 2017; Wang et al., 2017). This resection activity depends on the Mre11 subunit, whose endonuclease activity nicks the 5' strand near the DNA end, whereas its 3'-5' exonuclease activity generates a short 3'-overhang of up to 300 nucleotides in length (Neale et al., 2005; Reginato et al., 2017; Wang et al., 2017; Garcia et al., 2011; Shibata et al., 2014). The ssDNA tail is then elongated in the 5'-3' direction by the long-range resection nuclease Dna2 or Exo1 (Mimitou & Symington, 2008; Zhu et al., 2008; Cejka et al., 2010; Niu et al., 2010). Finally, MRX/MRN is required for the recruitment and activation of the Tel1/ATM kinase (Nakada et al., 2003; Uziel et al., 2003; Lee & Paull, 2005; Falck et al., 2005; Lee & Paull, 2004; You et al., 2005). In *S. cerevisiae*, Tel1, once loaded at DSBs by MRX, stabilizes MRX association with DSBs through a positive feedback loop (Cassani et al., 2016; Oh et al., 2018).

The two Rad50 subunits in the dimer constitute the binding sites for two ATP molecules. ATP binding to Rad50 induces a conformational rotation that increases the binding affinity of the two Rad50 subunits (Hopfner et al., 2000; Williams et al., 2011; Möckel et al., 2012; Liu et al., 2016; Seifert et al., 2016; Deshpande et al., 2014). In the ATP-bound state (resting state), the Rad50 dimer blocks the access of Mre11 to double-stranded DNA (dsDNA), thus preventing the MRX ability to incise the DNA ends (Rotheneder et al., 2023; Liu et al., 2016; Seifert et al., 2016; Deshpande et al., 2014). This MRX

conformation has been proposed to be the active state for Tel1 activation, as rad50 mutations that destabilize the ATP-bound state also impair Tel1 signalling activity (Deshpande et al., 2014; Lee et al., 2013; Cassani et al., 2019). Upon ATP hydrolysis, the Rad50 nucleotide-binding domains dissociate and Mre11 moves to one side of Rad50. This conformational change makes DNA accessible to the Mre11 nuclease active sites, thus licensing the endonucleolytic DNA cleavage by Mre11 (cutting state) (Gut et al., 2022). Activation of Mre11 endonuclease activity within the context of the MRX complex requires the Sae2 protein (CtIP in humans) that, once phosphorylated by cyclin-dependent kinases, interacts with Rad50, and was proposed to stabilize the nucleolytically active Mre11-Rad50 conformation (Cannavo & Cejka, 2014; Cannavo et al., 2018; Käshammer et al., 2019).

Recent data indicate that the activity of the MRX complex is negatively regulated by Rif2, a *S. cerevisiae* protein originated from duplication of the essential *ORC4* gene (Marcand et al., 2008). Rif2 inhibits the Mre11 endonuclease activity *in vitro* (Khayat et al., 2021; Marsella et al., 2021), MRX-mediated resection of telomeric DNA ends (Bonetti et al., 2010; Martina et al., 2012; Ribeyre & Shore, 2012), and MRX association with both DSBs and telomeres (Cassani et al., 2016; Hirano et al., 2009). These Rif2 inhibitory functions depend on a short amino acid motif, called MIN (MRN-Inhibitor), which is part of the BAT domain (Blocks Addition of Telomeres), previously identified as responsible for the negative regulation of telomere length (Kaizer et al., 2015). The MIN motif inhibits Mre11 endonuclease activity and interacts

with Rad50 in the same region where Rad50 binds Sae2 (Khayat et al., 2021; Marsella et al., 2021; Roisné-Hamelin et al., 2021).

These data lead to a working model, as depicted in Figure 8, in which MRX, in its ATP-bound conformation, can bind DNA but cannot cleave it. Following ATP hydrolysis by Rad50, the two Rad50 coiled coils zip up and Mre11 reaches the dsDNA by moving to the side of Rad50. Sae2 binding on the Rad50-Mre11 interface stabilizes this nucleolytically active ADP-bound MRX conformation, whereas Rif2 binding to Rad50 inhibits Mre11 nuclease activity by antagonizing the association of Sae2 with Rad50.

Interestingly, despite sharing no sequence homology with Rif2, the mammalian telomere-binding protein TRF2 carries an amino acid sequence, called iDDR (inhibitor of DNA Damage Response), that was recently found to interact with Rad50 similarly to MIN and to inhibit MRN-mediated resection of telomeric DNA ends (Myler et al., 2023).

In addition to limiting the Mre11 endonuclease activity, the Rif2 MIN motif counteracts Tel1-mediated telomere elongation by telomerase (Khayat et al., 2021; Kaizer et al., 2015; Roisné-Hamelin et al., 2021), MRX association at DNA ends (Roisné-Hamelin et al., 2021), and MRX-dependent stimulation of Tel1 kinase *in vitro* (Hailemariam et al., 2019). The mechanism through which Rif2 inhibits Tel1 activity at DNA ends is poorly understood, and various hypotheses can be conceived. Firstly, Rif2 might indirectly reduce Tel1 activation by diminishing the association of MRX with DSBs, which is necessary for recruiting Tel1 to DNA ends (Nakada et al., 2003; Uziel et al., 2003; Lee & Paull, 2005; Falck et al., 2005; Lee & Paull, 2004; You et al., 2005).

Secondly, Rif2 might directly inhibit Tel1 activation by interfering with Tel1-MRX interaction. Thirdly, since Rif2 stimulates the Rad50 ATPase activity *in vitro* (Cassani et al., 2016; Hailemariam et al., 2019), this might lead to a conformational change that might render the MRX complex unable to stimulate Tel1 kinase or to bind Tel1 effectively.

To test these hypotheses, we initially used AlphaFold Multimer to analyze the interaction interface between Rif2 MIN with Rad50. We then explored the effects of Rif2 binding to Rad50 by introducing mutations in Rif2 that enhance its interaction with Rad50. Our results show that the predicted Rad50-Rif2 interface involves hydrophobic residues conserved in the Rif2 yeast protein family but not in the mammalian TRF2 iDDR. Mutations of these residues reduce Rad50-Rif2 interaction and Rif2 functions at DNA ends. Furthermore, the substitution of S6 to E in Rif2 increases Rif2 affinity for Rad50 and enhances its inhibitory effect. In fact, unlike *rif2*Δ cells, *rif2-S6E* cells exhibit reduced hairpin cleavage. Furthermore, Rif2^{S6E} hampers Tel1 activation by reducing Tel1 association with DSBs without impairing MRX persistence at DSBs, indicating that Rif2 can directly reduce Tel1 recruitment to DNA ends. Rif2^{S6E} also diminishes Tel1-MRX interaction and stimulates ATPase by Rad50 more efficiently than wild-type Rif2, indicating that Rif2 binding to Rad50 counteracts Tel1 functions by inducing an MRX conformation unsuitable for Tel1 binding. In *rif2-S6E* cells, the decreased Tel1 association with DSBs leads to defects in maintaining the DSB ends close to each other, and this defect can be suppressed by enhancing Tel1 binding to DSBs. This finding, coupled with the observation that the role of Tel1 in supporting DSB

end-bridging does not require its kinase activity, suggests a direct and structural role for Tel1 in DSB end-tethering.

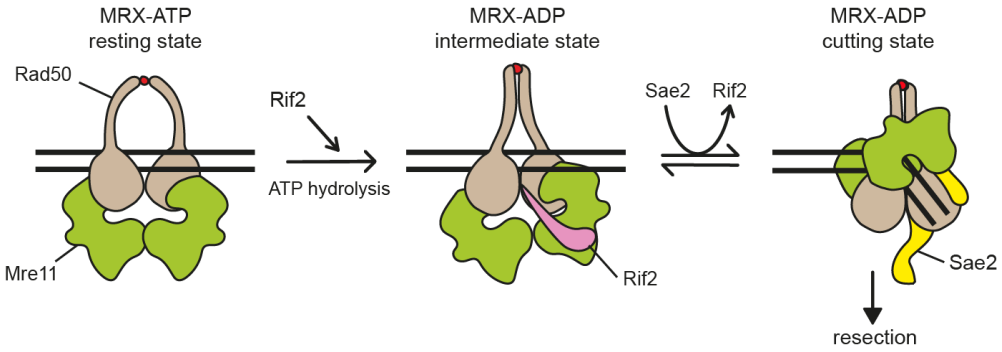

Figure 8. Model for regulation of MRX at DNA ends.) In the MRX ATP-bound state (resting state), Mre11 is inaccessible to dsDNA and therefore not competent to cleave it. Upon ATP hydrolysis, the two Rad50 coiled coils zip up and the Mre11 dimer rotates with respect to the Rad50 dimer globular domains. Rif2 binding to Rad50 stabilizes an Mre11-Rad50 ADP-bound state that is not competent for DNA cleavage. Sae2 antagonizes Rif2 binding to the Rad50-Mre11 interface and stabilizes an ADP-bound Mre11-Rad50 conformation (cutting state) that is proficient to cleave DNA. For simplicity, Xrs2 is not represented. The red dots indicate Zn^{2+} ions.

Analysis of the binding interface between the Rif2 MIN and Rad50

Rif2 inhibits MRX-dependent stimulation of Tel1 activity *in vitro* and Tel1 function at telomeres *in vivo* through a motif, termed MIN, that is situated at the Rif2 N-terminus (1-36 residues) (Hailemariam et al., 2019; Khayat et al., 2021; Marsella et al., 2021; Roisné-Hamelin et al., 2021). The inhibitory role of Rif2 in Tel1 activation might encompass several potential mechanisms, including indirect regulation by reducing MRX association with DNA ends, direct interference with Tel1-MRX interaction, and/or modulation of Rad50 ATPase activity. As the Rif2 MIN motif interacts with Rad50 (Hailemariam et al., 2019; Khayat et al., 2021; Roisné-Hamelin et al., 2021), to understand how Rif2 inhibits Tel1 activation, first we used the AlphaFold-Multimer predictor to generate models for the 1-36 amino acid MIN motif of Rif2 in complex with the Rad50 monomer from *S. cerevisiae*. As expected, the predictor found several structures of similar protein to exploit as templates for Rad50 modeling, but no template is available for Rif2 N-terminal region (Figure 9A). However, the structural prediction for Rif2 N-terminal was evaluated as a good and high-confidence prediction (Figure 9B and 9C).

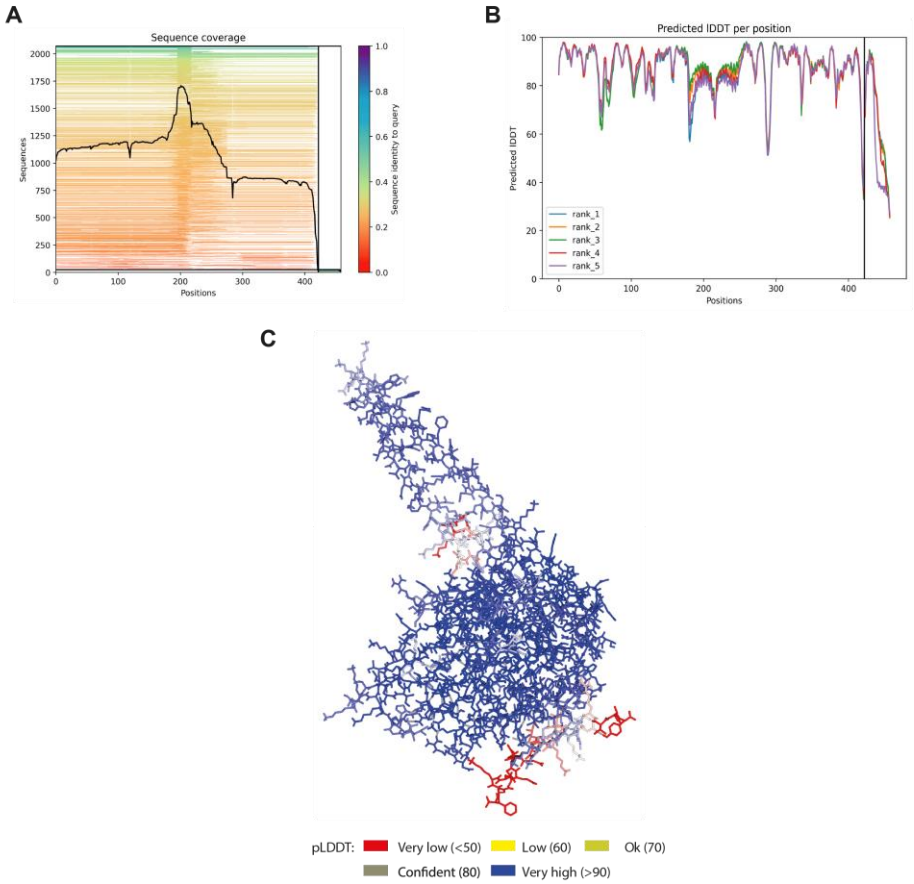

Figure 9. Quality assessment of the AlphaFold-multimer generated Rad50-Rif2 N-terminal complex. (A) Coverage from the multiple sequence alignment. Rad50 sequence is on the left section, Rif2 on the right. (B) LDDT parameter for the 5 top-ranked models. (C) LDDT-colored representation of the model. The most C-terminal region of Rif2 fragment is predicted at very low confidence.

The top-ranking model is shown in Figure 10A. The amino acids on the Rad50 surface that were previously identified as required for interaction with the Rif2 MIN domain (Roisné-Hamelin et al., 2021) are present in the interface predicted by AlphaFold-Multimer (Figure 10A). All the polar contacts between the two proteins are visualized in Figure 10B and C, and several of them involve amino acids previously shown to be conserved in the yeast Rif2 protein family. In detail, D5 and D7, which are highly conserved in both Rif2 and Orc4 homologs (Khayat et al., 2021; Roisné-Hamelin et al., 2021), are involved, respectively, in salt bridges with Rad50 K6 and K81 that were formerly identified as required for Rad50-Rif2 interaction (Figure 10B) (Roisné-Hamelin et al., 2021). The residue F8 in Rif2 is also invariant in Rif2 and Orc4 families, and its substitution with A affects Rif2-Rad50 interaction and Rif2 function in the regulation of telomere length (Kaizer et al., 2015; Roisné-Hamelin et al., 2021). In the model, the Rad50 F8 is within 6 Å to Rad50 K81, which allows a cation-π interaction. Moreover, F8 is also less than 5 Å from I93, which is close enough for van der Waals interaction (Figure 10B). The Rif2 R12 conserved residue interacts with D19 and E21 amino acids of Rad50. It is interesting to notice that D19 is localized in a tight turn near the N18 residue, previously reported as affected by N18S mutation that impinges on Rad50 affinity for Rif2 binding (Marsella et al., 2021). The model would suggest that N18 is important for the structural properties of this turn, more than for the direct interaction with Rif2.

Interesingly, the α-helix composed of amino acids 20-33 in Rif2 is positioned below the globular domain of Rad50, representing a new binding surface for Rif2 on the Rad50 C-terminal lobe of (Figure 10C). The interaction is mediated

by amino acids in Rif2 N-terminal domain that are conserved in Rif2 protein family but not in TRF2 iDDR (Myler et al., 2023). In detail, V18 and I23 face a hydrophobic cluster involving F1289 and V1305 of Rad50. The D21 and S28 partially conserved residues and the highly conserved D30 residue in Rif2 make contact, respectively, with Rad50 Y1312, E1274, and K1291.

Since this second interface could be inaccessible to Rif2 when MRX complex is in resting conformation, we superimposed the Rif2-Rad50 subcomplex to a model of the ATP-bound heterotetrameric state of Mre11-Rad50 that we previously described (Cassani et al., 2019a). The N-terminal of Rif2 occupies a space that is empty in the Mre11-Rad50 tetramer and should be accessible when the Mre11-Rad50 complex is in resting conformation, as required for Rif2 to stimulate Rad50 ATPase activity (Figure 10D).

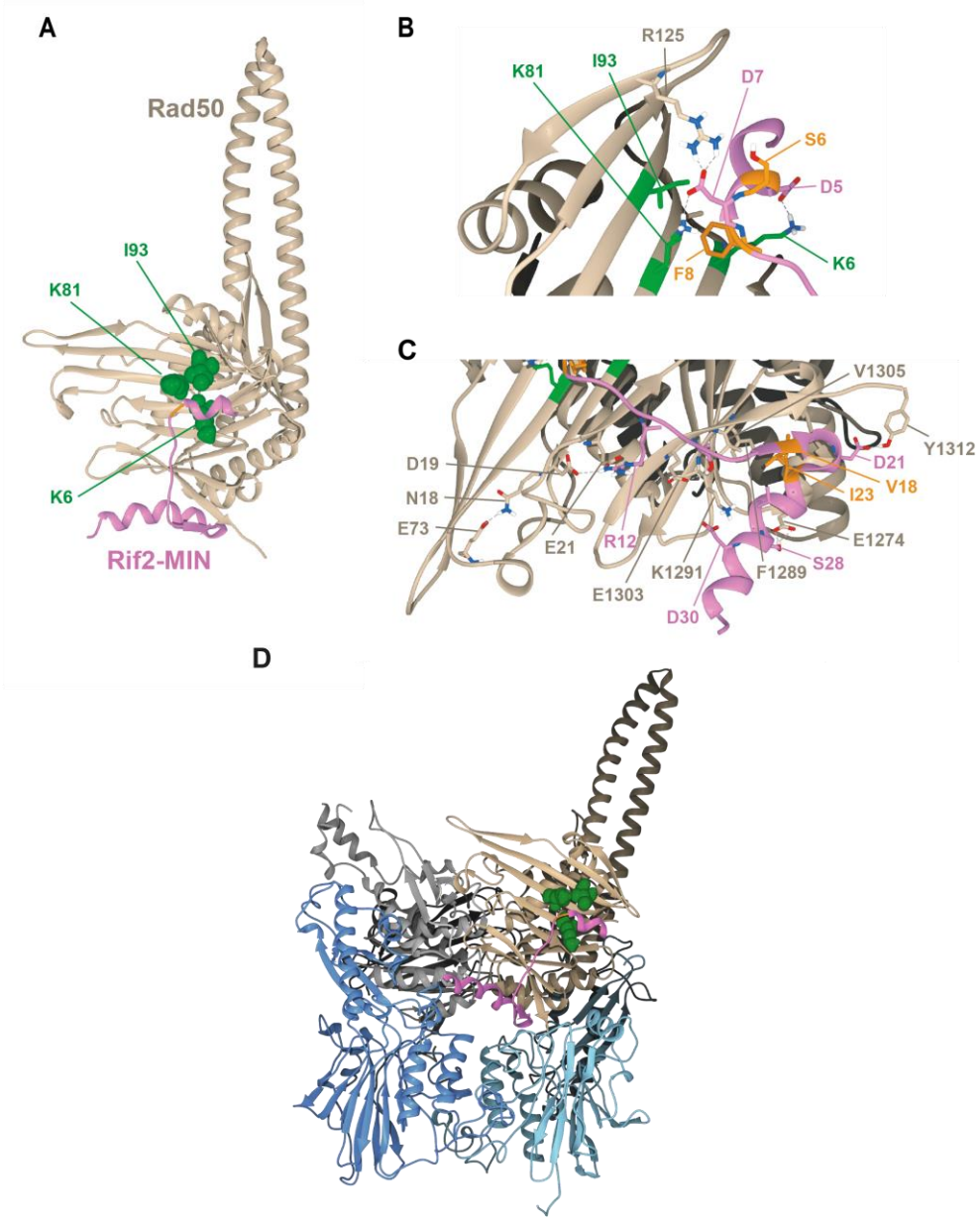
A
Rad50
I93
K81
K6
Rif2-MIN
B
R125
K81
I93
D7
S6
D5
K6
F8
C
V1305
Y1312
D21
V18
I23
D19
N18
E73
E21
R12
E1274
S28
K1291
F1289
E1303
D30
D

Figure 10. AlphaFold-Multimer generated model of the Rad50 complex with Rif2 N-terminal 36 amino acids. (A) Cartoon representation of the Rad50 (tan) and Rif2 N-terminal region (pink). The amino acids identified as necessary for interaction with Rif2 MIN domain on the surface of Rad50 β-sheet are represented as green spheres. (B) Detail of the interface between N-terminus of Rif2 and Rad50 β-sheet. (C) Detail of the second interface identified. Residues in the interface are represented as sticks. Rad50 residues previously known to be involved in the interaction are in green. Residues in Rif2 that were targeted for site-specific mutagenesis are in orange. (D) The model of Rad50-Rif2 N-terminal complex was superimposed to one of the two Rad50 in a heterotetrameric Mre11-Rad50 complex and is represented as a tan cartoon for Rad50 and a pink cartoon for Rif2. The amino acid from Rad50 previously known to be involved in this interaction are represented as green spheres. The other Rad50 subunit is represented as a grey cartoon, while the two Mre11 subunits are in blue and light blue.

Validation of the Rif2-Rad50 binding interface through the identification of MIN mutations that decrease or increase the Rif2 inhibitory function

To further validate the predicted Rif2-Rad50 interacting region, we replaced the highly conserved Rif2 residues V18 and I23 with E to introduce a negative charge, which was expected to disrupt the hydrophobic cluster that forms the core of the second interface. Furthermore, we engineered mutations that could enhance Rif2 inhibitory functions by further stabilizing the interaction of Rif2 with Rad50. To increase Rif2-Rad50 affinity, we considered mutations in the first interface, in particular the substitution of F8 to E. In fact, as F8 was predicted to interact with K81, its mutation to E might substitute the cation-π interaction with a salt bridge interaction. Besides, we decided to mutagenize the S6 residue to E to allow its interaction with the nearby Rad50 R125 residue (Figure 10B).

The deletion of *RIF2* has been shown to partially restore the DNA damage resistance of cells carrying the *rad50-V1269M* allele (referred to as *rad50-VM*), which we previously identified by searching for mutations that sensitize *tel1*Δ cells to the type I topoisomerase inhibitor camptothecin (CPT) (Cassani et al., 2016). The DNA damage sensitivity of *rad50-VM* cells was shown to be due to a decreased association of $MR^{VM}X$ with DNA DSBs, and the lack of Rif2 restored DNA damage resistance of *rad50-VM* cells by increasing $MR^{VM}X$ persistence at DSBs (Cassani et al., 2016). Hence, to determine whether the above *rif2-V18E*, *rif2-I23E*, *rif2-F8E*, and *rif2-S6E* alleles abolish or enhance Rif2 function, we combined them with the *rad50-VM* allele. Our rationale was that mutations resulting in Rif2 loss of function are expected to alleviate the

DNA damage sensitivity of *rad50-VM* cells, whereas those inducing hyperactivation should exacerbate it. In addition, as *RIF2* deletion results in over elongation of telomeres (Levy & Blackburn, 2004; McGee et al., 2010; Wotton & Shore, 1997), telomere length was also assessed. Similar to *rif2*Δ, the *rif2-V18E* and *rif2-I23E* alleles partially restored resistance to CPT of *rad50-VM* cells (Figure 11A) and caused telomere over elongation (Figure 11B), indicating that they impair Rif2 function Given that I23E is the mutation that causes the most severe overelongation of telomeres, we investigated whether this mutation impairs Rif2 function by reducing Rad50-Rif2 interaction. Utilizing a two-hybrid approach in cells that express the Rad50 head domain along with either wild-type Rif2 or Rif2^{I23E} (Khayat et al., 2021), we found that *rif2-I23E* reduced the ability of Rif2 to interact with Rad50 (Figure 11C), thereby substantiating the critical role of this region in mediating the Rad50-Rif2 interaction.

Unfortunately, the *rif2-F8E* mutation, which was designed to increase Rif2 affinity for Rad50 and therefore Rif2 inhibitory function, behaved similarly to *rif2-V18E* and *rif2-I23E* (Figure 11A and 11B), likely due to the impossibility of creating the right geometry for interaction with K81 or to the inadequate interaction with the hydrophobic pocket on the Rad50 surface (nearby I93). Interesingly, the *rif2-S6E* allele, which was also designed to enhance Rif2-Rad50 interaction, did not lead to an increase in telomere length (Figure 11B) and exacerbated the DNA damage sensitivity of *rad50-VM* cells (Figure 11A), raising the possibility that it could enhance Rif2 functions. In the predicted Rad50-Rif2 binding region, S6 is nearby the Rad50 R125 residue (Figure 10B), which interacts with Rif2 D7. The substitution of S6 with E introduces a

negative charge that allows the formation of a bond between Rif2 E6 and Rad50 R125, in addition to the already existing interaction of R125 with Rif2 D7. If the effect of the S6E substitution depends on a stronger interaction of Rif2 with Rad50 R125, then replacing R125 with K should only permit alternative interactions with D7 or with E6, but not with both, and therefore is expected to restore a wild-type Rif2-Rad50 affinity and to suppress the ability of *rif2-S6E* to exacerbate the *rad50-VM* DNA damage sensitivity. As shown in Figure 11D, *rif2-S6E rad50-R125K-VM* were as sensitive as *rad50-R125K-VM* cells, indicating that the *rif2-S6E* allele was unable to increase the CPT sensitivity of cells expressing a *rad50-VM* allele that also carries the R125K amino acid substitution. This finding demonstrates that the effect of the *rif2-S6E* mutation depends on a direct interaction between Rad50 and Rif2.

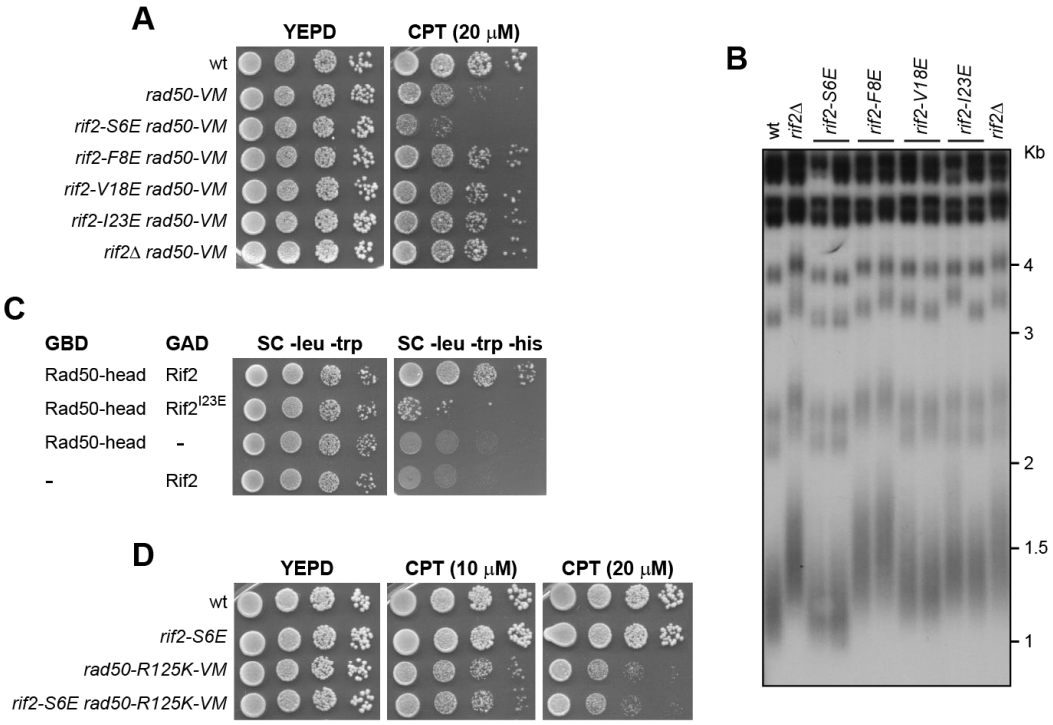

Figure 11. The *rif2* alleles and DNA sensitivity of *rad50-VM* cells, telomeres length and interaction between Rif2^{I23E} and Rad50-head. (A) Exponentially growing cultures were serially diluted (1:10) and each dilution was spotted out onto YEPD plates with or without camptothecin (CPT). (B) Telomere length. XhoI-cut genomic DNA from exponentially growing cells was subjected to Southern blot analysis using a radiolabeled poly(GT) telomere-specific probe. (C) Yeast two-hybrid assays of the fusion proteins indicated. Plates are minimal medium lacking the nutrients indicated on top. Four-fold serial dilutions were spotted left to right and incubated for 3–4 days at 30 °C. (D) Exponentially growing cultures were serially diluted (1:10) and each dilution was spotted out onto YEPD plates with or without CPT.

The *rif2-S6E* mutation increased neither Rif2 protein level nor Rif2 association with DSBs. In fact, similar amounts of Rif2 and Rif2^{S6E} were detected in protein extracts (Figure 12A). Furthermore, by using JKM139 derivative strains, where a single irreparable DSB at the *MAT* locus can be generated by expressing the site-specific HO endonuclease from a galactose-inducible promoter (S. E. Lee et al., 1998), similar amount of Rif2 and Rif2^{S6E} bound to DNA sequences close to the HO endonuclease cut site was found by chromatin immunoprecipitation (ChIP) and quantitative PCR (qPCR) after DSB formation (Figure 12B).

As expected from the predicted Rad50-Rif2 interaction interface, the *rif2-S6E* mutation indeed increases the interaction between Rif2 and Rad50. In fact, when we created yeast strains expressing epitope-tagged versions of Rad50, Rif2, and Rif2^{S6E} from their native genomic loci and Rad50-hemagglutinin (HA) was immunoprecipitated with an anti-HA antibody, an increase of Rif2^{S6E}-Myc was detected in HA-tagged Rad50 immunoprecipitates compared with wild-type Rif2-Myc (Figure 12C).

Taken together, these results, supported by previous mutational analyses examining binding capability, provide experimental support for the accuracy of the predicted Rif2-Rad50 interaction region.

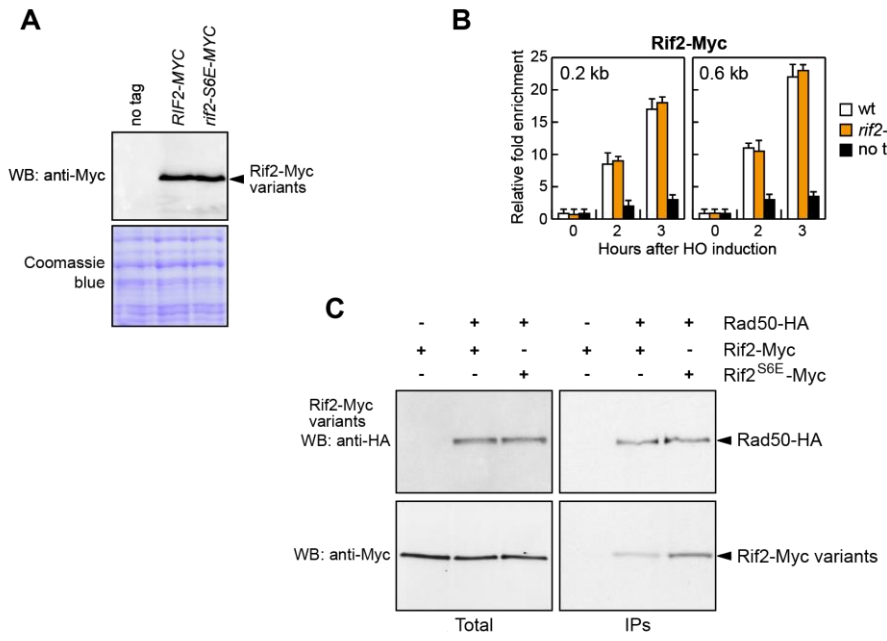

Figure 12. The *rif2-S6E* allele increases Rif2 interaction with Rad50. (A) Western blot with anti-Myc antibodies of extracts used for the ChIP analysis shown in (B). The same amount of protein extracts was separated on SDS-PAGE and stained with Coomassie blue as loading control. (B) Rif2-Myc ChIP at the indicated distances from the HO-cut site. Data are expressed as fold enrichment at the HO-cut site over that at a non-cleavable locus (ARO1), after normalization to the corresponding input for each time point. Fold enrichment was normalized to cut efficiency. Plotted values are the mean value of three independent experiments with error bars denoting standard deviation (s.d.). (C) Protein extracts from exponentially growing cells were analyzed by western blotting with anti-HA and anti-Myc antibodies either directly (Total) or after immunoprecipitation (IPs) of Rad50-HA with an anti-HA antibody.

Rif2^{S6E} reduces hairpin cleavage but not resection of an HO-induced DSB

Rif2 is less effective in inhibiting MRX-mediated resection and Tel1 activation at DSBs than at telomeres, where Rif2, in conjunction with Rif1 and Rap1 proteins, forms a higher-order architecture that provides a protective cap and limits telomerase access (Shi et al., 2013). To understand why Rif2 inhibition of MRX and Tel1 is kept low at DSBs compared to telomeric ends, we explored the consequences of expressing the Rif2^{S6E} variant that strengthens Rif2 interaction with Rad50 and potentially its inhibitory function. We and others have shown that Rif2 inhibits the Sae2-stimulated endonuclease activity of the Mre11-Rad50 subcomplex (Marsella et al., 2021; Roisné-Hamelin et al., 2021). The Mre11 endonuclease activity is essential for the processing of DSBs with non-canonical structures such as DNA hairpins or protein adducts (K. S. Lobachev et al., 2002a; Neale et al., 2005; Reginato et al., 2017; W. Wang et al., 2017), whereas it is dispensable at clean DSBs such as those generated upon induction of the HO endonuclease (Llorente & Symington, 2004). To assess whether the *rif2-S6E* mutation increases Rif2 inhibition of Mre11 endonuclease activity, we analyzed the effect of this mutation on MRX-mediated hairpin resolution. To this purpose, we used a genetic assay in which inverted Alu elements inserted in the *LYS2* gene on chromosome II induce a hairpin-capped DSB that is cleaved by MRX-Sae2 and subsequently repaired by HR using a truncated *lys2* gene (*lys2-Δ5'*) located on chromosome III (Figure 13A) (K. S. Lobachev et al., 2002a). As expected, the inverted Alu elements stimulate ectopic recombination and this stimulation depends on the Mre11 nuclease, as nuclease defective

mre11-H125N (*mre11-nd*) cells decreased the rates of Lys$^+$ recombinants compared to wild-type cells (Figure 13B). The generation of Lys$^+$ recombinants remained unaltered in *rif2*Δ cells, possibly because the low amount of Rif2 bound at DSBs compared to Sae2 is not enough to limit Sae2-mediated stimulation of Mre11 endonuclease. By contrast, it was decreased in *rif2-S6E* cells relative to wild-type cells (Figure 13B), suggesting that this allele increases Rif2 inhibition of MRX-mediated hairpin cleavage.

Consistent with previous findings that the nuclease activity of Mre11 is dispensable for the processing of clean DSBs such as that generated upon induction of the HO endonuclease (Llorente & Symington, 2004), we anticipated that *rif2-S6E* cells were capable to resect an HO-induced DSB at the *MAT* locus (Figure 13C and D). To measure DSB resection, we used JKM139 derivative strains, where a single DSB at the *MAT* locus can be generated by expressing the HO endonuclease upon galactose addition (S. E. Lee et al., 1998a). Resection of DNA regions flanking the HO-induced DSB renders the DNA sequence resistant to cleavage by restriction enzymes, resulting in the appearance of slower migrating bands (r1-r6) that can be detected after hybridization with a probe that anneals to the unresected strand on one side of the DSB. The appearance of the ssDNA intermediates at the HO-induced DSB occurred with similar kinetics in both wild-type and *rif2-S6E* cells (Figure 13C and D), indicating that the *rif2-S6E* mutation does not affect resection of the HO-induced DSB.

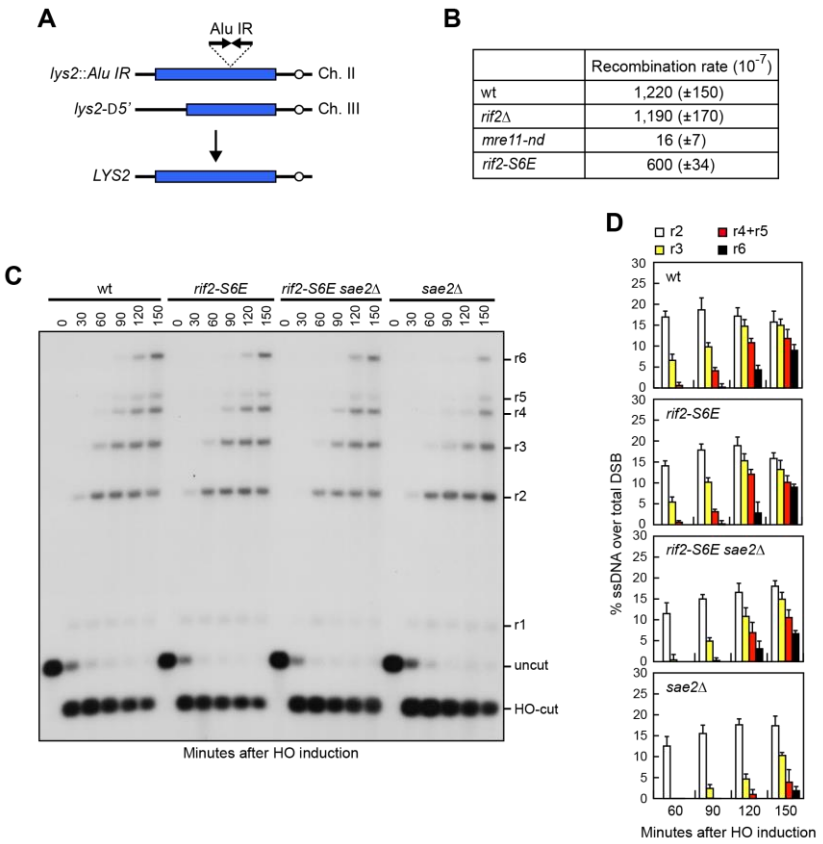

Figure 13. Hairpin resolution and resection of an HO-induced DSB in *rif2-S6E* cells. (A) Schematic representation of the lys2-Alu IR and lys2-Δ5' ectopic recombination system. (B) Recombination frequency of strains with the lys2-Alu IR and lys2-Δ5' ectopic recombination system. The rate of Lys+ recombinants was derived from the median recombination frequency. The reported values are the mean values of 3 independent experiments with s.d. indicated in brackets. (C) DSB resection. JKM139 derivative strains were transferred to YEPRG at time zero. SspI-digested genomic DNA was hybridized with a single-stranded MAT probe that anneals with the unresected strand. 5'-3' resection produces SspI fragments (r1 through r6) detected by the probe. (D) Densitometric analysis of the resection products. The mean values of three independent experiments as in (C) are represented with error bars denoting s.d.

It has been shown that the lack of Sae2 impairs DSB resection because it enhances MRX/Tel1 signaling activity that leads to an increased Rad9 association with DSBs that, in turn, inhibits the resection activity of Exo1 and Dna2 nucleases(Bonetti et al., 2015b; Ferrari et al., 2015; Yu et al., 2018). *rif2-S6E* cells possess wild-type levels of Rad9 both in protein extracts (Figure 14A) and bound at the HO-induced DSB (Figure 14B). Consistent with the suppression of *sae2*Δ resection defect, *rif2-S6E sae2*Δ cells showed a decreased Rad9 association with sequences close to HO cut site compared to *sae2*Δ cells (Figure 14B), although a similar amount of Rad9 can be detected by western blot in all protein extracts (Figure 14A). As the increased Rad9 binding at DSBs in *sae2*Δ cells is due to the hyperactivation of Tel1 signaling activity (Bonetti et al., 2015b; Ferrari et al., 2015; Yu et al., 2018), the diminished Rad9 association with DSBs in *rif2-S6E sae2*Δ cells might be due to a defective Tel1 signalling activity

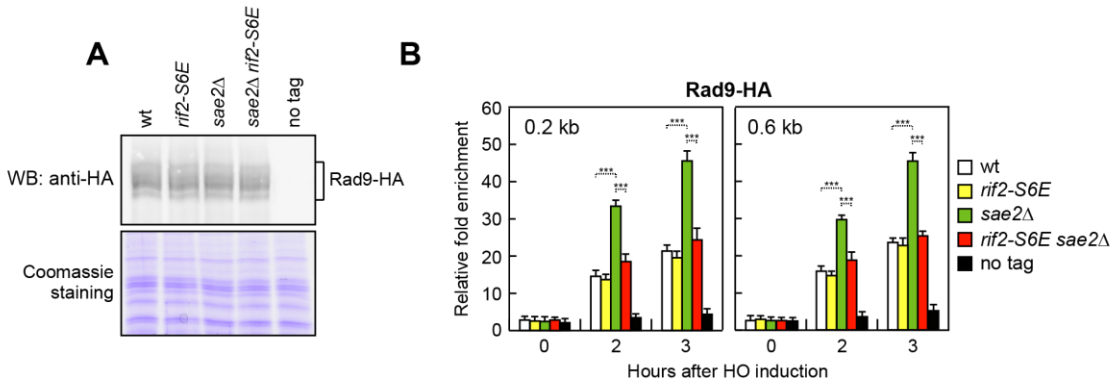

Figure 14. Quantification of amount of Rif2 bound to DSB. (A) Western blot with an anti-HA antibody of extracts used for the ChIP analysis shown in (B). The same amount of protein extracts was separated on SDS-PAGE and stained with Coomassie blue as loading control. (B) ChIP and qPCR. Exponentially growing YEPR cell cultures were transferred to YEPRG to induce HO expression, followed by ChIP analysis of the recruitment of Rad9-HA at the indicated distance from the HO-cut site. In all diagrams, ChIP signals were normalized for each time point to the corresponding input signal. Plotted values are the mean value of three independent experiments with error bars denoting s.d. ***$p<0.005$ (Student's t-test).

Rif2^{S6E} reduces Tel1 activation by decreasing Tel1 association with DSBs

Tel1-deficient cells do not exhibit marked sensitivity to DNA damaging agents and show no significant defects in checkpoint activation in response to a single DSB (Mantiero et al., 2007). Therefore, to assess the impact of the *rif2-S6E* mutation on Tel1 activation, we employed various approaches. Initially, we leveraged a previous discovery that adding galactose to cells expressing the *TEL1* gene under the galactose inducible *GAL1* promoter (*GAL-TEL1*) triggers a transient checkpoint activation that correlates with an increased MRX association with telomeres (Clerici et al., 2001; Viscardi et al., 2003; Viscardi et al., 2007). The cell-cycle arrest induced by this checkpoint activation heightens the sensitivity of *GAL-TEL1* cells to DNA damaging agents by reinforcing the checkpoint-mediated cell-cycle arrest induced by genotoxic exposure. Interestingly, Rif2 was identified as a multicopy suppressor of the DNA damage sensitivity of galactose-induced *GAL-TEL1* cells likely because it counteracts Tel1 activation (Viscardi et al., 2003). Therefore, we compared the effects of *rif2*Δ and *rif2-S6E* on the DNA damage sensitivity of *GAL-TEL1* cells in the presence of galactose, which induces Tel1 overexpression. We hypothesized that if the *rif2-S6E* mutation suppresses Tel1 activation more efficiently than wild-type Rif2, it should mimic the effect of *RIF2* overexpression and therefore alleviate the DNA damage sensitivity of galactose-induced *GAL-TEL1* cells. Conversely, *RIF2* deletion is expected to increase this sensitivity by enhancing Tel1 activation. As expected, *GAL-TEL1* cells spotted on galactose containing plates showed a slight growth defect compared to wild-type cells that increases in the presence of CPT or

phleomycin (Figure 15A). The *rif2-S6E* allele suppressed the DNA damage sensitivity of *GAL-TEL1* cells, whereas *rif2*Δ slightly increased it (Figure 15A), suggesting that Rif2^{S6E} mutant variant limits Tel1 activation more efficiently than wild-type Rif2.

Next, we took advantage of the finding that the lack of Sae2 suppresses the sensitivity to DNA-damaging agents of *mec1*Δ cells (kept viable by *SML1* deletion) by increasing Tel1 activation (Usui et al., 2001). This observation prompts us to evaluate the effect of *rif2-S6E* in *mec1*Δ cells. Consistent with a reduced Tel1 activity, when the *rif2-S6E* allele was combined with *mec1*Δ, the double mutant exhibited higher sensitivity to DNA damaging agents than *mec1*Δ alone (Figure 15B). By contrast, *rif2-S6E* did not increase the CPT sensitivity of *tel1*Δ cells (Figure 15C). Furthermore, it failed to suppress the severe growth defect of *mec1*Δ *tel1*Δ (Figure 15D), suggesting that the increased DNA damage sensitivity of *rif2-S6E mec1*Δ is due to a defect in Tel1 activation.

Finally, to confirm an impaired Tel1 signalling activity in *rif2-S6E* cells, we analyzed Mre11 that is known to be specifically phosphorylated by Tel1 and whose phosphorylation results in a decrease of its electrophoretic mobility (Clerici et al., 2006; D'Amours & Jackson, 2001). Wild-type cells phosphorylated Mre11 in response to phleomycin treatment, whereas Mre11 phosphorylation was reduced in *rif2-S6E* cells (Figure 15E).

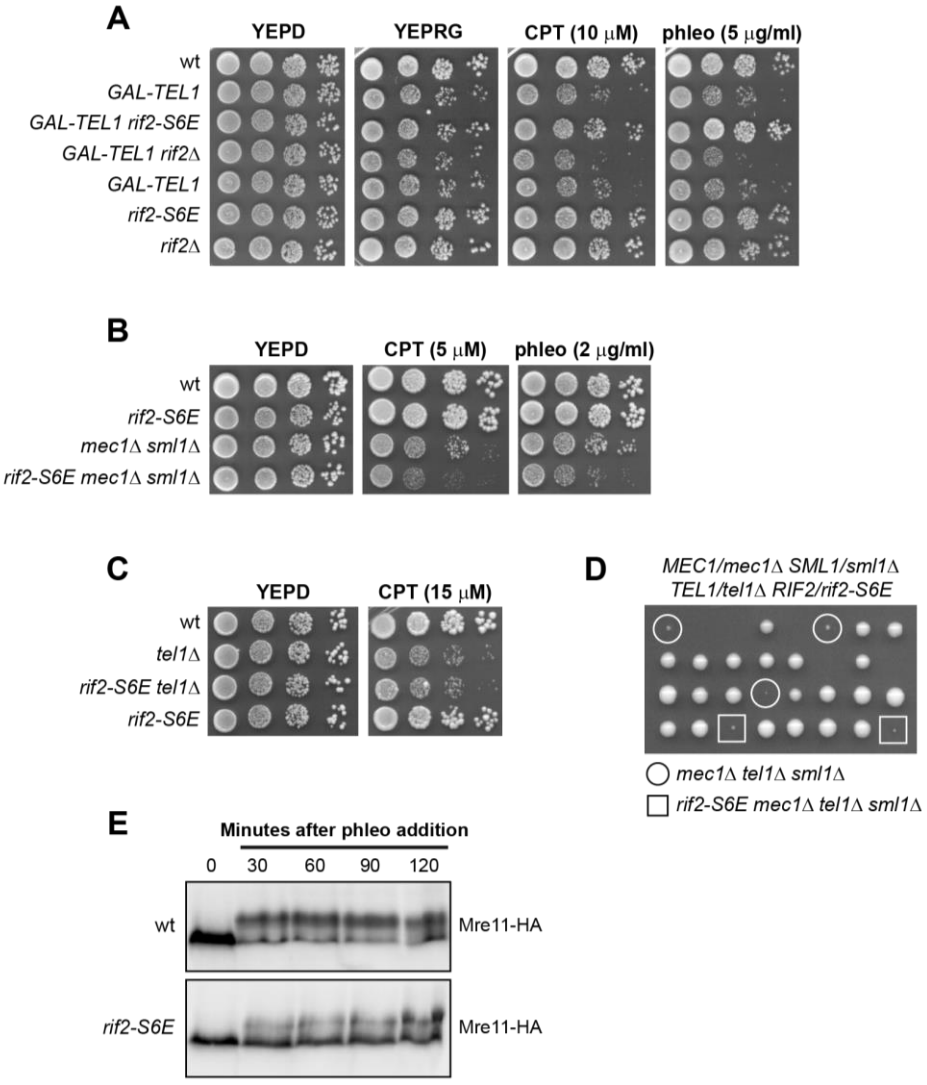

Figure 15. The *rif2-S6E* allele affects Tel1 activation. (A) Exponentially growing cultures were serially diluted (1:10) and each dilution was spotted out onto YEPD plates or onto YEPRG plates with or without CPT or phleomycin. (B, C) Exponentially growing cultures were serially diluted (1:10) and each dilution was spotted out onto YEPD plates with or without CPT or phleomycin. (D) Meiotic tetrads were dissected on YEPD plates, followed by spore genotyping. (E) Phleomycin (10 μg/mL) was added to exponentially growing cells followed by western blot analysis with anti-HA antibodies.

The accumulation of MRX and Tel1 is enhanced in *rif2*Δ and *sae2*Δ cells, with *sae2*Δ showing the strongest effect (Cassani et al., 2016; Marsella et al., 2021). To investigate whether the defective Tel1 signalling in *rif2-S6E* cells was due to a decreased MRX and/or Tel1 persistence at DSBs, we measured Mre11 and Tel1 association with sequences close to the HO endonuclease cut site at the *MAT* locus. The presence of the *rif2-S6E* mutation decreased retention of Tel1 at DSBs in both wild-type and *sae2*Δ cells (Figure 16A), although similar amounts of Tel1 were detected in all protein extracts (Figure 16B). By contrast, neither Mre11 binding at the HO-induced DSB nor Mre11 levels was significantly altered in *rif2-S6E* and *rif2-S6E sae2*Δ cells compared to wild-type and *sae2*Δ cells, respectively (Figure 16C and D), indicating that the dampening of Tel1 association with DSBs by Rif2^{S6E} is not due to the inhibition of MRX stable interaction with DNA ends.

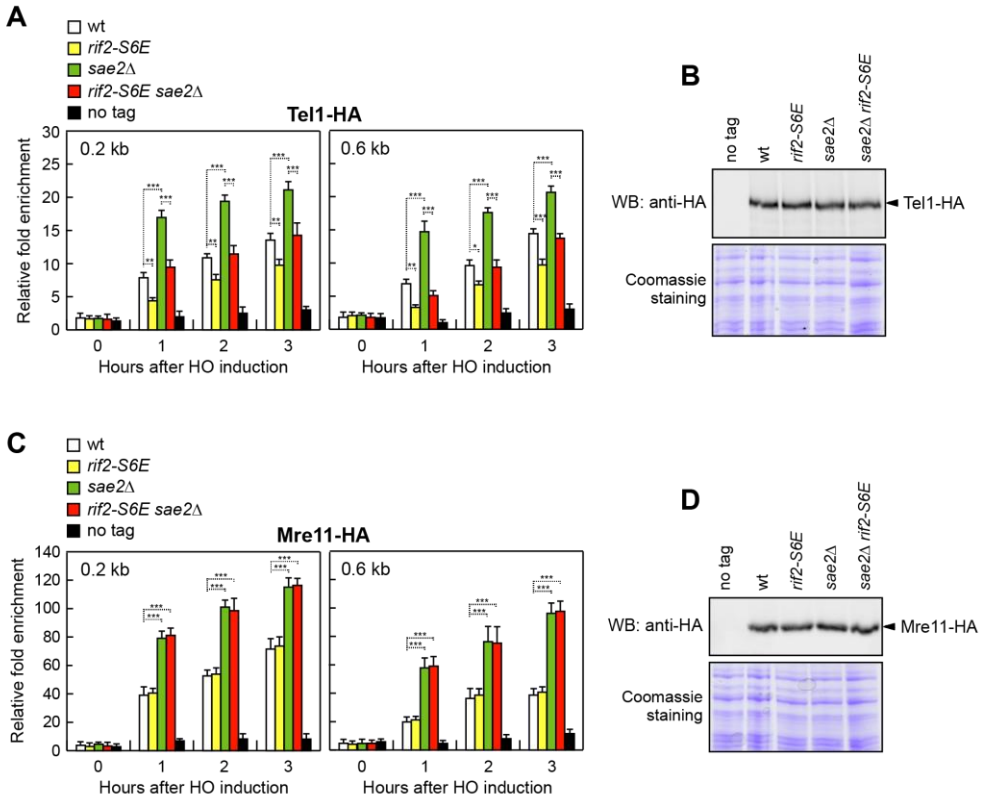

Figure 16. The *rif2-S6E* allele decreases Tel1 but not Mre11 association with the HO-induced DSB. (A) Tel1-HA ChIP at the indicated distances from the HO-cut site. Data are expressed as fold enrichment at the HO-cut site over that at a non-cleavable locus (*ARO1*), after normalization to the corresponding input for each time point. Fold enrichment was normalized to cut efficiency. Plotted values are the mean value of three independent experiments with error bars denoting s.d. ***p<0.005, **p<0.01, *p<0.05 (Student's t-test). (B) Western blot with an anti-HA antibody of extracts used for the ChIP analysis shown in (A). (C) Mre11-HA ChIP was performed as described in (A). Plotted values are the mean value of three independent experiments with error bars denoting s.d. ***p<0.005 (Student's t-test). (D) Western blot with an anti-HA antibody of extracts used for the ChIP analysis shown in (C).

Rif2^{S6E} impairs DSB end-tethering and DSB repair by SSA

Our previous finding that *RIF2* deletion increases DSB end-tethering and suppresses the end-tethering defect of *rad50-VM* cells (Cassani et al., 2016) prompted us to examine the effect of the *rif2-S6E* allele on DSB bridging. To detect the ability of cells to keep the DSB ends close to each other, we used a genetic background in which multiple repeats of the LacI repressor binding site are integrated 50 kb upstream and downstream of an HO cleavage site located on chromosome VII in cells constitutively expressing a LacI-GFP fusion protein (Kaye et al., 2004). The level of end-tethering was determined by measuring the generation of one or two LacI-GFP foci, upon expression of HO by galactose addition to cell cultures that were kept blocked in G2 by nocodazole (Figure 17A) or in G1 by α-factor (Figure 17B). Most wild-type cells showed a single LacI-GFP focus both before and after HO induction, indicating their ability to hold the broken DNA ends together (Figure 17A and B). By contrast, *rif2-S6E* cells showed an increase of two LacI-GFP spots compared to wild-type cells (Figure 17A and B), indicating an end-tethering defect.

The maintenance of the DSB ends in close proximity involves MRX, Sae2, and Tel1 (Clerici et al., 2005; Kaye et al., 2004; K. Lee et al., 2008; K. Lobachev et al., 2004; Nakai et al., 2011). The absence of Tel1 reduces the ability of cells to keep the DSB ends tethered to each other (Lee et al., 2008) and this defect was exacerbated when *TEL1* was deleted in cells carrying the *rad50-VM* allele (Cassani et al., 2016). Interestingly, opposite to *rif2*Δ that suppresses the end-

tethering defect of *sae2*Δ and *rad50-VM* cells (Cassani et al., 2016), the *rif2-S6E* allele exacerbated the end-tethering defect of both *rad50-VM* and *sae2*Δ cells, but not of *tel1*Δ cells (Figure 17A and B), suggesting that Rif2 and Tel1 regulate end-tethering by acting in the same pathway. The role of Tel1 in supporting DSB tethering does not require its kinase activity, as cells expressing a Tel1 kinase-dead allele (*tel1-kd*) did not show an end-tethering defect (Figure 17A and B).

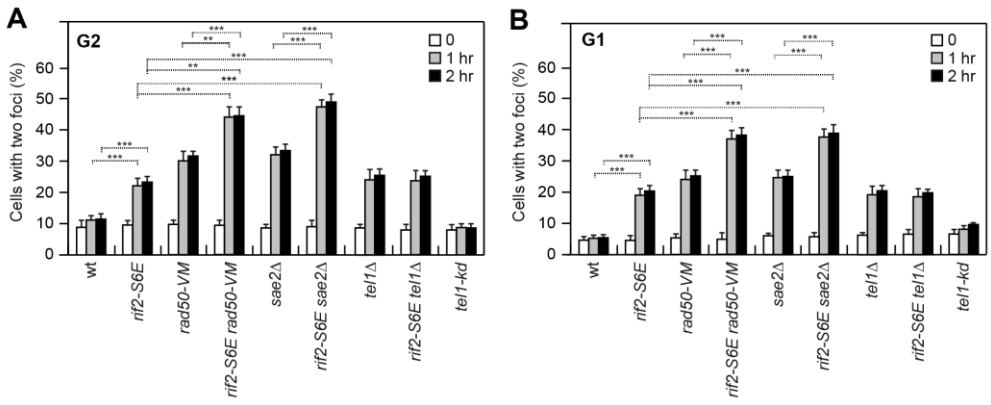

Figure 17. DSB end-tethering in *rif2-S6E* cells. DSB end-tethering. Exponentially growing YEPR cell cultures were arrested in G2 with nocodazole (A) or in G1 with α-factor (B) at time zero and transferred to YEPRG in the presence of nocodazole or α-factor, respectively. 200 cells for each strain were analyzed to determine the percentage of cells showing two LacI-GFP foci. Plotted values are the mean value of three independent experiments with error bars denoting s.d. ***p<0.005, **p<0.01 (Student's t-test).

A DSB flanked by direct DNA repeats can be repaired by single-strand annealing (SSA), a mechanism that requires that resection reaches the complementary DNA sequences followed by Rad52-dependent annealing of the resulting complementary ssDNA (Fishman-Lobell et al., 1992). We have previously shown that the lack of Sae2 impairs DSB repair by SSA and the poor SSA efficiency is in part due to the end-tethering defect (Clerici et al., 2005), prompting us to test the ability of *rif2-S6E* cells to repair a DSB by SSA. To measure the efficiency of SSA, we used YMV45 derivative strains carrying tandem repeats of the *LEU2* gene, located 4.6 kb apart on chromosome III, with the HO cutting site adjacent to one of the repeats (Figure 18A) (Vaze et al., 2002). HO was induced by galactose addition to exponentially growing cells and galactose was maintained in the medium in order to re-cleave the HO sites that can be rejoined by NHEJ. When DSB repair was monitored by Southern blot analysis with a *LEU2* probe, accumulation of the SSA repair product was reduced in *rif2-S6E cells* compared to wild-type cells (Figure 18B and C), indicating a role for Rif2 in the SSA repair mechanism. The finding that *rif2-S6E* cells did not affect resection of the HO-induced DSB (Figure 13C and D) indicates that the poor SSA efficiency of *rif2-S6E* cells cannot be explained by a resection defect, but it can be due to the low degree of end-tethering. Consistent with this hypothesis, the *rif2-S6E* allele, which increases the end-tethering defect of *sae2*Δ cells (Figure 17A and B), exacerbates the SSA defect of these cells as well (Figure 18B and C). Again, this SSA defect cannot be due to a reduced DSB resection, as *rif2-S6E sae2*Δ cells resect the HO-induced DSB faster than *sae2*Δ cells (Figure 13C and D).

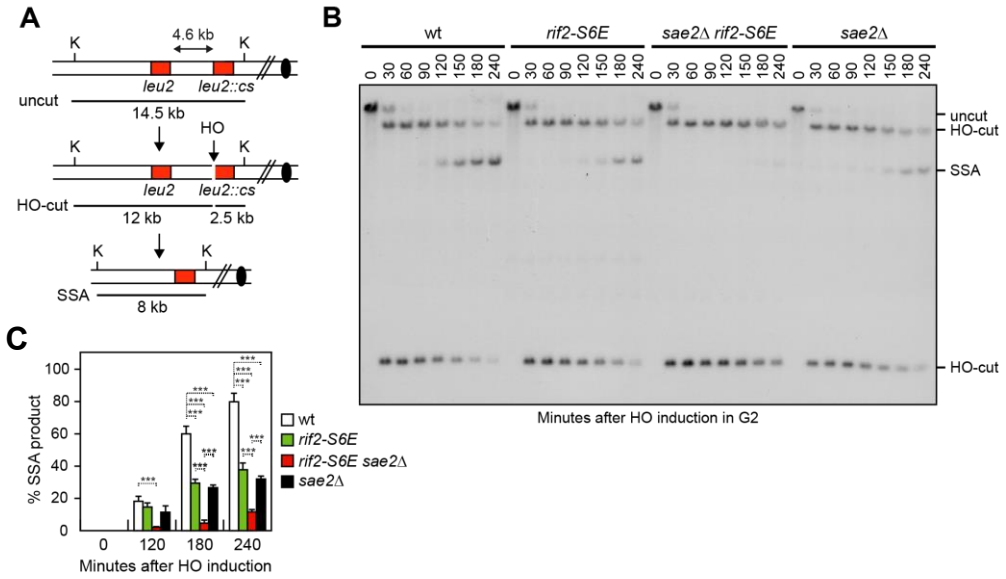

Figure 18. DSB repair by SSA in *rif2-S6E* cells. (A) System to detect DSB repair by SSA. HO induction by galactose addition generates a DSB between two homologous leu2 sequences that are 4.6 kb apart. K, KpnI. (B) Exponentially growing YEPR cell cultures were arrested in G2 with nocodazole and transferred to YEPRG. Southern blot analysis of KpnI-digested genomic DNA with a LEU2 probe revealed a 2.5 kb and 12 kb DNA fragments (HO-cut) resulting from HO-induced DSB formation. DSB repair by SSA generates an 8 kb fragment (SSA). (C) Densitometric analysis of the SSA band signals. Plotted values are the mean value of three independent experiments with error bars denoting s.d. ***$p<0.005$ (Student's t-test).

The end-tethering defect of *rif2-S6E* cells is due to a reduced Tel1 association with DSBs

Tel1 supports end-tethering independently of its kinase activity (Figure 17A and B) and Rif2 counteracts this function by decreasing Tel1 association with DSBs (Figure 16A). If the end-tethering defect of *rif2-S6E* cells is due to a reduced Tel1 association with DSBs, enforcing Tel1 recruitment at DSBs should restore the ability of *rif2-S6E* cells to bridge the DSB ends. To address this question, we used the hypermorphic *tel1-hy909* allele that we identified by searching for *tel1* mutations that compensate for the lack of Mec1 function (Baldo et al., 2008). The *tel1-hy909* allele, which carries the missense mutations A2287V, I2336T, and K2751R, increases Tel1 kinase activity and Tel1 association with DNA DSBs, while leaving Tel1 level within the cell unchanged (Baldo et al., 2008; Martina et al., 2012). Furthermore, it causes telomere overelongation in an MRX-independent manner (Keener et al., 2019). When we monitored DSB end-tethering by measuring the generation of one or two LacI-GFP foci upon expression of HO by galactose addition, *tel1-hy909 rif2-S6E* cells showed a decreased percentage of two LacI-GFP spots compared to *rif2-S6E* cells (Figure 19A). Furthermore, the presence of the *tel1-hy909* mutation increased the amount of Tel1 bound at the HO-induced DSB in both wild-type and *rif2-S6E* cells (Figure 19B). These findings indicate that the *tel1-hy909* mutation suppresses the end-tethering defect of *rif2-S6E* cells by increasing Tel1 association with DNA DSBs. This finding, together with the observation that the *rif2-S6E* allele decreased Tel1 association but not MRX binding at DSBs, supports a structural and direct role of Tel1 in DSB end-bridging.

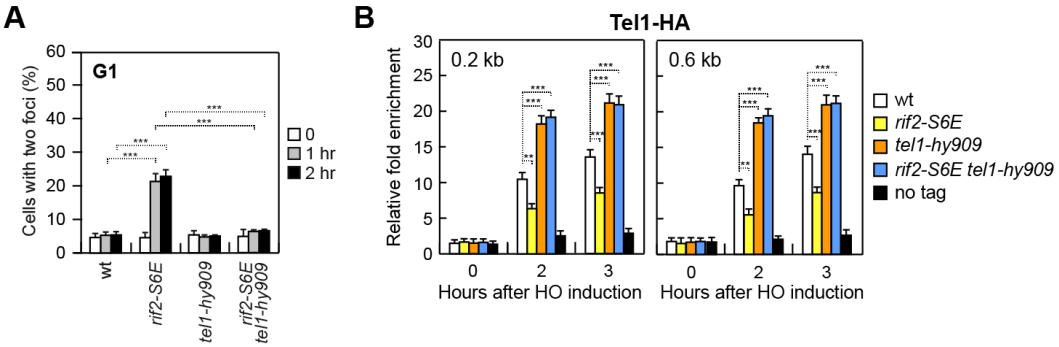

Figure 19. The allele *tel1-hy909* suppress the end-tethering defect and Tel1 decreased at DSBs of *rif2-S6E* cells. (A) Exponentially growing YEPR cell cultures were arrested in G1 with α-factor at time zero and transferred to YEPRG in the presence of α-factor. 200 cells for each strain were analyzed to determine the percentage of cells showing two LacI-GFP foci. Plotted values are the mean value of three independent experiments with error bars denoting s.d. ***p<0.005 (Student's t-test). (B) Tel1-HA ChIP and qPCR at the indicated distances from the HO-cut site as described in Figure 2F.

Rif2^{S6E} limits Tel1-MRX interaction

Because Rif2 is known to interact with Rad50 and to stimulate its ATPase activity (Cassani et al., 2016a; Hailemariam et al., 2019; Kaizer et al., 2015), we investigated the effect of the *rif2-S6E* mutation on Rad50 ATPase. The addition of purified Rif2^{S6E} to the Mre11-Rad50 subcomplex increased the ATP hydrolysis activity by Rad50 more efficiently than wild-type Rif2 (Figure 20A), indicating that Rif2^{S6E} possesses an increased ability to stimulate ATPase by Rad50 possibly due to its more robust interaction with Rad50 (Figure 12C).

As Tel1 recruitment at DSBs requires MRX (Lee & Paull, 2004; Nakada et al., 2003; Uziel et al., 2003; You et al., 2005), we tested whether Rif2^{S6E} binding to Rad50 can disrupt MRX-Tel1 interaction. When Tel1 was immune-precipitated with an anti-HA antibody, we observed a reduction in the amount of Rad50-Myc detected in HA-tagged Tel1 immunoprecipitates from *rif2-S6E* cells compared to wild-type cells (Figure 20B). Altogether, these findings indicate that the Rif2^{S6E} mutant variant impairs MRX-Tel1 interaction more efficiently than wild type Rif2, possibly because it possesses an enhanced ability to promote ATP hydrolysis by Rad50 that facilitates the transition to an ADP-bound MRX intermediate incapable to bind Tel1.

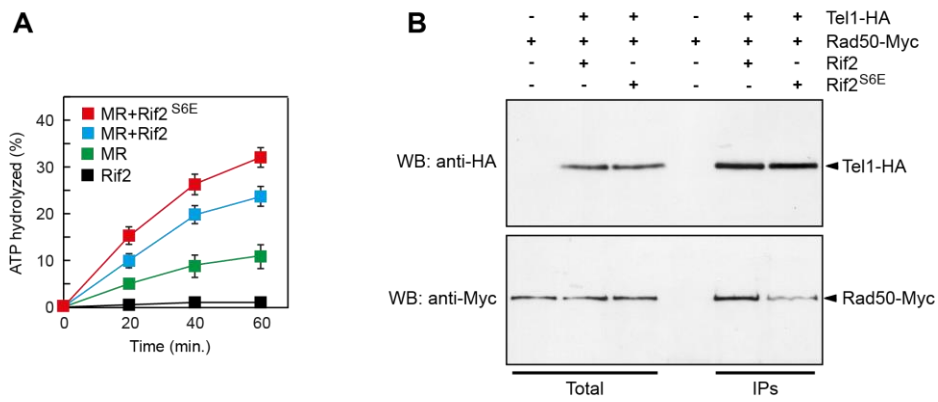

Figure 20. Rif2^{S6E} increases ATP hydrolysis by Rad50 and reduces Tel1-MRX interaction. (A) ATPase assays of Mre11-Rad50 subcomplex in the presence of Rif2 or Rif2^{S6E}. Plotted values are the mean value of three independent experiments with error bars denoting s.d. (B) Protein extracts from exponentially growing cells were analyzed by western blotting with anti-HA and anti-Myc antibodies either directly (total) or after immunoprecipitation (IPs) of Tel1-HA with an anti-HA antibody.

DISCUSSION

Chapter 1

Rif2 exerts inhibitory effects on both Mre11 endonuclease activity and the activation of the Tel1 kinase. These Rif2 inhibitory functions reside in the MIN motif, a 36 amino acid sequence located at the N-terminal that binds Rad50 ATPase head and stimulates its ATPase activity *in vitro* (Marcand et al., 2008; Marsella et al., 2021; Myler et al., 2023). The available evidence supports a model in which the MIN motif reduces Mre11 nuclease activity by counteracting Sae2 interaction with Rad50 and therefore the stabilization of the Mre11-Rad50 cutting state. However, the mechanisms through which the MIN motif limits Tel1 activation and the *in vivo* implications of this inhibition at DNA DSBs is poorly understood.

To comprehend the outcomes of Rif2 binding to Rad50, we used the multimer algorithm of AlphaFold to provide structural modelling of the interaction interface between the 36 residues of Rif2-MIN with Rad50. The predicted model is consistent with previous mutational data (Roisné-Hamelin et al., 2021) and our engineering of mutations that decrease or increase Rif2-Rad50 interaction strongly supports the accuracy of the predicted interaction interface. Furthermore, the finding that the effect of the *rif2-S6E* allele, which in the model is supposed to strengthen the interaction of Rif2 with Rad50 R125, can be abrogated by changing R125 to K, not only contributes to validating the model but also indicates that the Rif2 inhibitory function depends on a direct interaction between Rad50 and Rif2.

The increased Rif2-Rad50 interaction in *rif2-S6E* cells allowed us to study the *in vivo* consequences of Rif2 binding to Rad50 at DNA DSBs. We found that *rif2-S6E* cells reduce MRX-mediated hairpin cleavage, thus indicating that Rif2 can limit Mre11 endonuclease activity at DSBs not only *in vitro* but also within

the cellular environment. The finding that a heightened Rif2 activity at DSBs can limit DNA cleavage by MRX can explain the need for having higher levels of Sae2 than Rif2 at these sites to guarantee that there is adequate nuclease active Mre11-Rad50 subcomplex to initiate DSB resection.

We also found that the Rif2^{S6E} mutant variant inhibits Tel1 activation more efficiently than wild type Rif2 by decreasing Tel1 association with DSBs. It should be noted that the reduction of Tel1 activity in *rif2-S6E* cells is not enough to shorten telomeres. As Rif2 and its interacting proteins Rif1 and Rap1 have been shown to form a molecular Velcro that covers the telomeric DNA (Shi et al., 2013), it is possible that the rif2-S6E mutation is not capable of further increasing the already severe Rif2-mediated inhibition of Tel1 activity. Conversely, the *rif2-S6E* allele reduces Tel1 association with DSBs to such an extent that Rad9 binding at DSBs is diminished in *sae2*Δ cells, possibly allowing the *rif2-S6E* allele to suppress the *sae2*Δ resection defect.

The low Tel1 association at DSBs in rif2-S6E cells reduces the efficiency of DSB end-tethering and the contribution of Tel1 in the maintenance of the DSB ends in close proximity does not require its kinase activity. Given that MRX supports DNA tethering (Kaye et al., 2004; Lee et al., 2008; Lobachev et al., 2004; Nakai et al., 2011) and Tel1 is known to stabilize MRX persistence with DSBs (Cassani et al., 2016; Oh et al., 2018), the tethering defect resulting from diminished Tel1 association with DSBs in *rif2-S6E* cells might be attributed to lower Mre11 retention at DSBs. However, the finding that the *rif2-S6E* mutation reduces Tel1 association with DSBs without diminishing MRX association at these sites indicates that the decreased end-tethering in *rif2-S6E* cells is not caused by reduced MRX persistence at DSBs. This

observation, together with the finding that increasing Tel1 enrichment at DSBs by expressing the Tel1^{hy909} mutant variant is enough to suppress the end-tethering defect of *rif2-S6E* cells, supports a direct and structural role of Tel1 in bridging DSB ends.

The finding that the Rif2^{S6E} mutant variant decreases Tel1 binding at DSBs, whereas MRX association with DSBs remains unaffected, also indicates that Rif2 can negatively regulate Tel1 recruitment at DSBs independently of the control of MRX persistence at the DNA ends. Consistent with such a role, Rif2^{S6E} reduces the physical association between Tel1 and MRX, indicating that Rif2 limits Tel1 activation by antagonizing MRX-Tel1 interaction. Biochemical studies have shown that Rif2 stimulates the ATPase activity by Rad50 (Cassani et al., 2016; Myler et al., 2023). As Rif2^{S6E} stimulates Rad50 ATPase more efficiently than wild-type Rif2, these data suggest that Rif2 binding to Rad50 and stimulation of its hydrolyzing activity induces a conformational state of Mre11-Rad50 that is not competent for Tel1 binding and therefore for stimulation of its kinase activity. These data support a model where the ATP-bound form of MRX (resting state) is effective at interacting with Tel1 and tethering the DSB ends (Figure D1). In this model, the association of Rif2 with Rad50 stimulates the ATP hydrolysis by Rad50, facilitating the transition to an ADP-bound MRX intermediate state, which is incapable to bind Tel1 and to perform its endonuclease function. The high amount of Sae2 bound at DSBs compared to Rif2 displaces Rif2 from its association with Rad50. Sae2 binding to Rad50 stabilizes MRX in a nucleolytically active ADP-bound conformation (cutting state), capable of initiating DSB resection yet still unable to bind Tel1. Therefore, the ATPase

activity of Rad50 on one hand allows MRX-mediated nucleolytic degradation of DSBs, and on the other hand, releases Tel1 from Rad50 binding, thus explaining a previous observation that the generation of ssDNA at the DSB ends leads to a transition from Tel1- to Mec1-mediated checkpoint signalling (Mantiero et al., 2007)). Conversely, at normal-length telomeres, the presence of a Rif2-mediated higher-order structure locks MRX in an ADP-bound state that neither binds Tel1 nor exhibits MRX nuclease activity, preventing unwanted telomere elongation and checkpoint activation. Considering that mammalian TRF2 suppresses ATM signalling (de Lange, 2018), it would be intriguing to explore whether this suppression is mediated through the TRF2 iDDR motif.

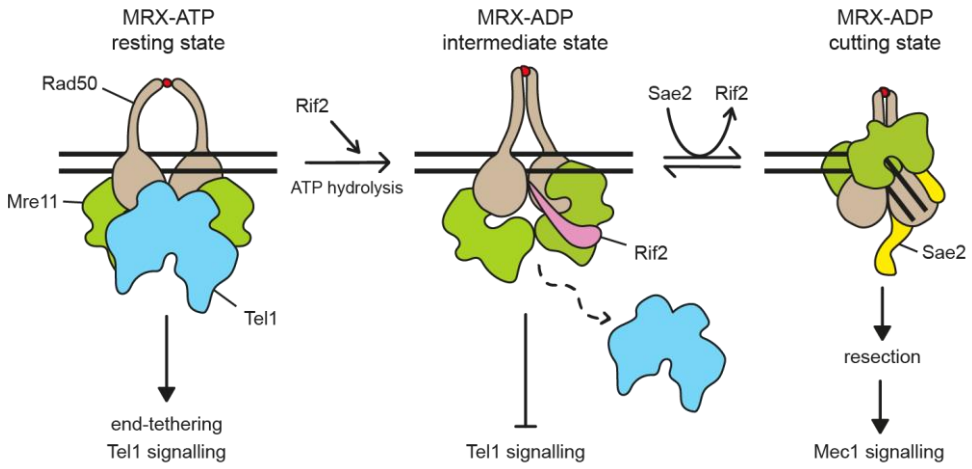

Figure D1. Model for Rif2 regulation of Tel1 activity at DNA ends. Tel1 binds the MRX ATP-bound state (resting state) and supports DSB end-tethering. Rif2 binding to the MRX ATP-bound conformation and stimulation of ATP hydrolysis facilitates the transition to an ADP-bound MRX intermediate that is not competent to bind Tel1 and to cleave DNA. Sae2 antagonizes Rif2 binding to Rad50 and stabilizes an ADP-bound MRX conformation (cutting state) that is proficient to initiate DSB resection but is still not able to bind Tel1. The release of Tel1 from Rad50 binding and the generation of ssDNA leads to a transition from a Tel1- to a Mec1-mediated checkpoint signalling. The red dots indicate Zn^{2+} ions.

RESULTS

Chapter 2

Nucleic Acids Research
2023 February 28
51(4):1783-1802.
doi:10.1093/nar/gkad062

Nucleic Acids Research

The Ku complex promotes DNA end-bridging and this function is antagonized by Tel1/ATM kinase

Carlo Rinaldi[1], **Paolo Pizzul**[1], Erika Casari[1], Renata Tisi[1], Maria Pia Longhese[1*]

[*] Corresponding Author

[1] Dipartimento di Biotecnologie e Bioscienze, Università degli Studi di Milano-Bicocca, Milano, 20126, Italy

The Ku complex, which comprises the two Ku70 and Ku80 subunits, recognizes with avid affinity and no sequence specificity a large variety of DNA ends, including blunt ends, hairpin DNA, and ends with protruding single-stranded overhangs (Blier et al., 1993; Griffith et al., 1992; Mimori & Hardin, 1986). Ku orthologs are found in organisms ranging from bacteria to humans (Aravind & Koonin, 2001; Downs & Jackson, 2004b). In eukaryotes, the two Ku subunits share three structural domains, consisting of an N-terminal von Willebrand A (vWA)-like domain, a central -barrel domain, and an -helical C-terminal arm. Structural analyses have revealed that Ku70 and Ku80 form a heterodimer that adopts a quasi-symmetric structure with a ring that encircles the duplex DNA (Walker et al., 2001; Yaneva et al., 1997). Furthermore, Ku binds DNA ends asymmetrically, with the Ku70 vWA-like domain facing outwards in close proximity to the DNA end and the Ku80 vWA-like domain facing inwards (Ribes-Zamora et al., 2007; Rivera-Calzada et al., 2007; Walker et al., 2001).

In addition of protecting the DSB ends from degradation by preventing the access of Exo1 to the DSB ends, the Ku complex acts as a hub to directly or indirectly recruit downstream NHEJ components (Zahid et al., 2021). Canonical proteins involved in NHEJ in mammals include the DNA-dependent protein kinase catalytic subunit (DNA-PKcs) that interacts with Ku to form the DNA-PK holoenzyme, XRCC4 (Lif1 in yeast), XLF (Nej1 in yeast) and PAXX. The final NHEJ step relies on DNA ligase IV (Dnl4 in yeast), which forms a constitutive complex with XRCC4/Lif1 to ligate the DNA ends (Chaplin & Blundell, 2020).

A central aspect of NHEJ is the maintenance of the DNA ends in close proximity to direct repair, a function that in *Saccharomyces cerevisiae* involves the MRX complex and Sae2 (Clerici et al., 2005; Kaye et al., 2004; K. Lee et al., 2008; K. Lobachev et al., 2004; Nakai et al., 2011). Disparate conclusions have been drawn about the involvement of NHEJ proteins in this phenomenon. In fact, pull-down assays using either purified proteins or cell-free extracts have reported that Ku alone (Ramsden & Gellert, 1998), DNA-PKcs alone (DeFazio et al., 2002), or the DNA-PK holoenzyme (Cary et al., 1997; Hammel et al., 2010; Spagnolo et al., 2006; J. L. Wang et al., 2018; Weterings et al., 2003) could bridge the DNA ends. Furthermore, Ku and the XRCC4-DNA ligase IV complex have been found to be necessary and sufficient to mediate a flexible synapsis of two DNA ends, whereas either alone is not (Chang et al., 2016; Reid et al., 2015; Zhao et al., 2019). Single-molecule FRET studies in *Xenopus* egg extracts showed that the NHEJ factors can assemble into a long-range complex, in which the DNA ends are laterally aligned and are held together by Ku, DNA-PKcs, DNA Ligase IV, XRCC4 and XLF (Chaplin et al., 2021; Chen et al., 2021; Graham et al., 2016). Upon dissociation of DNA-PKs, this high-order structural assembly is converted into an end-to-end close contact configuration, in which the DNA ends are aligned for ligation (Chaplin et al., 2021; Chen et al., 2021; Graham et al., 2016). On the other hand, a single molecule study of bacterial NHEJ, a mechanism relying on a homodimeric Ku and Ligase D, revealed that the Ku dimer alone is sufficient to form DNA bridges that are stabilized upon addition of Ligase D (Öz et al., 2021). This situation is similar to the NHEJ mechanism found in yeast cells, which do not possess DNA-PKcs, leaving open the possibility that Ku may be a central component in the formation of a molecular DSB bridge.

Despite these observations, whether the Ku complex is important to support DSB end-tethering remains to be elucidated.

Here, we report the identification and characterization of the *S. cerevisiae ku70-C85Y* allele that, like *KU70* deletion, restores DNA damage resistance of *sae2*Δ cells. However, unlike *KU70* deletion that suppresses the resection defect of *sae2*Δ cells by relieving inhibition of Exo1 resection activity (Foster et al., 2011; Mimitou & Symington, 2010; Shim et al., 2010), the *ku70-C85Y* mutation suppresses the DSB end-tethering defect of *sae2*Δ cells, whereas the lack of Ku70 exacerbates it. The C85Y mutation, which increases Ku affinity for DNA, enhances Ku persistence closeness to the DSB end and decreases it at more distant sites. Suppression of *sae2*Δ end-tethering defect and increased Ku persistence very close to the DSB ends can also be observed when histone removal around a DSB is defective either by eliminating Tel1 kinase activity or nucleosome remodelers. Altogether, these findings lead to a model whereby Ku contributes to keeping the DNA ends tethered to each other, whereas Tel1 kinase antagonizes this Ku function by promoting histone removal around DSBs.

Identification of *ku70* alleles that suppress the DNA damage sensitivity of *sae2*Δ cells

The lack of Sae2, which leads to hypersensitivity to DNA damaging agents, impairs resection and tethering of DNA DSB ends (Clerici et al., 2005). Deletion of *KU70* suppressed the sensitivity to camptothecin (CPT) and methyl methanesulfonate (MMS) of *sae2*Δ cells by relieving inhibition of Exo1 nuclease (Foster et al., 2011; Mimitou & Symington, 2010; Shim et al., 2010), whereas it conferred no rescue of sensitivity to phleomycin (Figure 21A). We have previously identified *mre11* mutations that increase resistance of *sae2*Δ cells to phleomycin and suppress their end-tethering but not their resection defect (Cassani et al., 2018), suggesting that end-tethering can be particularly important to repair phleomycin-induced DNA lesions. To understand the contribution of DSB end-tethering in DNA damage resistance and the possible role of Ku in this phenomenon, we searched for *ku70* mutations that restored the resistance to phleomycin of *sae2*Δ cells. *KU70* gene was amplified by low-fidelity PCR, followed by transformation into *sae2*Δ cells with linear *KU70* PCR products in order to replace the corresponding *KU70* wild-type sequence with the mutagenized DNA fragments. Transformants were then screened for increased viability in the presence of phleomycin compared to *sae2*Δ cells. This analysis allowed us to identify the *ku70-G79S*, *ku70-C85Y*, *ku70-A90T*, *ku70-N104Y*, and *ku70-D173G* alleles. These mutations restored DNA damage resistance of *sae2*Δ cells not only to phleomycin but also to CPT and MMS, whereas, as expected, *ku70*Δ was effective only in the suppression of *sae2*Δ CPT and MMS sensitivities (Figure 21A).

The Ku70 and Ku80 subunits share a similar topology. Their structure is composed of three domains: an N-terminal / domain similar to a vWA domain, a -barrel with the function of enclosing the nucleic acid, and a helical C-terminal arm that leans towards the vWA-like domain of the other subunit (Walker et al., 2001) (Figure 21B). The identified Ku70 mutations are all localized in the conserved N-terminal vWA-like domain. None of the substitutions generates critical problems to the protein structure according to an analysis with Missense 3D suite (Ittisoponpisan et al., 2019) and, with the exception of A90 and N104, many of the residues are buried inside the structure. In detail, both C85Y and A90T mutations introduce a bulkier amino acid (with a reduction in the surrounding cavity volume of 31.752 and 9.288 $Å^3$, respectively) and target the same -hairpin structure, which is localized in the nearby region of the conserved 5 helix that was shown to be involved in Ku–Ku self-association in humans (Ribes-Zamora et al., 2013) (Figure 21B and C). The N104 resides in a loop exposed to solvent immediately adjacent to the same -hairpin and the N104Y substitution leads to exposition of an aromatic amino acid. The G79S and D173G mutations affect residues localized in the embedded -sheet within the vWA-like domain, with G79 being nearby the 84–93 amino acid -hairpin and substituting a buried G residue with a bulkier amino acid, while D173 forming a saline bridge with K213 that is lost in the D173G mutant (Figure 21B and C). None of the residues is in conserved vWA traits and none of the substitutions is likely to disrupt the domain structure, although all of them are non-conservative substitutions.

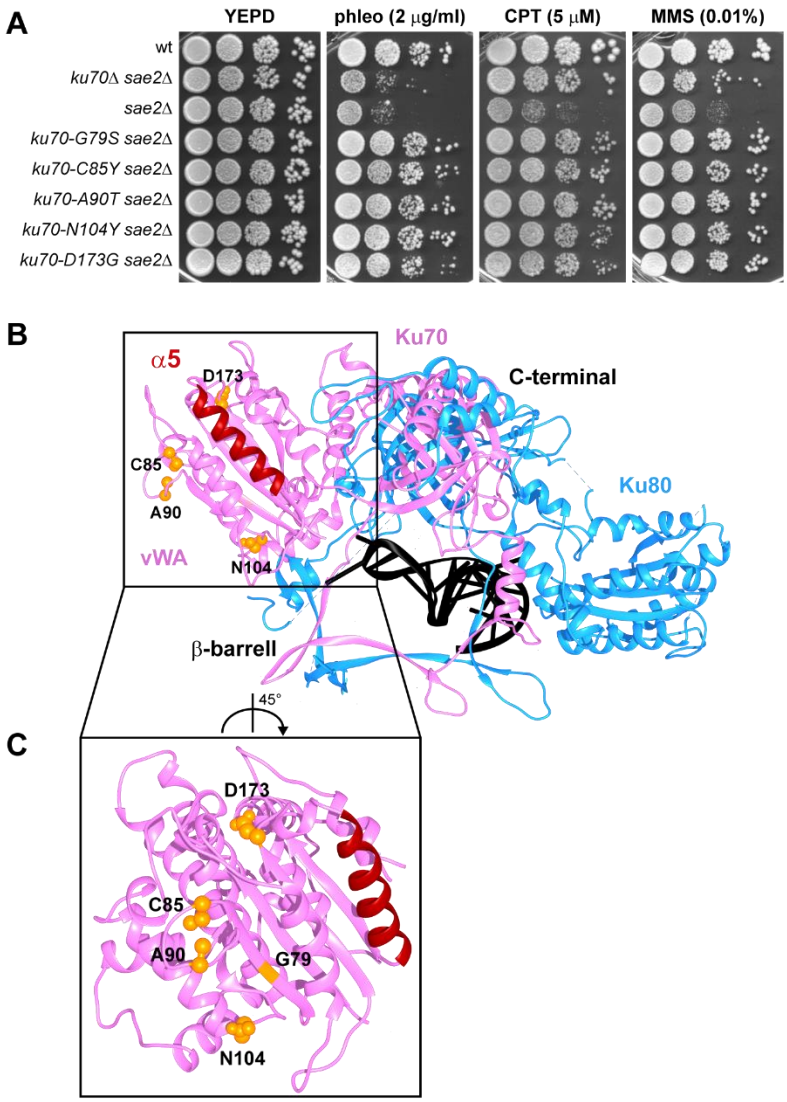

Figure 21. Identification of *ku70* alleles that suppress the sensitivity to phleomycin of *sae2*Δ cells. (A) Exponentially growing cultures were serially diluted (1:10) and each dilution was spotted out onto YEPD plates with or without phleomycin (phleo), camptothecin (CPT) or methyl methanesulfonate (MMS). (B) The structure of yeast Ku70–Ku80 heterodimer (PDB ID: 5Y58)

is shown as a cartoon. Ku70 is in pink (with α5 helix in red), Ku80 in blue, and the nucleic acid in black. The residues affected by the mutations are shown as orange balls. (C) The structure of Ku70 vWA-like domain is shown in detail with α5 helix in red. The residues affected by the mutations are shown as orange balls.

The lack of Ku affects the length of telomeres by destabilizing the interaction between the telomerase subunit Est1 and the telomeric DNA (Bertuch & Lundblad, 2003; Porter et al., 1996; J. M. Williams et al., 2014). We found that the *ku70-G79S*, *ku70-A90T*, and *ku70-N104Y* alleles shortened telomeres although not severely as *ku70*Δ, whereas both *ku70-C85Y* and *ku70-D173G* did not (Figure 22A). As the C85Y mutation does not affect telomere length, we focused the analysis on this mutation.

The ability of *ku70-C85Y* to suppress the sensitivity of *sae2*Δ to genotoxic agents was dominant, as *KU70*/*ku70-C85Y sae2*Δ/*sae2*Δ diploid cells were less sensitive to phleomycin and CPT compared to *KU70*/*KU70 sae2*Δ/*sae2*Δ diploid cells (Figure 22C), suggesting that *ku70-C85Y* allele encodes an hypermorphic variant. The mutation did not alter protein level, as similar amount of Ku70 was detected in protein extracts from wild-type and *ku70-C85Y* cells (Figure 22B).

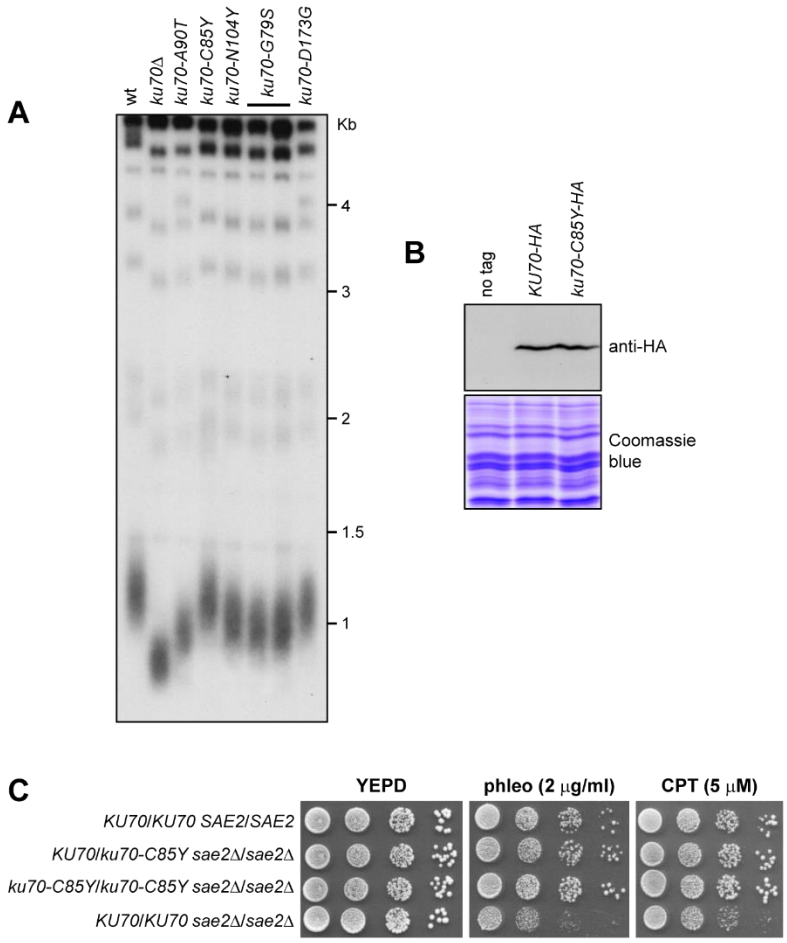

Figure 22. Telomere length analysis of *ku70* mutants and genetic dominance of *ku70-C85Y*. (A) Telomere length. XhoI-cut genomic DNA from exponentially growing cells was subjected to Southern blot analysis using a radiolabeled poly(GT) telomere-specific probe. (B) Exponentially growing cultures were serially diluted (1:10) and each dilution was spotted out onto YEPD plates with or without phleomycin or CPT. (C) Western blot with an anti-HA antibody of protein extracts. The same amount of protein extracts was separated on an SDS-PAGE and stained with Coomassie blue as loading control.

The *ku70-C85Y* allele does not suppress the resection defect and checkpoint hyperactivation of *sae2*Δ cells

The lack of Sae2 enhances MRX/Tel1 signaling activity that leads to an increased Rad9 association with DSBs and hyperactivation of the downstream checkpoint kinase Rad53 that causes a persistent cell-cycle arrest (Clerici et al., 2006; Usui et al., 2001). The increased Rad9 binding at DSBs acts as a barrier to Sgs1- Dna2-mediated DSB resection (Bonetti et al., 2015a; Ferrari et al., 2015; Gobbini et al., 2015; Yu et al., 2018), whereas Rad53 hyperactivation results in inhibitory phosphorylation of Exo1 (Morin et al., 2008), thus accounting for the *sae2*Δ resection defect. Both the resection defect and persistent checkpoint activation contribute to the DNA damage hypersensitivity of *sae2*Δ cells. In fact, deletion of *KU70* partially suppresses both the DNA damage sensitivity and the resection defect of *sae2*Δ cells because inhibition of Exo1 resection activity is relieved (Foster et al., 2011; Mimitou & Symington, 2010; Shim et al., 2010). Furthermore, dampening checkpoint activation either by reducing MRX/Tel1 binding to DSBs or by impairing Rad53 or Tel1 kinase activity restores DNA damage resistance and DSB resection of *sae2*Δ cells (Cassani et al., 2018; H. Chen et al., 2015; Gobbini et al., 2015; Puddu et al., 2015; Yu et al., 2018).

To assess the mechanism underlying suppression by the *ku70-C85Y* allele, first we investigated whether the *ku70- C85Y* allele can partially suppress the DNA damage sensitivity of *sae2*Δ cells by dampening checkpoint activation. To measure checkpoint activation, we used a haploid JKM139 strain background that expresses the site-specific *HO* endonuclease gene from a galactose-inducible promoter (S. E. Lee et al., 1998a). In this strain, induction of HO

upon galactose addition leads to the generation of a single DSB at the *MAT* locus that cannot be repaired by HR because the homologous donor loci *HML* and *HMR* are deleted. When G1-arrested cell cultures were spotted on galactose-containing plates to induce HO, most wild-type, *ku70-C85Y*, *sae2*Δ, and *ku70-C85Y sae2*Δ cells arrested as large budded cells within 4 hours after HO induction (Figure 23A), indicating that the checkpoint is activated. A checkpoint response triggered by a single unrepairable DSB can be turned off, allowing cells to resume cell-cycle progression through a process called adaptation (Pellicioli et al., 2001; Toczyski et al., 1997). The enhanced checkpoint activation in *sae2*Δ cells prevents cells from adapting to the checkpoint triggered by an unrepaired DSB (Clerici et al., 2006; Usui et al., 2001). We found that wild-type and *ku70-C85Y* cells were capable to adapt to the checkpoint and to form microcolonies with more than 2 cells within 24 h, whereas most *sae2*Δ and *ku70-C85Y sae2*Δ cells remained arrested at the 2-cell dumbbell stage (Figure 23A). Thus, we can conclude that *ku70-C85Y* does not suppress the DNA damage sensitivity of *sae2*Δ cells by decreasing checkpoint activation triggered by an unrepaired DSB.

Next, we asked whether the *ku70-C85Y* allele behaves like *ku70*Δ and therefore restores DNA damage resistance of *sae2*Δ cells by suppressing their resection defect. To monitor DSB resection we used JKM139 derivative strains, where a single irreparable DSB at the *MAT* locus can be induced by HO expression. Because ssDNA cannot be cleaved by restriction enzymes, ssDNA generation was assessed by testing resistance to cleavage as resection proceeds beyond the *Ssp*I restriction site located at different distances from the HO-cut site. *Ssp*I-resistant ssDNA can be detected as appearance of slower migrating bands (r1-r6) after denaturing gel electrophoresis of *Ssp*I-digested

genomic DNA and hybridization with a probe that anneals to the unresected strand at one side of the DSB (Figure 23B). As expected, *sae2*Δ cells showed a resection defect of the HO-induced DSB that was similar to that of *ku70-C85Y sae2*Δ cells (Figure 23C and D), indicating that *ku70-C85Y* does not suppress the DNA damage sensitivity of *sae2*Δ cells by restoring DSB resection.

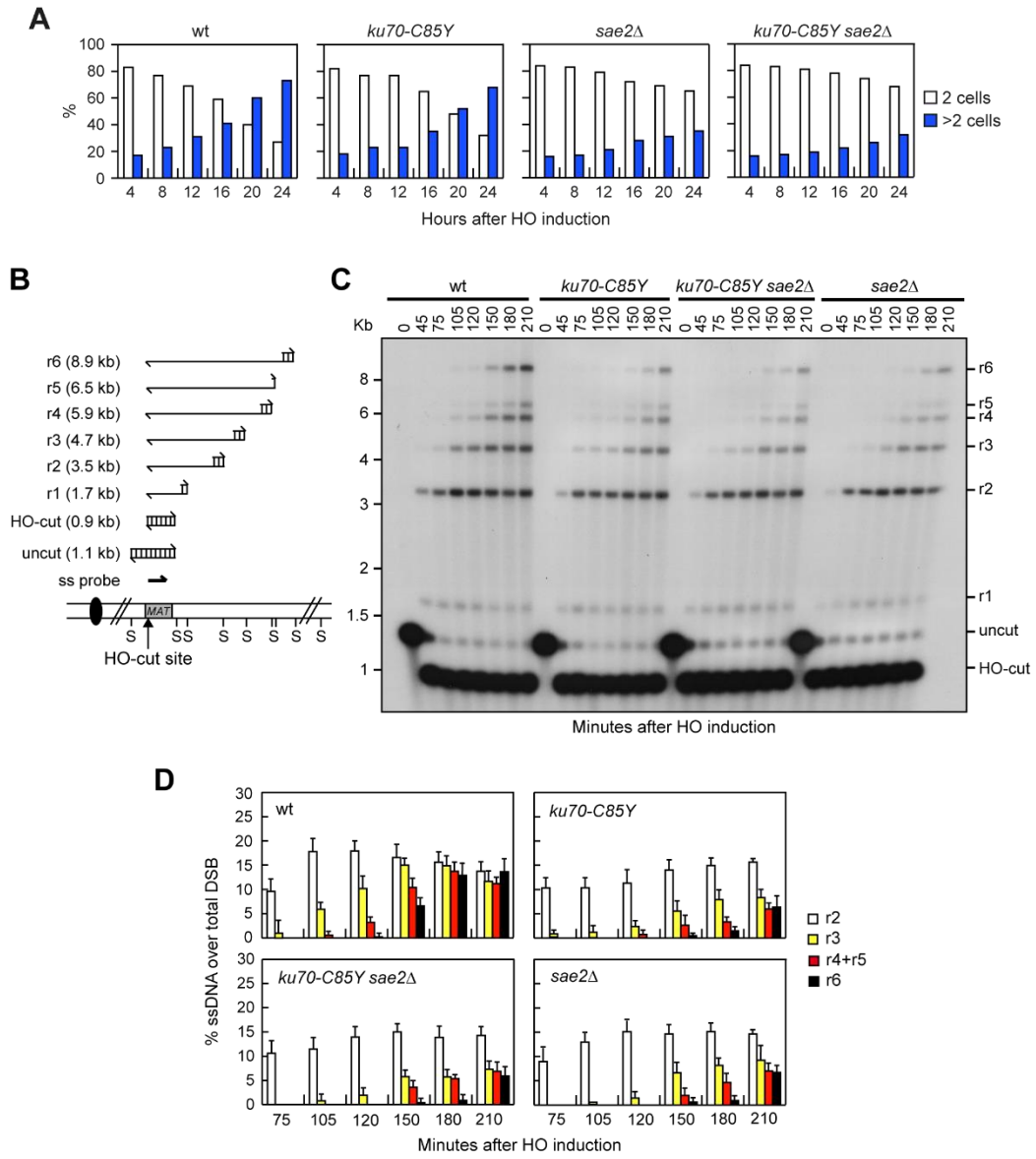

Figure 23. Suppression of *sae2Δ* DNA damage sensitivity by *ku70-C85Y* does not involve DSB resection. (A) YEPR G1-arrested cell cultures of JKM139 derivative strains, carrying the HO cut site at the *MAT* locus, were plated on galactose-containing plates (time zero). 200 cells for each strain were

analyzed to determine the frequency of cells forming microcolonies with two cells (2 cells) and of more than two cells (>2 cells). (B) System used to detect DSB resection. Resection of the DSB end progressively eliminates *Ssp*I sites (S), producing longer *Ssp*I fragments (r1 through r6) that can be separated on an alkaline agarose gel and visualized after hybridization with a single-strand RNA probe that anneals to the unresected strand at one side of the DSB. (C) DSB resection. JKM139 derivative strains were transferred to YEPRG at time zero. *Ssp*I-digested genomic DNA was hybridized with a single-stranded *MAT* probe that anneals with the unresected strand. 5'-3' resection produces *Ssp*I fragments (r1 through r6) detected by the probe. (C) Densitometric analysis of the resection products. The mean values of three independent experiments as in (D) are represented with error bars denoting standard deviation (s.d.).

Removal of Ku70 suppresses the DNA damage sensitivity and the resection defect of *sae2*Δ cells in an Exo1-dependent manner (Foster et al., 2011; Mimitou & Symington, 2010; Shim et al., 2010). Consistent with different suppression mechanisms by the *ku70*Δ and *ku70-C85Y* alleles, *ku70*Δ failed to suppress the sensitivity to CPT and MMS of *sae2*Δ *exo1*Δ cells, whereas *ku70-C85Y sae2*Δ *exo1*Δ cells were more resistant to CPT and MMS than *sae2*Δ *exo1*Δ cells (Figure 24A), indicating that Exo1 is not required for *sae2*Δ suppression by *ku70-C85Y*. Similar results have been obtained with the other *G79S*, *A90T*, *N104Y* and *D173G* mutations (Figure 24B). Furthermore, while deletion of *KU70* suppressed the sensitivity to CPT and MMS of cells expressing the nuclease defective *mre11-H125N* allele and restored viability of *sae2*Δ *sgs1*Δ cells, *ku70-C85Y* did not (Figure 24C and D), suggesting that the C85Y mutation bypasses a Sae2 function that does not involve Sgs1 and DSB resection.

Interestingly, while *KU70* deletion did not affect DSB resection (Clerici et al., 2008), *ku70-C85Y* cells showed a resection defect compared to wild-type cells (Figure 23C and D). As Ku limits DSB resection by inhibiting the recruitment of Exo1 to DSBs (Shim et al., 2010), we analyzed the effect of the ku70-C85Y mutation on Exo1 association with DSBs. To minimize the effect of DSB resection on protein binding to DSBs, HO was induced in G1-arrested cells that were kept arrested in G1 with -factor throughout the experiment. In fact, the low Cdk1 activity in G1 cells prevents resection of the HO-induced DSB (Aylon et al., 2004; Ira et al., 2004). Consistent with previous observations (Shim et al., 2010), chromatin immunoprecipitation (ChIP) and quantitative PCR (qPCR) showed that the lack of Ku70 increased Exo1 association with the HO-induced DSB (Figure 24E). By contrast, although protein extract from wild-type and *ku70-C85Y* cells contained a similar amount of Exo1 (Figure 24F), *ku70-C85Y* cells showed a decreased Exo1 association with the HO-induced DSB compared to wild-type cells (Figure 24E). This finding indicates that the *ku70-C85Y* allele encodes a hypermorphic Ku70 variant that limits Exo1 association with the DSB ends more efficiently than wild-type Ku70.

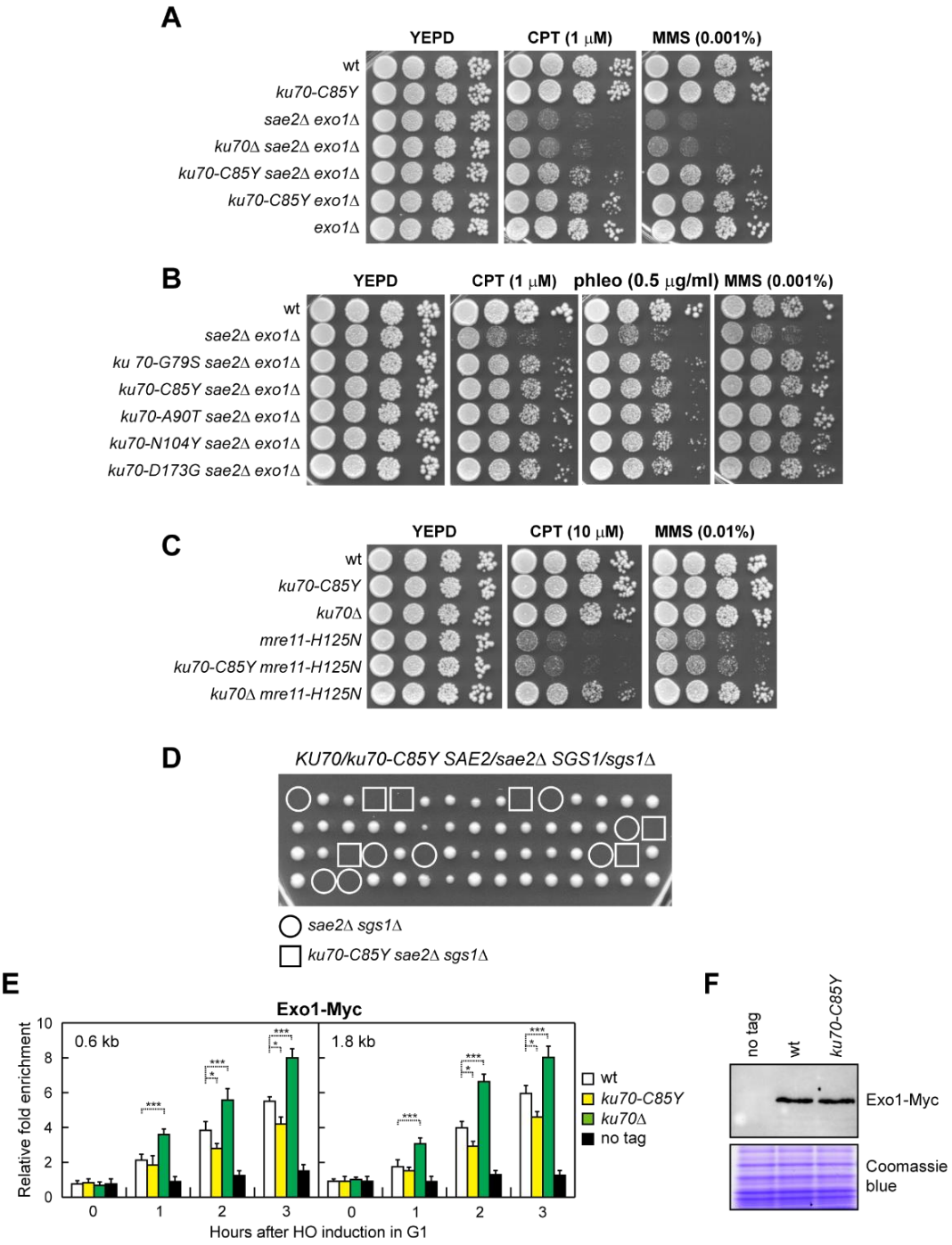
A
YEPD
CPT (1 μM)
MMS (0.001%)
wt
ku70-C85Y
sae2Δ exo1Δ
ku70Δ sae2Δ exo1Δ
ku70-C85Y sae2Δ exo1Δ
ku70-C85Y exo1Δ
exo1Δ
B
YEPD
CPT (1 μM)
phleo (0.5 μg/ml)
MMS (0.001%)
wt
sae2Δ exo1Δ
ku 70-G79S sae2Δ exo1Δ
ku70-C85Y sae2Δ exo1Δ
ku70-A90T sae2Δ exo1Δ
ku70-N104Y sae2Δ exo1Δ
ku70-D173G sae2Δ exo1Δ
C
YEPD
CPT (10 μM)
MMS (0.01%)
wt
ku70-C85Y
ku70Δ
mre11-H125N
ku70-C85Y mre11-H125N
ku70Δ mre11-H125N
D
KU70/ku70-C85Y SAE2/sae2Δ SGS1/sgs1Δ
sae2Δ sgs1Δ
ku70-C85Y sae2Δ sgs1Δ
E
Exo1-Myc
0.6 kb
1.8 kb
Relative fold enrichment
Hours after HO induction in G1
wt
ku70-C85Y
ku70Δ
no tag
F
no tag
wt
ku70-C85Y
Exo1-Myc
Coomassie blue

Figure 24. Suppression of *sae2*Δ DNA damage sensitivity by *ku70* mutants does not involve Exo1. (A, B, C) Exponentially growing cultures were serially diluted (1:10) and each dilution was spotted out onto YEPD plates with or without CPT, MMS or phleomycin. (D) Meiotic tetrads were dissected on YEPD plates that were incubated at 25°C, followed by spore genotyping. (E) ChIP and qPCR. YEPR G1-arrested cell cultures of JKM139 derivative strains were transferred to YEPRG to induce HO in the presence of α-factor. Relative fold enrichment of Exo1-Myc at the indicated distances from the HO cleavage site was determined after ChIP with an anti-Myc antibody and qPCR. The mean values of three independent experiments are represented with error bars denoting s.d. ***$p < 0.005$; *$p < 0.05$ (unpaired two-tailed Student's t-test). (F) Western blot with an anti-Myc antibody of extracts used for the ChIP analysis shown in (E). The same amounts of extracts were separated on an SDS-PAGE and stained with Coomassie blue as loading control.

The *ku70-C85Y* allele suppresses the end-tethering defect of *sae2*Δ cells

We investigated the effect of *ku70-C85Y* on the DNA damage sensitivity of cells lacking Mre11 or expressing the *rad50-VM* allele, which encodes a Rad50 mutant variant that specifically impairs the tethering of the DSB ends (Cassani et al., 2016a). The *ku70-C85Y* allele failed to suppress the severe DNA damage sensitivity of *mre11*Δ cells (Figure 25A), whereas it was capable of partially restoring DNA damage resistance of *rad50-VM* cells (Figure 25B). This result, together with the observation that Sae2 is involved in keeping the DSB ends tethered to each other (Clerici et al., 2005; K. Lee et al., 2008), raises the possibility that the *ku70-C85Y* allele can suppress the DNA damage sensitivity of *sae2*Δ cells by restoring DSB end-tethering.

To visualize DNA regions flanking to an HO-induced DSB, we used a strain background where multiple repeats of the LacI repressor binding site are integrated 50 kb upstream and downstream of an irreparable HO break site located on chromosome VII in cells constitutively expressing a LacI-GFP fusion protein (Kaye et al., 2004). The level of end-tethering upon DSB formation was determined by measuring the generation of one or two LacI-GFP foci. HO expression was induced by galactose addition to cell cultures that were arrested in G2 with nocodazole and kept blocked in G2 by nocodazole in order to ensure that all cells would arrest in metaphase. Consistent with an end-tethering defect (Clerici et al., 2005), *sae2*Δ cells showed an increase of two LacI-GFP foci compared to the uninduced condition, whereas ~90% of wild-type cells showed a single LacI-GFP focus

1–2 h after HO induction (Figure 25C). Strikingly, *sae2*Δ cells harboring the *ku70-C85Y* allele showed a decrease in the percentage of two LacI-GFP foci (Figure 25C), indicating that this mutation suppresses the end-tethering defect caused by the lack of Sae2. A slight but significant decrease of two LacI-GFP foci can be detected also in *ku70-C85Y* cells compared to wild-type cells (Figure 25C), suggesting that the $Ku70^{C85Y}$ mutant variant possesses by itself an increased ability to support DSB end-tethering. Consistent with a role of the Ku complex in DSB end-tethering, the lack of Ku70 slightly increased the percentage of untethered ends after HO induction and this percentage was further increased in *ku70*Δ *sae2*Δ cells compared to each single mutant (Figure 25C). The effect of *ku70*Δ and *ku70-C85Y* alleles on the frequency of LacI-GFP foci after HO induction was primarily due to end-tethering and not to cohesion defects. In fact, similar results have been obtained when HO was induced in α-factor-arrested cells that were kept arrested in G1 in the presence of galactose (Figure 25D).

The function of Ku in DSB end-tethering appears to be independent of MRX, as *ku70-C85Y* decreased the amount of two LacI-GFP foci of both *mre11*Δ and *rad50-VM* cells (Figure 25C and D). While the severe DNA damage hypersensitivity of *mre11*Δ cells, which was not suppressed by the *ku70-C85Y* allele (Figure 3A), is due to the lack of MRX functions in several aspects of the DNA damage response, *rad50-VM* cells are specifically defective in DSB tethering (Cassani et al., 2016). Therefore, the increased DNA damage resistance of *ku70-C85Y rad50-VM* cells compared to *rad50-VM* cells (Figure 25B) can be due to the suppression of their DSB tethering defect.

A role for Ku in DSB end-bridging predicts that two Ku70–Ku80 heterodimers can interact. Consistent with this hypothesis, atomic force microscopy showed that DNA-bound human Ku can self-associate (Cary et al., 1997) and an interaction between two Ku heterodimers has been observed by coimmunoprecipitation in human cells (Ribes-Zamora et al., 2013). To assess a possible interaction between Ku70–Ku80 heterodimers in yeast, we performed coimmunoprecipitation using protein extracts prepared from diploid cells carrying differentially tagged versions of Ku70. We detected Ku70-HA in Ku70-Flag immunoprecipitates from both wild-type and *ku70-C85Y* protein extracts (Figure 25E). As neither Ku70 nor Ku80 homodimerizes (Errami et al., 1998; Griffith et al., 1992; Ono et al., 1994), these results are consistent with differentially tagged Ku heterodimers forming multimers.

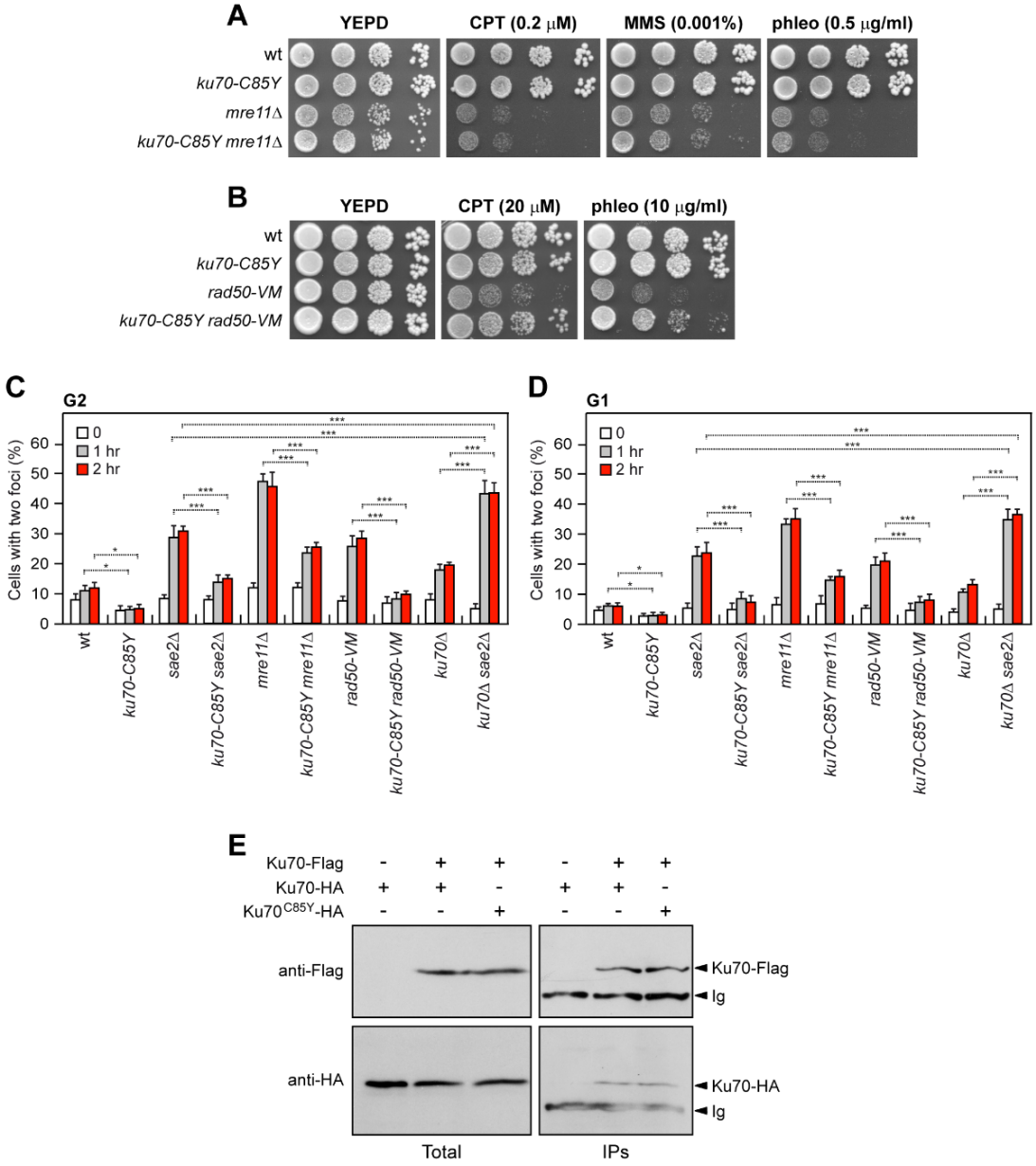
A
YEPD
CPT (0.2 μM)
MMS (0.001%)
phleo (0.5 μg/ml)
wt
ku70-C85Y
mre11Δ
ku70-C85Y mre11Δ
B
YEPD
CPT (20 μM)
phleo (10 μg/ml)
wt
ku70-C85Y
rad50-VM
ku70-C85Y rad50-VM
C
G2
Cells with two foci (%)
0
1 hr
2 hr
wt
ku70-C85Y
sae2Δ
ku70-C85Y sae2Δ
mre11Δ
ku70-C85Y mre11Δ
rad50-VM
ku70-C85Y rad50-VM
ku70Δ
ku70Δ sae2Δ
D
G1
Cells with two foci (%)
0
1 hr
2 hr
wt
ku70-C85Y
sae2Δ
ku70-C85Y sae2Δ
mre11Δ
ku70-C85Y mre11Δ
rad50-VM
ku70-C85Y rad50-VM
ku70Δ
ku70Δ sae2Δ
E
Ku70-Flag
Ku70-HA
Ku70C85Y-HA
anti-Flag
anti-HA
Ku70-Flag
Ig
Ku70-HA
Ig
Total
IPs

Figure 25. The *ku70-C85Y* allele suppresses the end-tethering defect of *sae2*Δ cells. (A, B) Exponentially growing cultures were serially diluted (1:10) and each dilution was spotted out onto YEPD plates with or without CPT, MMS or phleomycin. (C, D) DSB end-tethering. Exponentially growing YEPR cell cultures were arrested in G2 with nocodazole (C) or in G1 with α-factor (D) at time zero and transferred to YEPRG in the presence of nocodazole or α-factor, respectively. 200 cells for each strain were analyzed to determine the percentage of cells showing two LacI-GFP foci. The mean values of three independent experiments are represented with error bars denoting s.d. ***$p < 0.005$; **$p < 0.01$; *$p < 0.05$ (unpaired two-tailed Student's *t*-test). (E) Ku70 can self-associate. Protein extracts were analyzed by western blotting with an anti-Flag or an anti-HA antibody either directly (Total) or after immunoprecipitation (IPs) with an anti-Flag antibody.

The *ku70-C85Y* allele suppresses the HR defects of *sae2*Δ cells

The maintenance of the DSB ends tethered to each other can be important to repair a DSB by both NHEJ and HR. As DSB repair by NHEJ is increased in *sae2*Δ cells possibly due to the reduced DSB resection (Cassani et al., 2018), it is unlikely that the restored end-tethering in *ku70-C85Y sae2*Δ cells leads to DNA damage resistance by increasing the efficiency of NHEJ. In fact, when we measured DSB repair by NHEJ as the ability of cells to religate a plasmid that was linearized before being transformed into the cells, *sae2*Δ cells, as expected, showed an increase in the efficiency of plasmid religation compared to wild-type cells (Figure 26A). By contrast, *ku70-C85Y* cells decreased it either in the presence or in the absence of Sae2 (Figure 26A), indicating that the *ku70-C85Y* mutation impairs DSB end-joining. Furthermore, the *ku70-C85Y* allele still suppressed the DNA damage sensitivity of *sae2*Δ cells lacking the NHEJ component Nej1 (Figure 26B), whose loss leads to end-joining defects (Frank-Vaillant & Marcand, 2001; Kegel et al., 2001), indicating that NHEJ is not required for *sae2*Δ suppression.

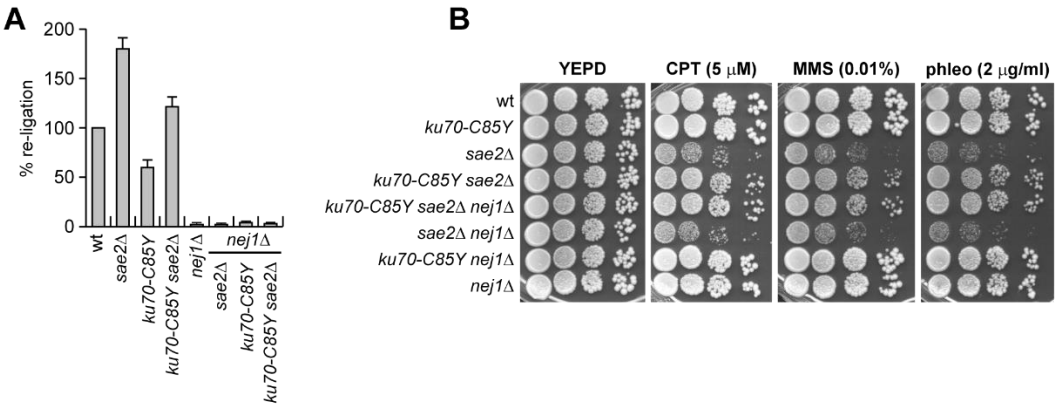

Figure 26. The *ku70-C85Y* mutant increases the efficiency of NHEJ (A) Plasmid religation assay. The same amounts of *Bam*HI-linearized or uncut pRS316 plasmid DNA were transformed into the cells. Data are expressed as percentage of religation relative to wild type that was set up at 100% after normalization to the corresponding transformation efficiency of the uncut plasmid. (B) Exponentially growing cultures were serially diluted (1:10) and each dilution was spotted out onto YEPD plates with or without CPT, MMS or phleomycin.

In the canonical HR pathway, the 3'-ended ssDNA tail at one of the DSB ends invades the homologous template, forming a D-loop structure that primes DNA synthesis. Then, the complementary sequence on the second end of the DSB can anneal to the displaced ssDNA to generate a double Holliday junction, whose random cleavage yields to noncrossover (NCO) and crossover (CO) products. Alternatively, if the newly synthesized strand is unwound by the D-loop, its annealing with the 3' ssDNA end at the other side of the DSB leads to the generation of NCO products in a process called synthesis-dependent strand-annealing (SDSA). Finally, when homology is present only

for one end of the DSB, this single end invades the template and initiates extensive DNA synthesis that can reach even the end of the chromosome in a process called break-induced replication (BIR) (Mehta & Haber, 2014).

We have previously shown that the lack of Sae2 impairs DSB repair by SDSA (Cassani et al., 2018). Furthermore, *mre11* mutations that suppressed the end-tethering defect of *sae2*Δ cells also suppressed their SDSA defect (Cassani et al., 2018). Thus, we investigated whether the increased DNA damage resistance of *sae2*Δ cells conferred by the *ku70-C85Y* mutation might be due to a more efficient DSB repair by SDSA. To monitor CO and NCO formation, we used a haploid strain that carries a *MATa* gene on chromosome V that can be cleaved by HO and repaired by using a *MATa* (*MATa-inc*) sequence on chromosome III that contains a single base pair substitution that prevents HO cleavage (Saponaro et al., 2010) (Figure 27A). Galactose was added to induce HO and then it was maintained in the medium to cleave the HO sites that were eventually reconstituted by NHEJ. As expected (Cassani et al., 2018), the 3 kb *MATa* band resulting from NCO recombination events reaccumulated less efficiently in *sae2*Δ cells compared to wild-type cells (Figure 27B and C), while the 3.4 kb band resulting from CO recombination events was similar in wild-type and *sae2*Δ cells (Figure 27B and D). The presence of the *ku70-C85Y* mutation, which did not affect by itself the generation of both COs and NCOs events, increased the NCO products in *sae2*Δ cells (Figure 27B–D). As most NCO products arise from the SDSA mechanism, this finding indicates that the *ku70-C85Y* allele suppresses the SDSA defect of *sae2*Δ cells.

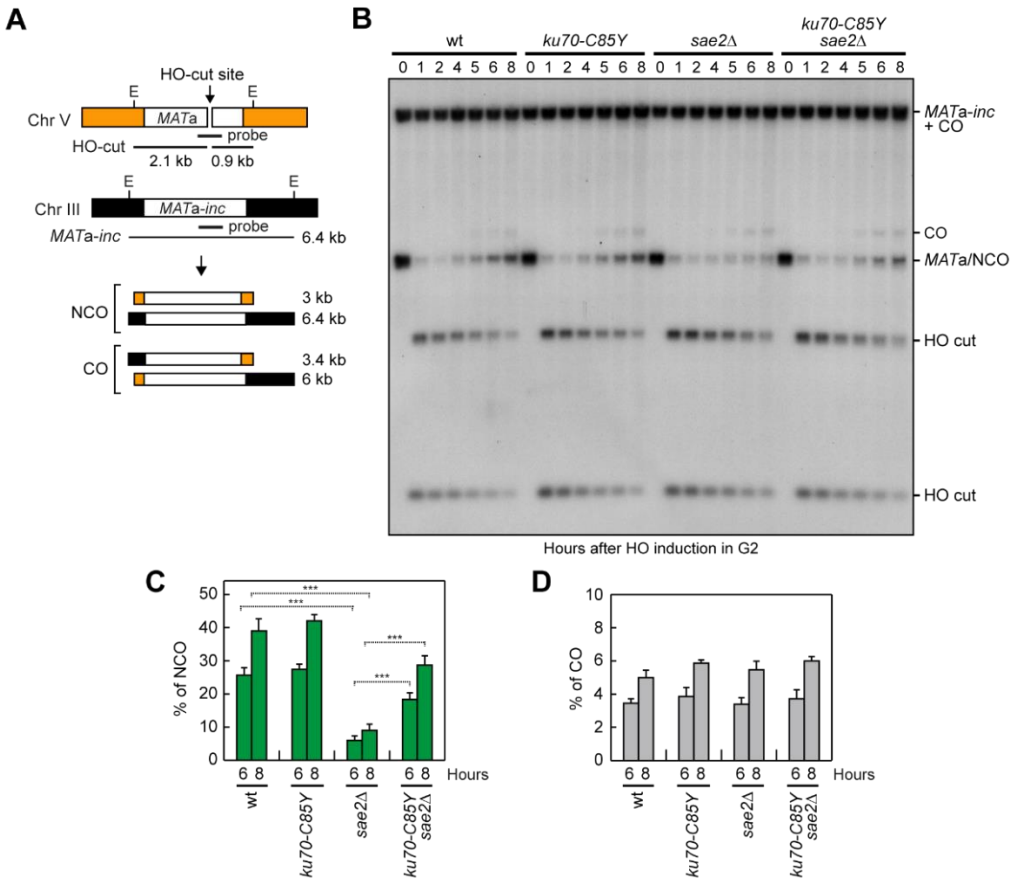

Figure 27. The *ku70-C85Y* allele suppresses the SDSA defect of *sae2Δ* cells. DSB repair by ectopic recombination. (A) System to detect ectopic recombination. HO induction generates a DSB at a *MATa* DNA sequence on chromosome V, while the homologous *MATa-inc* region on chromosome III cannot be cut by HO and is used as a donor for HR-mediated repair that generate noncrossover (NCO) and crossover (CO) products. E, *Eco*RI. (B) YEPR cell cultures were arrested in G2 with nocodazole and transferred to YEPRG at time zero in the presence of nocodazole. Southern blot analysis of *Eco*RI-digested genomic DNA with a *MATa* probe. (C, D) Densitometric analysis of NCO (C) and CO (D) band signals. The mean values of three independent experiments are represented with error bars denoting s.d. ***p< 0.005 (unpaired two-tailed Student's t-test).

A DSB that is flanked by direct repeats can be repaired by single-strand annealing (SSA), which requires resection of the direct repeats followed by annealing of the resulting complementary ssDNA (Mehta & Haber, 2014). We have previously shown that the lack of Sae2 impairs DSB repair by SSA and that this SSA defect cannot be solely explained by the reduced DSB resection (Clerici et al., 2005), raising the possibility that the end-tethering defect displayed by *sae2*Δ cells can contribute to the poor SSA efficiency. To investigate the effect of the *ku70-C85Y* allele on DSB repair by SSA, we used a strain carrying tandem repeats of the *LEU2* gene, with a recognition site for HO adjacent to one of the repeats (Vaze et al., 2002) (Figure 28A). Galactose was added to G2-arrested cells to induce HO expression and it was maintained in the medium to recleave the HO sites reconstituted by NHEJ. We found that *sae2*Δ cells reduced the accumulation of the SSA repair products compared to wild-type cells, whereas the SSA repair events increased in *ku70-C85Y sae2*Δ cells (Figure 28B and C), indicating that *ku70-C85Y* suppresses the SSA defect caused by the lack of Sae2.

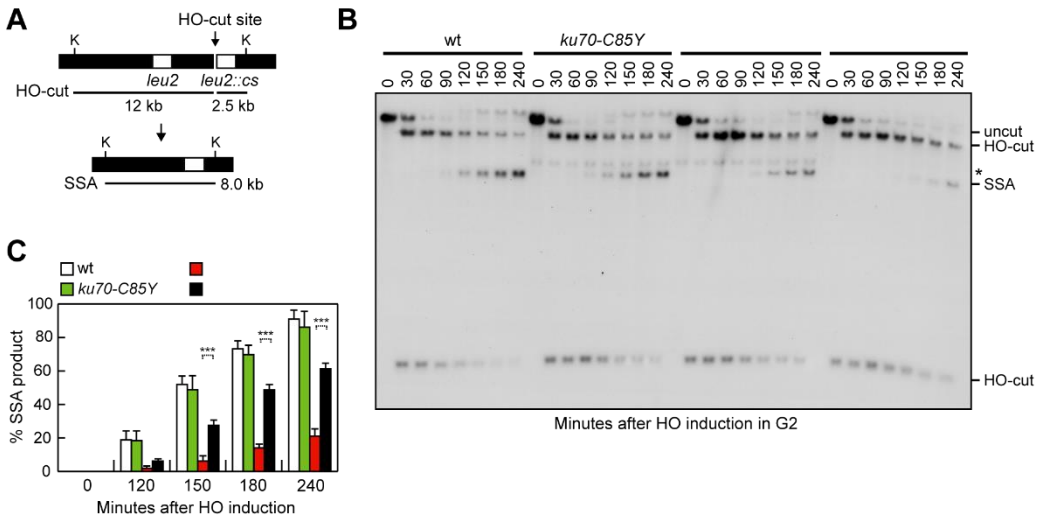

Figure 28. The *ku70-C85Y* allele suppresses the SSA defect of *sae2*Δ cells. (A) System to detect DSB repair by SSA. HO induction generates a DSB between two homologous *leu2* sequences that are 4.6 kb apart. K, *Kpn*I. (B) YEPR cell cultures were arrested in G2 with nocodazole and transferred to YEPRG at time zero in the presence of nocodazole. Southern blot analysis of *Kpn*I-digested genomic DNA with a *LEU2* probe revealed a 2.5 kb and 12 kb DNA fragments (HO-cut) resulting from HO-induced DSB formation. DSB repair by SSA generates an 8 kb fragment (SSA). * indicates cross-hybridization. (C) Densitometric analysis of the SSA band signals. The mean values of three independent experiments are represented with error bars denoting s.d. ***p< 0.005 (unpaired two-tailed Student's t-test).

The C85Y mutation increases Ku70 association with the DSB ends

The C85Y mutation might facilitate the tethering of the DSB ends either by increasing Ku–Ku self-interaction or by stabilizing Ku70 association with the DSB end. As we failed to detect an increase in Ku70–Ku70 interaction by coimmunoprecipitation in *ku70-C85Y* cells (Figure 25E), wild-type and mutant Ku protein complexes were tested for DNA-binding by gel electrophoretic mobility shift assay (EMSA). Both Ku70–Ku80 and Ku70^{C85Y}–Ku80 heterodimers were produced and purified from *E. coli* cells to homogeneity (Figure 29A) and tested for the ability to bind a 21 bp blunt-ended double-stranded DNA (dsDNA) that is capable of binding one Ku heterodimer (Blier et al., 1993). Size Exclusion Chromatography (SEC) analyses on purified complexes showed that Ku70–Ku80 and Ku70C85Y–Ku80 were dimers (Figure 29B), indicating that the C85Y substitution does not affect the complex quaternary structure. Increasing concentrations of Ku heterodimer were added to a fixed amount of radiolabeled dsDNA substrate. The addition of either wild-type Ku70–Ku80 or Ku70^{C85Y}–Ku80 complex resulted in one shifted band, likely representing DNA bound to one Ku dimer (Figure 29C). This single-bound species became detectable at a 4-fold ratio of wild-type Ku70–Ku80 to DNA substrate and at a 2-fold ratio of Ku70^{C85Y}–Ku80 to DNA substrate (Figure 29C), indicating that the C85Y mutation increases the DNA binding affinity of the Ku heterodimer.

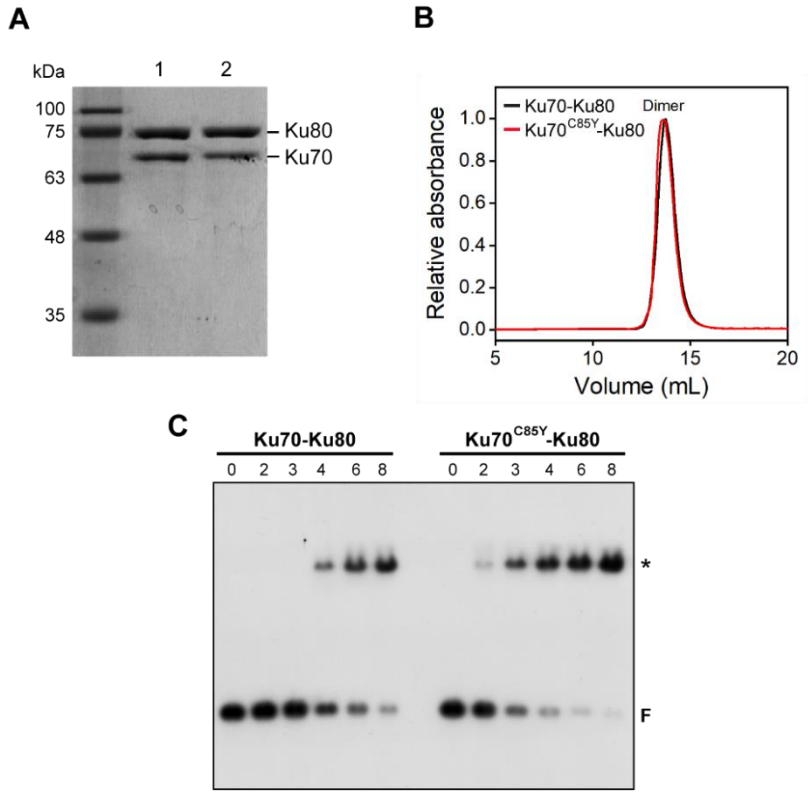

Figure 29. Purification of Ku70-Ku80 and Ku70^{C85Y}-Ku80 complexes and analysis of protein-DNA binding *in vitro*. (A) SDS-PAGE analysis of purified Ku70-Ku80 (lane 1) and Ku70^{C85Y}-Ku80 (lane 2) complexes. (B) Quaternary structure of Ku70-Ku80 and Ku70^{C85Y}-Ku80 complexes determined by SEC analysis. One of three independent measurements was shown. The molecular weight estimated by SEC is 164.93 ± 4.56 kDa and 153.20± 5.71 kDa for Ku70-Ku80 and Ku70^{C85Y}-Ku80 complexes, respectively. (A) EMSA with a 21 bp dsDNA and increasing concentrations of Ku70–Ku80 and Ku70^{C85Y}–Ku80 complexes. Bands corresponding to free DNA (F) and to a protein-DNA complex (asterisk) are denoted.

Next, we performed ChIP analysis to assess the consequences of the C85Y mutation on Ku70 association with DSBs. Consistent with an increased DNA binding propensity of Ku70^{C85Y}–Ku80 (Figure 29C), the amount of Ku70C85Y bound very close to the HO-induced DSB (0.2 kb) was increased compared to wild-type Ku70 (Figure 30A), although similar amount of Ku70 and Ku70C85Y can be detected in the protein extracts used for the ChIP analysis (Figure 30B). Interestingly, as the distance from the DSB increased (0.6 and 1.8 kb), the amount of Ku70^{C85Y} bound to the HO-induced DSB was lower than wild-type Ku70 (Figure 30A). As the Ku complex has been proposed to slide along DNA (de Vries et al., 1989), this finding suggests that the increased DNA affinity of the mutant Ku70^{C85Y}–Ku80 complex for DNA ends can result in a decreased propensity of the complex to diffuse over the broken DNA end and in an increased ability to support the tethering of the DSB ends. Consistent with this hypothesis, the *ku70-Y494N* mutation, which was identified as a suppressor of the CPT sensitivity of mre11 nuclease mutants, was shown to reduce DNA binding of the Ku heterodimer and to increase its probability to slide inwards once bound to dsDNA (Balestrini et al., 2013). Interestingly, the *ku70-Y494N* allele, which was capable of partially suppressing the CPT sensitivity of *sae2*Δ cells in an Exo1-dependent manner because of its failure to inhibit Exo1, did not suppress the phleomycin sensitivity of *sae2*Δ cells (Figure 30C). Furthermore, it exacerbated the DNA damage sensitivity and the end-tethering defect of *rad50-VM* cells (Figure 30E), thus supporting the hypothesis that the ability of Ku to support DSB end-tethering is influenced by its DNA binding properties.

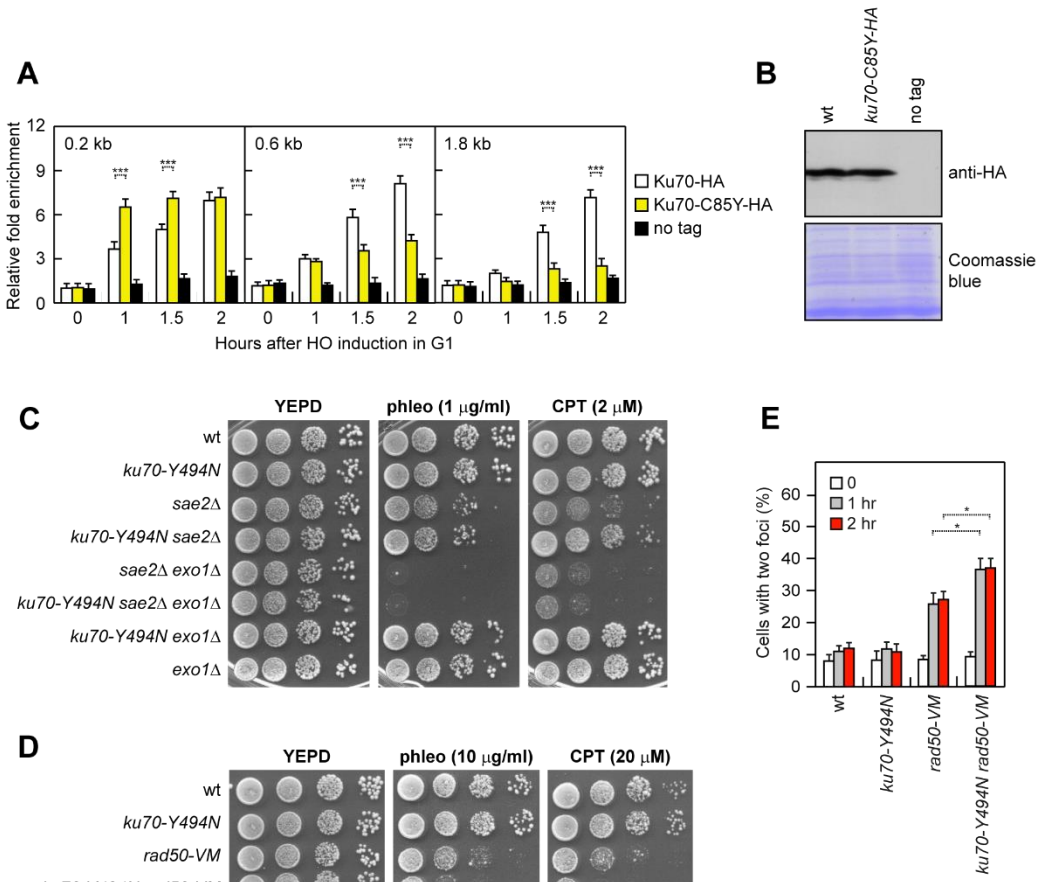

Figure 30. Ku association with DSB and *ku70-Y494N* phenotypes. (A) ChIP and qPCR. Exponentially growing YEPR cell cultures of JKM139 derivative strains were arrested in G1 with α-factor and transferred to YEPRG to induce HO in the presence of α-factor. Relative fold enrichment of Ku70-HA and Ku70^{C85Y}-HA at the indicated distances from the HO cleavage site was determined after ChIP with an anti-HA antibody and qPCR. The mean values of three independent experiments are represented with error bars denoting s.d. **p <0.01 (unpaired two-tailed Student's t-test). (B) Western blot with an anti-HA antibody of extracts used for the ChIP analysis shown in (A). The same amount of protein extracts was separated on an SDS-PAGE and

stained with Coomassie blue as loading control. (C, D) Exponentially growing cultures were serially diluted (1:10) and each dilution was spotted out onto YEPD plates with or without phleomycin or CPT. (E) DSB end-tethering. Exponentially growing YEPR cell cultures were arrested in G2 with nocodazole at time zero and transferred to YEPRG in the presence of nocodazole. 200 cells for each strain were analyzed to determine the percentage of cells showing two LacI-GFP foci. The mean values of three independent experiments are represented with error bars denoting s.d. *$p < 0.05$ (unpaired two-tailed Student's t-test).

In order to investigate the interaction of wild-type and mutant Ku heterodimers with a DNA end, and since no structure is available for yeast Ku bound to DNA, we performed an integrative docking software HADDOCK2.4 simulation for both wild-type Ku70–Ku80 and mutant $Ku70^{C85Y}$–Ku80 heterodimers versus a 13 bp dsDNA molecule. Only with the $Ku70^{C85Y}$–Ku80 heterodimer the docking protocol explored far different conformations and was able to position the DNA molecule inside the β-barrel, similarly to what observed in the human Ku complex with DNA (Walker et al., 2001). In order to obtain a wild-type Ku–DNA complex as well, we built a homology modeling structure of the wild-type heterodimer bound to DNA with the mutant heterodimer structure as a model. The models obtained were refined by the HADDOCK2.4 refinement protocol (Neijenhuis et al., 2022), which exploits molecular dynamics simulation in water solvent allowing freedom of movement first to the residues side chains all over the protein and then to the region of the protein taking contact with the interactor. The simulations generated structures with minimized energy and HADDOCK scores of -118.5 for the wild-type and -124.3 for the mutant heterodimer,

mainly due to a higher number of electrostatic interactions in the mutant complex (the specific scores for electrostatic interactions being -548.7 versus -516.8 for Ku70^{C85Y}–Ku80 versus Ku70–Ku80). By analyzing the structures, we could observe that the ring of the wild-type heterodimer is able to make only few electrostatic contacts with the DNA molecule (Figure 31A), as it was actually described in the available structures for the human Ku70–Ku80 complex (Walker et al., 2001). It is interesting to notice that the positive residues of the Ku70^{C85Y}–Ku80 ring appeared to be able to make more salt-bridges and H-bonds with the DNA (Figure 31B), suggesting that the β-barrel of Ku70^{C85Y}–Ku80 could be more flexible than that of the wild-type Ku70–Ku80, thus allowing the positive residues to orient their side chains towards the DNA molecule.

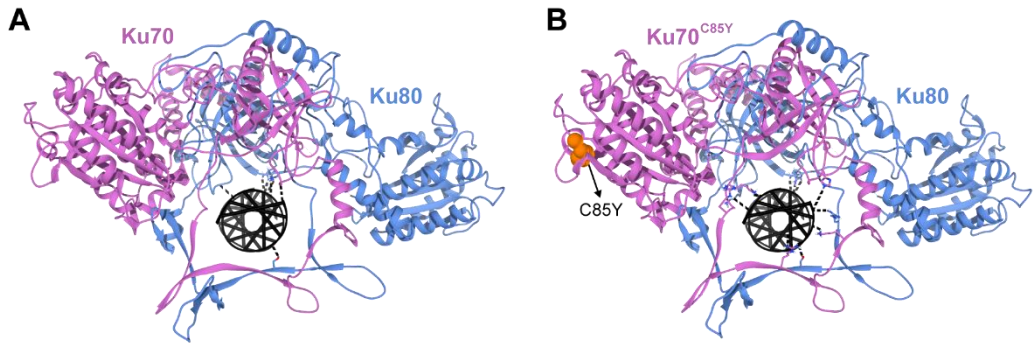

Figure 31. Structure of a Ku heterodimer bound to DNA. (A, B) Structures were obtained by docking protocol on HADDOCK2.4 platform as described in the Materials and Methods section. The complexes of wild-type Ku70–Ku80 (A) or Ku70^{C85Y}–Ku80 (B) bound to DNA, minimized by HADDOCK refinement protocol, are shown. Ku70 is in pink, Ku80 in blue, DNA in black. Residues making electrostatic contacts with DNA are exposed in sticks and the bonds are in dashed lines. The residue affected by the C85Y mutation in (B) is shown as orange balls.

Tel1 kinase antagonizes Ku function in DSB end-tethering

The lack of Tel1 increases Ku persistence very close to the DSB ends (Iwasaki et al., 2016). Furthermore, mammalian ATM antagonizes tethering at single-ended DSBs (Britton et al., 2020), raising the possibility that Tel1/ATM can modulate DSB tethering by regulating Ku association with DNA. However, the possible role of Tel1 in regulating Ku-mediated end-tethering can be masked by the fact that Tel1 has a structural role in promoting MRX persistence at DSBs and therefore the lack of Tel1 would impair end-tethering by decreasing the amount of MRX bound at DSBs (Cassani et al., 2016a; Oh et al., 2018). As Tel1 increases MRX retention at DSBs independently of its kinase activity (Cassani et al., 2016a), we analyzed DSB end-tethering and Ku association with DSBs in cells expressing a Tel1 kinase defective (*tel1-kd*) allele (Mallory & Petes, 2000), which has been already reported to suppress the DNA damage sensitivity of *sae2*Δ cells (Gobbini et al., 2015). We detected a significant decrease in percentage of two LacI-GFP foci in *tel1-kd sae2*Δ cells compared to *sae2*Δ cells (Roberts & Ramsden, 2007) (Figure 32A and B), indicating that Tel1 antagonizes DNA bridging. Furthermore, similar to Ku70^{C85Y}, the lack of Tel1 kinase activity increased the amount of Ku70 bound in close proximity to the HO-induced DSB ends and this effect was more pronounced in the presence of the Ku70^{C85Y} mutant variant (Figure 32C). The amount of Ku70 bound at more distant sites (0.6 and 1.8 kb) from the HO-induced DSB was much lower in *tel1-kd* cells compared to wild type (Figure 32C), indicating that Tel1 controls Ku persistence at the DSB ends.

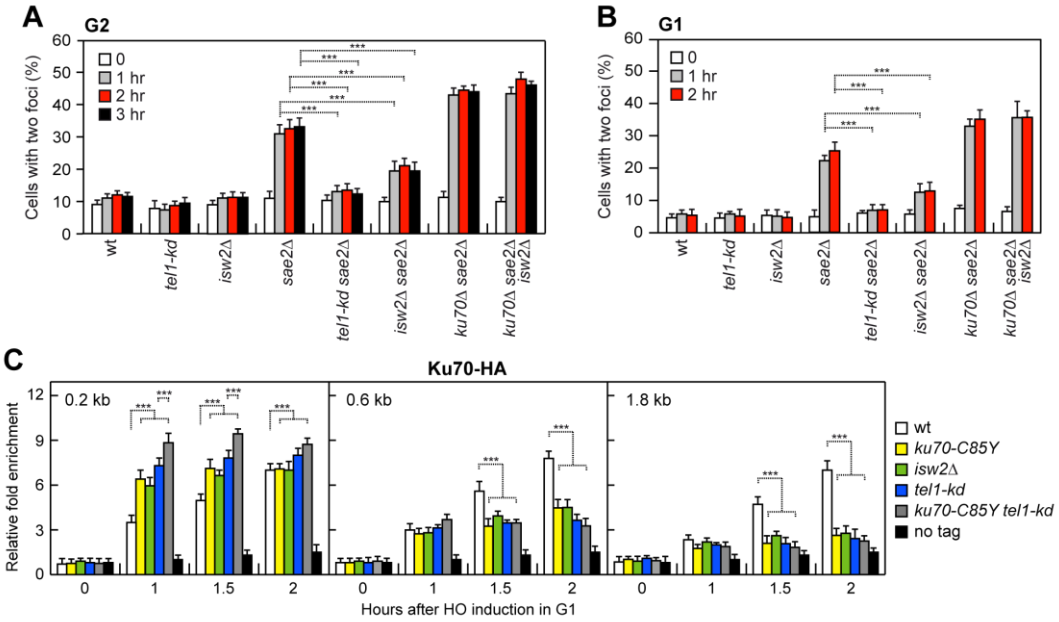

Figure 32. The lack of Tel1 kinase or of Isw2 suppresses the end-tethering defect of *sae2*Δ cells and increases Ku persistence close to the DSB ends. (A, B) DSB end-tethering. Exponentially growing YEPR cell cultures were arrested in G2 with nocodazole (A) or in G1 with α-factor (B) at time zero and transferred to YEPRG in the presence of nocodazole or α-factor, respectively. 200 cells for each strain were analyzed to determine the percentage of cells showing two LacI-GFP foci. The mean values of three independent experiments are represented with error bars denoting s.d. ***p<0.005 (unpaired two-tailed Student's t-test). (C) ChIP and qPCR. Exponentially growing YEPR cell cultures of JKM139 derivative strains were arrested in G1 with α-factor and transferred to YEPRG to induce HO in the presence of α-factor. Relative fold enrichment of Ku70-HA at the HO-induced DSB was evaluated after ChIP with an anti-HA antibody and qPCR. The mean values of three independent experiments are represented with error bars denoting s.d. ***p <0.005; *p< 0.05 (unpaired two-tailed Student's t-test).

Nucleosome removal from DSBs antagonizes Ku function in DSB end-tethering

Previous work has shown that Ku diffusion is inefficient on nucleosome-associated DNA ends (Roberts & Ramsden, 2007). Furthermore, Ku and phosphorylated histone H2AX (γH2AX) foci are mutually exclusive (Britton et al., 2013), suggesting that Ku localizes to DNA ends that are locally depleted of nucleosomes. ChIP experiments support nucleosome disassembly near DSBs (Tsukuda et al., 2005), with histone loss promoted by mammalian ATM (Berkovich et al., 2007; Li & Tyler, 2016). These findings lead to the hypothesis that Tel1 can control Ku spreading by promoting histone disassembly around a DSB. Thus, we evaluated the effect of the lack of Tel1 kinase activity on histone H2A and H3 occupancy centromere-proximal to the irreparable HO-induced DSB at the MAT locus. HO expression was induced by galactose addition to G2-arrested cells that were kept arrested in G2 with nocodazole to exclude possible effects of DNA replication on histone association with DNA. As expected, H2A and H3 signals near the HO-induced DSB decreased in wild-type cells, while they remained high in *tel1-kd* cells (Figure 33A), indicating that Tel1 kinase promotes nucleosome loss from DSBs.

If Tel1 antagonizes the Ku function in supporting DSB end-bridging by promoting histone removal from DSBs and Ku sliding inwards, failure to remove histones should mimic the effect caused by the lack of Tel1 kinase activity on DNA end-tethering and Ku association with DSBs. The density of nucleosome packaging is regulated by ATP-dependent chromatin remodelers, which use the energy derived from ATP hydrolysis to evict, assemble, reposition, or exchange histones throughout the genome. We have previously

shown that the lack of the chromatin remodeler Isw2 dramatically impairs nucleosome disassembly at DSBs (Casari, Gobbini, Gnugnoli, et al., 2021), prompting us to test the effect of its deletion on *sae2*Δ suppression, Ku association with DSBs, and DSB tethering. The lack of Isw2, which impaired H2A and H3 removal from the HO-induced DSB (Figure 33A), partially suppresses both the DNA damage sensitivity (Figure 33B) and the end-tethering defect of *sae2*Δ cells (Figure 32A and B). Furthermore, similar to both *ku70-C85Y* and *tel1-kd*, *isw2*Δ increased Ku70 association very close to the HO-induced DSB end, whereas it decreased it at more distant sites (Figure 32C).

Suppression of both the DNA damage sensitivity and the end-tethering defect of *sae2*Δ cells by *ISW2* deletion requires Ku70. In fact, *isw2*Δ failed to suppress the phleomycin sensitivity of *ku70*Δ *sae2*Δ cells and did not further increase resistance to CPT of *ku70*Δ *sae2*Δ cells (Figure 33B). Furthermore, *isw2*Δ did not restore end-tethering of *ku70*Δ *sae2*Δ cells (Figure 32A and B). Unfortunately, the effect of the *tel1-kd* mutation on *ku70*Δ *sae2*Δ cells cannot be tested due to the senescence phenotype of *ku70*Δ *tel1-kd* cells (Porter et al., 1996). Altogether, these data indicate that histone removal from DSBs antagonizes the Ku function in supporting DSB bridging.

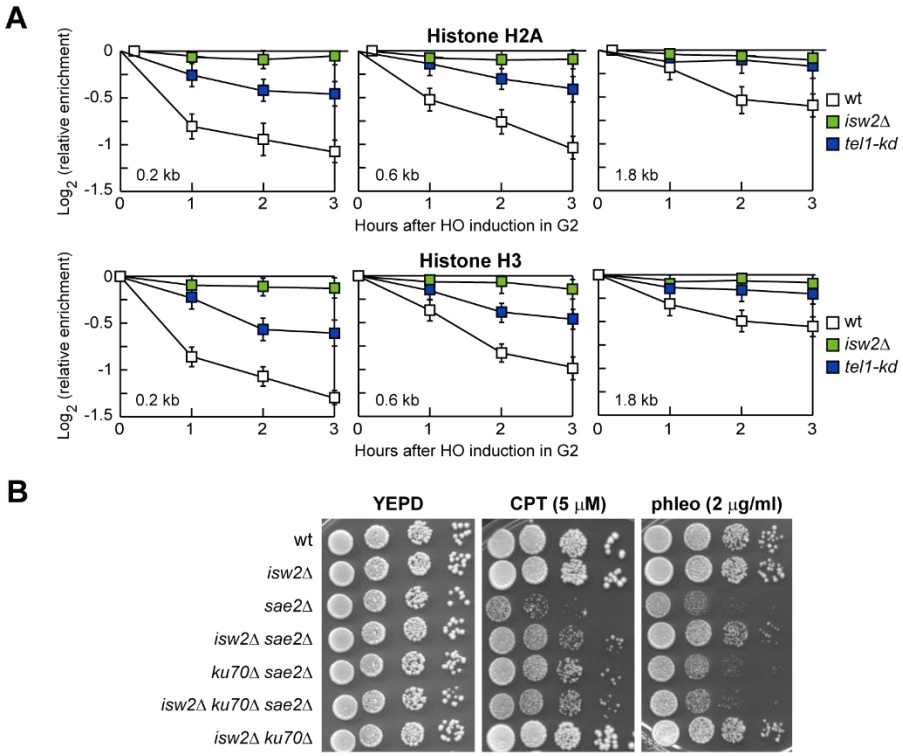

Figure 33. Tel1 kinase promotes nucleosome loss from DSB. (A) ChIP and qPCR. HO expression was induced at time zero by galactose addition to G2-arrested cells that were kept arrested in G2 by nocodazole throughout the experiment. Relative fold enrichment of H2A or H3 at the HO-induced DSB was evaluated after ChIP with an anti-H2A or an anti-H3 antibody and qPCR analysis. The mean values of three independent experiments are represented with error bars denoting s.d. (B) Serial dilutions of exponentially growing cultures onto YEPD plates with or without CPT or phleomycin.

DISCUSSION

Chapter 2

The maintenance of the DSB ends tethered to each other prevents the broken chromatid from physically separating from the rest of the chromosome, this process facilitates the correct repair by NHEJ and the homology search during HR. Whether the Ku heterodimer has an *in vivo* role in bridging the DSB ends together has remained somewhat obscure. By characterizing a *ku70* mutation that increases DNA damage resistance of *sae2*Δ cells in a Exo1-independent manner, we provide evidence that the Ku complex has a role in maintaining an intrachromosomal association between the ends of a broken chromosome (Figure D2). In fact, the *ku70-C85Y* allele increases DSB end-tethering and suppresses the end-tethering defect of *sae2*Δ cells. This Ku function in supporting end-bridging occurs independently of MRX, as the *ku70-C85Y* allele also partially suppresses the bridging defects of *mre11*Δ and *rad50-VM* cells. Consistent with a role of Ku in end-tethering, we found that Ku70 can self-associate and the lack of Ku70 exacerbates the end-tethering defect of *sae2*Δ cells.

The maintenance of the DSB ends tethered to each other can be important to repair a DSB by both NHEJ and HR. As *sae2*Δ cells are not defective in DSB repair by NHEJ and *ku70-C85Y* cells show a slight NHEJ defect, it is unlikely that the enhanced end-tethering activity conferred by the *ku70-C85Y* mutation might restore *sae2*Δ DNA damage resistance by increasing the NHEJ efficiency. We have previously shown that the lack of Sae2 impairs DSB repair by both SDSA and SSA (Cassani et al., 2018; Clerici et al., 2005). The *ku70-C85Y* mutation partially suppresses both the SDSA and SSA defects of *sae2*Δ cells, suggesting that a defective end-tethering contributes to the DNA damage sensitivity of *sae2*Δ cells by impairing DSB repair by HR. An essential step in

DSB repair by SDSA is that both ends of a DSB are engaged in HR at the same time, thus eliminating the possibility that a single DNA strand invades the template and primes DNA synthesis up to the end of the chromosome through the BIR mechanism. Both Sae2 and MRX have been found to suppress BIR events (Pham et al., 2021), raising the possibility that these proteins can promote SDSA by coordinating the usage of the two ends of a DSB. It was previously shown that MRX and Sae2 coordinate resection at the two DSB ends (Westmoreland & Resnick, 2013) and that restoration of synchronous resection in *mre11* mutants decreases DSB repair by BIR (Pham et al., 2021). Based on the finding that the *ku70-C85Y* mutation restores end-tethering and suppresses the SDSA defect of *sae2*Δ cells, we propose that the maintenance of the DSB ends in close proximity can promote DSB repair by SDSA by contributing to execute synchronous resection of the two DSB ends, thus facilitating the annealing of the displaced strand to the other DSB end. The same mechanism can also explain the suppression of the *sae2*Δ SSA defect.

Interestingly, whereas suppression of *sae2*Δ resection defect by *KU70* deletion results in an increased resistance to CPT and MMS (Foster et al., 2011; Mimitou & Symington, 2010; Shim et al., 2010), suppression of *sae2*Δ end-bridging defect by the *ku70-C85Y* allele also restores resistance to phleomycin. This finding suggests that end-tethering is more important than end-resection to repair phleomycin-induced DNA lesions. Consistent with this hypothesis, we have previously identified *mre11* mutations that increase resistance of *sae2*Δ cells to phleomycin by suppressing their end-tethering but not their resection defect (Cassani et al., 2018). Although phleomycin causes DNA cleavage events as ionizing radiation (IR), the finding that *KU70* deletion suppresses

the sensitivity of *sae2*Δ cells to IR but not to phleomycin suggests that the DNA ends generated by these two DNA damaging agents could differ in their nature and/or could be processed differently by the cells. Coherently with this observation it is know that phleomycin and the realted bleomycin are able the induce DSB when bound to the minor groove of DNA, a distint mechanism compared to IR (Sleigh, 1976). In any case, both end-resection and end-tethering can contribute to increase resistance to CPT that, due to the collision between the replication fork and Topoisomerase I trapped on DNA, can cause single-ended DSBs that can be repaired by sister chromatid recombination (M. Zhu et al., 2018).

How does Ku70^{C85Y} enhance end-tethering? The C85Y mutation increases the amount of Ku bound at the end of a DSB by enhancing its affinity for DNA, arguing that the increased Ku persistence at DNA ends can account for its better ability to support end-tethering and to inhibit Exo1 association with DSBs. The Ku heterodimer, once bound to a DSB, has been proposed to slide along DNA with an energy-free mechanism (de Vries et al., 1989). We found that the amount of DSB-bound Ku70^{C85Y} is higher than wild-type Ku70 very closely to the DSB end, whereas it decreases with increasing distance from the DSB end. This different Ku enrichment depending on the distance from the DSB ends is consistent with a sliding defect that retains Ku70^{C85Y}–Ku80 at the DNA end. The limited Ku70^{C85Y}–Ku80 diffusion can be due to the higher affinity of the mutant complex for DNA that imposes a higher energetic barrier to inward movement. In fact, in order to allow energy-free sliding of the Ku dimer along the DNA molecule, the interactions between the protein surface and the DNA have to be easily breakable by mere molecules vibration

energy. The more stable interaction established by the Ku70^{C85Y}–Ku80 heterodimer with DNA would impose a stronger energetic barrier, making its overrun a rarer event. An increased retention of the Ku70^{C85Y}–Ku80 heterodimer on DNA can also limit the accessibility of Exo1 and of other NHEJ proteins to the DSB ends, thus explaining the resection and the NHEJ defects of *ku70-C85Y* cells.

High-resolution microscopy experiments have shown that Ku translocation on DNA appears to be more limited in a cellular context (Britton et al., 2020), suggesting the existence of mechanisms that suppress Ku diffusion. We found that the lack of Tel1 kinase activity suppresses the end-tethering defect of *sae2*Δ cells. Furthermore, it increases the amount of Ku70 bound very closely to the DSB end, suggesting that Tel1 kinase antagonizes the ability of Ku to support DSB end-tethering by counteracting its persistence at the DSB end. Tel1 kinase might exert this function by regulating Ku conformational changes and/or the activity of proteins that promote or inhibit Ku translocation. Several studies conducted in mammals and yeast support nucleosome eviction in the immediate vicinity of DSB sites with phosphorylated H2AX (γH2AX) being accumulated in the adjacent chromatin (Berkovich et al., 2007; Kim et al., 2007; Shroff et al., 2004; Tsukuda et al., 2005). Interestingly, Ku was shown to be less able to load and translocate internally on nucleosome-associated DNA ends (Roberts & Ramsden, 2007; Walker et al., 2001). Furthermore, in mammals Ku and γH2AX foci are mutually exclusive, with Ku foci being flanked by γH2AX (Britton et al., 2013), suggesting that Ku localizes to DNA ends that are locally depleted of nucleosomes. We found that Tel1 promotes histone disassembly from DSBs. Furthermore, the lack of Isw2 chromatin

remodeler, which increases histone persistence at the DSB end, mimics the effect caused by the lack of Tel1 kinase on Ku-mediated DSB tethering and Ku association with DSBs, suggesting that the presence of nucleosomes helps to retain Ku at the DNA end and therefore to promote its function in end-bridging. In any case, although *ISW2* deletion impairs nucleosome removal from DSBs more severely than the lack of Tel1 kinase activity, the *tel1-kd* allele suppresses the end-tethering defect of *sae2*Δ cells more efficiently than *isw2*Δ, suggesting that Tel1, besides removing histones, could act directly on Ku to regulate its DSB association.

In summary, we propose that the Ku heterodimer is loaded on each side of a DSB and contributes to hold the DNA ends together (Figure D2). This function occurs independently of the MRX complex and Sae2, which also support DSB end-tethering. Tel1 kinase counteracts this Ku function by promoting nucleosome removal from DSBs and Ku sliding inwards. As the presence of Ku at the DSB ends prevents the access of resection nucleases, this Tel1-mediated regulation of Ku association with the DSB ends provides an important layer of control in the choice between NHEJ and HR.

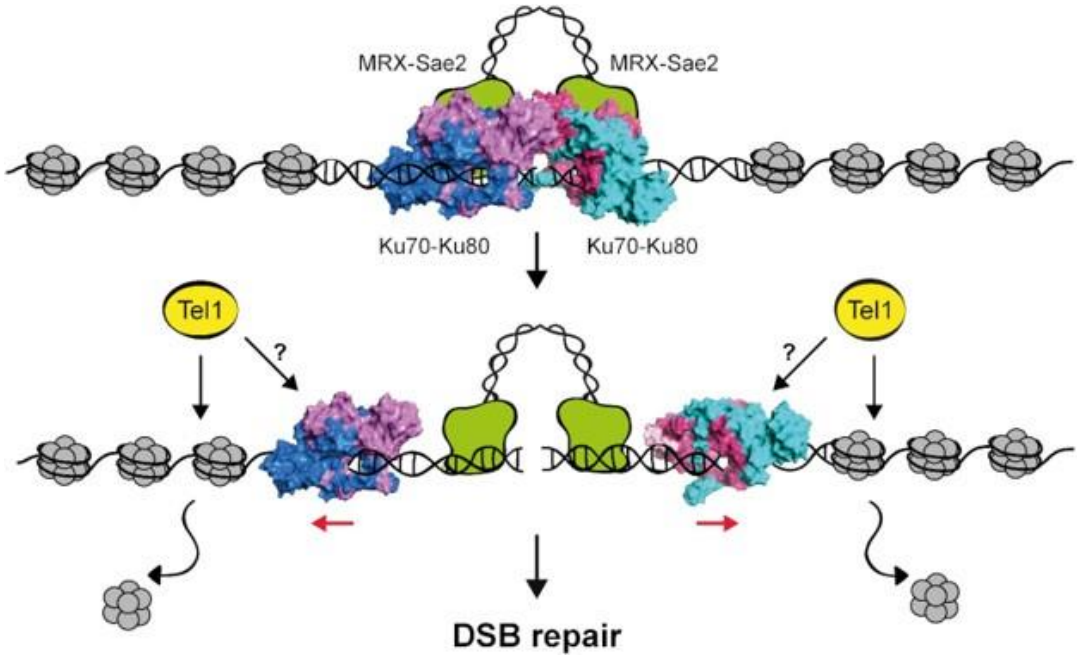

Figure D2. Model for Ku function at DSBs. After DSB formation, two Ku heterodimers are loaded onto both sides of the DSB and contribute to maintain them in close proximity by interacting to each other. This function occurs independently of the MRX complex and Sae2, which also contribute to tether the DSB ends. Tel1 counteracts Ku persistence at the DSB ends by promoting histone removal from DSBs and Ku sliding inwards (red arrows). We cannot exclude the possibility that Tel1 can also act directly on Ku to control its association with DSB. Ku sliding can allow the loading of nucleases that initiate DSB resection and channel DSB repair into HR. The structure of the Ku heterotetramer was built by protein-protein docking simulations, where the interface spans the two vWA-like domains of the Ku70 subunits.

METHODS

Yeast strain

Saccharomyces cerevisiae is the experimental model used in this study. The strains are derivatives of W303 (*MATa/a ade2-1 can1-100 his3-11,15 leu2- 3,112 trp1-1 ura3-1 rad5-535*), JKM139 (*MATa ho hml*Δ*::ADE1 hmr*Δ*::ADE1 ade1-100 leu2-3,112 lys5 trp1::hisG ura3-52 ade3::GAL-HO*), and HS21 (*MATa ade5-1 his7-2 ura3*⊿ *trp1-289 leu2-3,112::p305L3 LEU2 lys2::Alu*IR). Strain genotypes are listed in Table 1. Strain JKM139, used to detect DSB resection, HO checkpoint and to perform ChIP analysis, was kindly provided by J. Haber (Brandeis University, Waltham, USA). Strain used to monitor Lys+ recombinants was kindly provided by S. Jinks-Robertson (Duke University School of Medicine, Durham, USA). Strains YJK40.6, used to detect end-tethering, was kindly provided by D. P. Toczyski (University of California, San Francisco, USA). Gene disruptions and tag fusions were generated by one-step PCR homology cassette amplification and standard yeast transformation method.

Table 1. *Saccharomyces cerevisiae* strains used in this studies.

Strain	Relevant Genotype	Source
W303	*MAT*a/α *ade2-1 can1-100 his3-11,15 leu2-3,112 trp1-1 ura3-1 rad5-535*	
YLL 1134.2	W303 *MAT*a *rif2*Δ*::KANMX*	(Cassani et al., 2016)
YLL 4689.1	W303 *MAT*a *rif2-S6E::LEU2*	This study
YLL 4690.3	W303 *MAT*a *rif2-F8E::LEU2*	This study
YLL 4691.1	W303 *MAT*a *rif2-V18E::LEU2*	This study
YLL 4692.4	W303 *MAT*a *rif2-I23E::LEU2*	This study
DMP 5781/1B	W303 *MAT*a *rad50-V1269M::KANMX*	(Cassani et al., 2016)
DMP 7823/1C	W303 *MAT*a *rif2-S6E::LEU2 rad50-V1269M::KANMX*	This study

DMP 7824/6C	W303 *MATa rif2-F8E::LEU2 rad50-V1269M::KANMX*	This study
DMP 7825/1A	W303 *MATa rif2-V18E::LEU2 rad50-V1269M::KANMX*	This study
DMP 7826/1A	W303 *MATa rif2-I23E::LEU2 rad50-V1269M::KANMX*	This study
YLL 1133	W303 *ura3::TEL1::URA3 tel1::GAL1-TEL1::LEU2*	(Viscardi et al., 2003)
DMP 7827/2D	W303 *GAL1-TEL1::LEU2 rif2-S6E::LEU2*	This study
DMP 7828/1D	W303 *GAL1-TEL1::LEU2 rif2Δ::KANMX*	This study
YLL 490.4	W303 *mec1Δ::HIS3 sml1Δ::KANMX*	(Longhese et al., 2000)
DMP 7829/4A	W303 *mec1Δ::HIS3 sml1Δ::KANMX rif2-S6E::LEU2*	This study
DMP 3335/2A	W303 *tel1Δ::HIS3*	(Casari et al., 2021)
DMP 7830/2A	W303 *tel1Δ::HIS3 rif2-S6E::LEU2*	This study
YLL 4720	W303 *rad50-R125K-VM::KANMX*	This study
DMP 7871	W303 *rad50-R125K-VM::KANMX rif2-S6E::LEU2*	This study
YLL 1069.3	W303 *MATa sae2Δ::KANMX*	(Gobbini et al., 2015)
YLL 4537.3	W303 *MATa ku70-C85Y::URA3 sae2Δ::KANMX*	This study
YLL 4610.8	W303 *MATa ku70-A90T::URA3 sae2Δ::KANMX*	This study
YLL 4611.7	W303 *MATa ku70-N104Y::URA3 sae2Δ::KANMX*	This study
YLL 4612.20	W303 *MATa ku70-G79S::URA3 sae2Δ::KANMX*	This study
YLL 4551.2	W303 *MATa ku70-D173G::URA3 sae2Δ::KANMX*	This study
DMP 7521/1A	W303 *MATa ku70-C85Y::URA3 sae2Δ::KANMX*	This study
DMP 7523/2A	W303 *MATa ku70-C85Y::URA3*	This study
YLL 4609.4	W303 *MATa ku70-G79S::URA3*	This study
YLL 4535.2	W303 *MATa ku70-A90T::URA3*	This study
YLL 4608.2	W303 *MATa ku70-N104Y::URA3*	This study

DMP 7586/10B	W303 *MATa ku70-D173G::URA3*	This study
YLL 941.1	W303 *MATa ku70Δ::HIS3*	(Marsella et al., 2021)
DMP 7541/7B	W303 *MATa ku70Δ::HIS3 sae2Δ::KANMX*	This study
DMP 7560/4C	W303 *MATa ku70Δ::HIS3 sae2Δ::KANMX*	This study
DMP 7609.1	W303 *MATa/a KU70-3HA::URA3/KU70-FLAG::KANMX*	This study
DMP 7739.1	W303 *MATa/a ku70-C85Y-3HA::URA3/ku70-C85Y-FLAG::KANMX*	This study
DMP 7615/1B	W303 *MATa ku70-C85Y::URA3 rad50-V1269M::KANMX*	This study
DMP 7648/6D	W303 *MATa exo1Δ::HIS3*	This study
DMP 7648/3C	W303 *MATa ku70-C85Y::URA3 exo1Δ::HIS3*	This study
DMP 7648/4D	W303 *MATa ku70-C85Y::URA3 sae2Δ::KANMX exo1Δ::HIS3*	This study
DMP 7647/6D	W303 *MATa ku70-A90T::URA3 sae2Δ::KANMX exo1Δ::HIS3*	This study
DMP 7649/2A	W303 *MATa ku70-N104Y::URA3 sae2Δ::KANMX exo1Δ::HIS3*	This study
DMP 7650/1A	W303 *MATa ku70-D173G::URA3 sae2Δ::KANMX exo1Δ::HIS3*	This study
DMP 7651/4C	W303 *MATa ku70-G79S::URA3 sae2Δ::KANMX exo1Δ::HIS3*	This study
DMP 7652/22B	W303 *MATa sae2Δ::KANMX exo1Δ::HIS3*	This study
DMP 7657/4A	W303 *MATa ku70Δ::HIS3 sae2Δ::KANMX exo1Δ::HIS3*	This study
DMP 7653/3B	W303 *MATa mre11-H125N*	This study
DMP 7641/7C	W303 *MATa ku70Δ::HIS3*	This study
DMP 7653/9A	W303 *MATa ku70-C85Y::URA3 mre11-H125N*	This study
DMP 7654/7B	W303 *MATa ku70Δ::HIS3 mre11-H125N*	This study
DMP 7660/11A	W303 *MATa ku70-C85Y::URA3 mre11Δ::HIS3*	This study
DMP 7660/9B	W303 *MATa mre11Δ::HIS3*	This study

DMP 7613/10C	W303 *MATa ku70-C85Y::URA3 sae2Δ::KANMX nej1Δ::HIS3*	This study
DMP 7614/10D	W303 *MATa sae2Δ::KANMX nej1Δ::HIS3*	This study
DMP 7612/5A	W303 *MATa ku70-C85Y::URA3 nej1Δ::HIS3*	This study
DMP 7612/1A	W303 *MATa nej1Δ::HIS3*	This study
YLL 4189.3	W303 *MATa isw2Δ::HIS3*	(Casari, et al., 2021)
DMP 7636/5D	W303 *MATa isw2Δ::HIS3 ku70Δ::HIS3 sae2Δ::KANMX*	This study
DMP 7642/8C	W303 *MATa isw2Δ::HIS3 sae2Δ::KANMX*	This study
DMP 7642/8D	W303 *MATa sae2Δ::KANMX*	This study
DMP 7643/8B	W303 *MATa isw2Δ::HIS3 ku70Δ::HIS3*	This study
DMP 7731.1	W303 *MATa/a KU70/KU70 SAE2/SAE2*	This study
DMP 7732.1	W303 *MATa/a KU70/ku70-C85Y::URA3 sae2⊿::KANMX/ sae2⊿::KANMX*	This study
DMP 7733.1	W303 *MATa/a ku70-C85Y::URA3/ku70-C85Y::URA3 sae2⊿::KANMX/ sae2⊿::KANMX*	This study
DMP 7734.1	W303 *MATa/a KU70/KU70 sae2⊿::KANMX/ sae2⊿::KANMX*	This study
YLL 4634.3	W303 *MATa ku70-Y494N::URA3 sae2⊿::KANMX*	This study
DMP 7735/9A	W303 *MATa ku70-Y494N::URA3*	This study
DMP 7736/14A	W303 *MATa ku70-Y494N::URA3 sae2⊿::KANMX exo1⊿::HIS3*	This study
DMP 7737/6B	W303 *MATa ku70-Y494N::URA3 exo1⊿::HIS3*	This study
DMP 7738/16D	W303 *MATa ku70-Y494N::URA3 rad50-V1269M::KANMX*	This study
HS21	MATα *ade5-1 his7-2 ura3⊿ trp1-289 leu2-3,112::p305L3 LEU2 lys2::AluIR*	(K. S. Lobachev et al., 2002)
YLL 4694.1	HS21 *MAT*a *rif2Δ::KANMX*	This study
YLL 4348.1	HS21 MATα *mre11-H15N::LEU2*	(Marsella et al., 2021)
YLL 4695.2	HS21 *MAT*a *rif2-S6E::HPHMX*	This study

JKM139	*MAT*a *hml*Δ::*ADE1, hmr*Δ::*ADE1*, *ade1-100, lys5, leu2-3,112, trp1::hisG ura3-52, ho, ade3::GAL-HO site*	(S. E. Lee et al., 1998)
YLL 4693	JKM139 *MAT*a *rif2-S6E::LEU2*	This study
YLL 1523.3	JKM139 *MAT*a *sae2*Δ*::KANMX*	(Gobbini et al., 2015)
DMP 7831/2B	JKM139 *MAT*a *rif2-S6E::LEU2 sae2*Δ*::KANMX*	This study
YLL 3611.1	JKM139 *MATa RIF2-18MYC::TRP1*	(Cassani et al., 2016)
YLL 4696.2	JKM139 *MATa rif2-S6E-18MYC:: TRP1::LEU2*	This study
YLL 3421.2	JKM139 *MAT*a *RAD9-3HA::TRP1*	(Clerici et al., 2014)
DMP 6911/4B	JKM139 *MAT*a *RAD9-3HA::TRP1 sae2*Δ*::KANMX*	(Colombo et al., 2019)
DMP 7832/2A	JKM139 *MAT*a *RAD9-3HA::TRP1 rif2-S6E::LEU2*	This study
DMP 7832/12B	JKM139 *MAT*a *RAD9-3HA::TRP1 rif2-S6E::LEU2 sae2*Δ*::KANMX*	This study
YLL 3188.3	JKM139 *MAT*a *MRE11-3HA::URA3*	(Cassani et al., 2018)
DMP 6867/1B	JKM139 *MAT*a *MRE11-3HA::URA3 sae2*Δ*::KANMX*	This study
DMP 7833/7C	JKM139 *MAT*a *MRE11-3HA::URA3 rif2-S6E::LEU2*	This study
DMP 7833/4B	JKM139 *MAT*a *MRE11-3HA::URA3 rif2-S6E::LEU2 sae2*Δ*::KANMX*	This study
YLL 3222.6	JKM139 *MAT*a *TEL1-3HA::NATMX*	(Cassani et al., 2018)
DMP 6435/1A	JKM139 *MAT*a *TEL1-3HA::NATMX sae2*Δ*::KANMX*	(Marsella et al., 2021)
DMP 7834/5C	JKM139 *MAT*a *TEL1-3HA::NATMX rif2-S6E::LEU2*	This study
DMP 7834/2B	JKM139 *MAT*a *TEL1-3HA::NATMX rif2-S6E::LEU2 sae2*Δ*::KANMX*	This study
DMP 7837/1B	JKM139 *MATa RAD50-3HA::URA3 RIF2-18MYC::TRP1*	This study
DMP 7838/5B	JKM139 *MATa RAD50-3HA::URA3 rif2-S6E-18MYC::TRP1::LEU2*	This study
DMP 6905/1C	JKM139 *MATa RAD50-18MYC::URA3 TEL1-3HA::NATMX*	(Cassani et al., 2019)
DMP 7839/2A	JKM139 *MATa RAD50-18MYC::URA3 TEL1-3HA::NATMX rif2-S6E::LEU2*	This study
YLL 3786.1	JKM139 *MATa RAD50-18MYC::URA3*	(Cassani et al., 2019)

DMP 7529/2D	JKM139 *MATa ku70-C85Y::URA3*	This study
YLL 4548.6	JKM139 *MATa ku70-C85Y::URA3 sae2Δ::KANMX*	This study
DMP 6433/6C	JKM139 *MATa KU70-3HA::URA3 bar1Δ::TRP1*	(Gobbini et al., 2015)
DMP 7562/2B	JKM139 *MATa ku70-C85Y-3HA::TRP1 bar1Δ::TRP1*	This study
DMP 7621/12A	JKM139 *MATa KU70-3HA::URA3 tel1-kd::LEU2 bar1Δ::TRP1*	This study
DMP 7622/24A	JKM139 *MATa ku70-C85Y-3HA::URA3 tel1-kd::LEU2 bar1Δ::TRP1*	This study
DMP 7638/19D	JKM139 *MATa KU70-3HA::URA3 isw2Δ::HPHMX bar1Δ::TRP1*	This study
DMP 6758/8B	JKM139 *MATa EXO1-MYC bar1Δ::HPHMX*	(Gobbini et al., 2018)
DMP 7655/1A	JKM139 *MATa EXO1-18MYC::TRP1 ku70Δ::URA3 bar1Δ::HPHMX*	This study
DMP 7625/4C	JKM139 *MATa EXO1-MYC ku70-C85Y::URA3 bar1Δ::HPHMX*	This study
DMP 6187/3B	JKM139 *MATa tel1-kd::LEU2*	(Gobbini et al., 2015)
YLL 4264.1	JKM139 *MATa isw2Δ::HPHMX*	(Casari et al., 2021)
YJK40.6	*MATꓕ hmlΔ hmrΔ can1 lys5 ade2 leu2 trp1 ura3 his3 ade3:: GAL-HO VII::TRP1-HO LacI-GFP::URA3 LacO::LYS5 LacO::KanR*	(Kaye et al., 2004)
YLL 1709.11	YJK40.6 *sae2Δ::NATMX*	(Clerici et al., 2005)
YLL 4697.3	YJK40.6 *rif2-S6E::HPHMX*	This study
YLL 4698.1	YJK40.6 *sae2Δ::HPHMX rif2-S6E::LEU2*	This study
YLL 3641.6	YJK40.6 *rad50-V1269M::HPHMX*	(Cassani et al., 2016)
YLL 4699.1	YJK40.6 *rad50-V1269M::KANMX rif2-S6E::HPHMX*	This study
YLL 3617.2	YJK40.6 *tel1Δ::NATMX*	(Cassani et al., 2016)
YLL 4700.2	YJK40.6 *tel1Δ::NATMX rif2-S6E::LEU2*	This study
YLL 4706	YJK40.6 *tel1-hy909::LEU2*	This study
YLL 4707	YJK40.6 *tel1-hy909::LEU2 rif2::S6E::HPHMX*	This study
YLL 4538.11	YJK40.6 *ku70-C85Y::LEU2*	This study

YLL 4540.2	YJK40.6 *ku70-C85Y::LEU2 sae2Δ::NATMX*	This study
YLL 4555.4	YJK40.6 *ku70Δ::LEU2*	This study
YLL 4558.1	YJK40.6 *ku70Δ::LEU2 sae2Δ::NATMX*	This study
YLL 1731.29	YJK40.6 *mre11Δ::NATMX*	(Clerici et al., 2005)
YLL 4574.1	YJK40.6 *ku70-C85Y::LEU2 mre11Δ::NATMX*	This study
YLL 3641.6	YJK40.6 *rad50-V1269M::HPHMX*	(Cassani et al., 2016)
YLL 4570.1	YJK40.6 *ku70-C85Y::LEU2 rad50-V1269M::HPHMX*	This study
YLL 4589.4	YJK40.6 *tel1-kd::LEU2*	This study
YLL 4587.2	YJK40.6 *tel1-kd::LEU2 sae2Δ::NATMX*	This study
YLL 4591.2	YJK40.6 *isw2Δ::LEU2*	This study
YLL 4592.11	YJK40.6 *isw2Δ::LEU2 sae2Δ::NATMX*	This study
YLL 4608.3	YJK40.6 *isw2Δ::HPHMX ku70Δ::LEU2 sae2Δ::NATMX*	This study
YLL 4635.4	YJK40.6 *ku70-Y494N::LEU2*	This study
YLL 4636.1	YJK40.6 *ku70-Y494N::LEU2 rad50-V1269M::HPHMX*	This study
YMV45	*ho hml::ADE1 mata::hisG hmr::ADE1 leu2::leu2(Asp718-SalI)- URA3-pBR332-MATa ade3::GAL::HO ade1 lys5 ura3-52 trp1::hisG*	(Vaze et al., 2002)
YLL 1621.9	YMV45 *sae2Δ::KANMX*	(Gobbini et al., 2015)
YLL 4701.2	YMV45 *rif2-S6E::LEU2*	This study
YLL 4702.3	YMV45 *sae2Δ::KANMX rif2-S6E::LEU2*	This study
YLL 4639.10	YMV45 *ku70-C85Y::LEU2*	This study
YLL 4640.4	YMV45 *ku70-C85Y::LEU2 sae2Δ::KANMX*	This study

Y190	*MATa ura3-52 his3-200 lys2-801 ade2-101 trp1-901 leu2-3 gal4⊿ gal80⊿ cyhr2 LYS2::GAL1UAS-HIS3TATA-HIS3 URA3::GAL1UAS-GAL1TATA-lacZ*	(Roisné-Hamelin et al., 2021, 2021)
tGI354	*ho hml*Δ*::ADE1 MATa-inc hmr*Δ*::ADE1 ade1 leu2-3;112 lys5 trp1::hisG ura3-52 ade3::GAL::HO arg5,6::MATa::HPHMX*	(Saponaro et al., 2010)
YLL 3914.2	tGI354 *sae2*Δ*::NATMX*	(Cassani et al., 2018)
YLL 4637.3	tGI354 *ku70-C85Y::LEU2*	This study
YLL 4638.12	tGI354 *ku70-C85Y::LEU2 sae2*Δ*::NATMX*	This study

Yeast growth media

YEP (Yeast-Extract Peptone) is the standard rich medium for *S. cerevisiae* and contains 10 g/L yeast extract, 20 g/L peptone, and 50 mg/L adenine. YEP must be supplemented with 2% glucose (YEPD), 2% raffinose (YEPR) or 2% raffinose and 3% galactose (YEPRG) as carbon source. YEP-based selective media are obtained including 400 μg/mL G418, 300 μg/mL hygromicin-B (HPH) or 100 μg/ml nourseothricin (NAT). Solid media are obtained including 2% agar. Stock solutions are 50% glucose, 30% raffinose, 30% galactose, 80 mg/mL G418, 50 mg/mL hygromicin-B, 50 mg/mL nourseothricin. YEP and glucose stock solution are autoclave-sterilized and stored at RT. Sugars and antibiotics stock solutions are sterilized by microfiltration and stored at 30°C/37°C and -20°C, respectively. S.C. (Synthetic Complete) is the minimal growth medium for *S. cerevisiae* and contains 1.7 g/L YNB (Yeast Nitrogen Base) without amino acids, 5 g/L ammonium sulphate, 200 μM inositol, 25 mg/L uracil, 25 mg/L adenine, 25

mg/L hystidine, 25 mg/L leucine, 25 mg/L tryptophan. S.C. can be supplemented with drop-out solution (20 mg/L arginine, 60 mg/L isoleucine, 40 mg/L lysine, 10 mg/L methionine, 60 mg/L phenylalanine, 50 mg/L tyrosine), based on yeast strains requirements. One or more amino acid/base can be omitted to have S.C selective media (e.g., S.C. -ura is S.C. lacking uracil). Solid media are obtained by including 2% agar. Stock solutions are 17 g/L YNB + 50 g/L ammonium sulphate (or 10 g/L monosodic glutamic acid), 5 g/L uracil, 5 g/L adenine, 5 g/L hystidine, 5 g/L leucine, 5 g/L tryptophan, 100X drop out solution (2 g/L arginine, 6 g/L isoleucine, 4 g/L lysine, 1 g/L methionine, 6 g/L phenylalanine, 5 g/L tyrosine), 20 mM inositol. All these solutions are sterilized by micro-filtration and stored at 4°C. VB sporulation medium contains 13.6 g/L sodium acetate, 1.9 g/L KCl, 0.35 g/L MgSO4, 1.2 g/L NaCl and pH is adjusted to 7.0. To obtain solid medium include 2% agar. Media are autoclave sterilized.

Synchronization of yeast cells with α-factor

By using α-factor, it is possible to synchronize a population of yeast cells in G1 phase of the cell cycle. This pheromone activates a signal transduction cascade that arrests the cell cycle in G1 phase. Only *MATa* cells are responsive to α-factor. To synchronize a population of exponentially growing yeast cells in YEPD, 2 μg/mL α-factor are added to cell cultures at the concentration of around $8x10^6$ cells/mL. If the percentage of budded cells falls below 5%, cells are considered G1- arrested. To detect end-tethering, cells are then washed and resuspended in fresh medium with 5 μg/mL α-factor to maintain G1-arrested cells.

Synchronization of yeast cells with nocodazole

By using nocodazole, it is possible to synchronize a population of yeast cells in G2 phase of the cell cycle. This drug causes the depolymerization of microtubules, thus activating the mitotic checkpoint which arrests cell cycle at the metaphase to anaphase transition. To synchronize a population of exponentially growing yeast cells in YEPD, 5 μg/mL nocodazole, together with DMSO at a final concentration of 1% (use a stock solution of nocodazole 0,5 mg/mL in 100% DMSO), are added to cell cultures at the concentration of around $8x10^6$ cells/mL. If the percentage of dumbbell cells reaches 95%, cells are considered G2-arrested. To detect end-tethering, cells are then washed and resuspended in fresh medium with 15 μg/mL nocodazole to maintain G2-arrested cells.

Transformation of *S. cerevisiae* cells

YEPD exponentially growing yeast cells are harvested by centrifugation and washed with 1 mL 1 M lithium acetate (LiAc) pH 7.5. Cells are then resuspended in 1 M LiAc pH 7.5 to obtain a cells/LiAc 1:1 solution. 24 μL cells/LiAc are incubated 1 hour at RT with 90 μL 50% PEG (PolyEthylene Glycol) 4000, 8 μL carrier DNA (salmon sperm DNA) and 4-10 μL PCR DNA of interest (divide these quantities for transformation with plasmids). After the addition of 12 μL 60% glycerol, cells are incubated at RT for 1 hour, heat-shocked at 42°C for 10-20 minutes and plated on appropriate selective medium.

Search for *ku70* mutations that suppress the DNA damage sensitivity of *sae2*Δ cells

To search for *ku70* alleles that suppress the *sae2*Δ sensitivity to different genotoxic agents, genomic DNA from strains carrying the *URA3* gene located 500 bp upstream of the *KU70* ORF was used as template to amplify by low-fidelity PCR the *KU70* coding region, respectively. Thirty independent PCR reaction mixtures were prepared, each containing 5U EuroTaq DNA polymerase (Euroclone), 10 ng genomic DNA, 500 ng each primer, 0.5 mM each dNTP (dATP, dTTP, dCTP), 0.1 mM dGTP, 0.5 mM MnCl2, 10 Mm Tris-HCl pH 8.3, 50 mM KCl, and 1.5 mM MgCl2. The resulting PCR amplification products, containing the *KU70* coding sequence and the *URA3* marker gene, were used to transform a *sae2*Δ strain (YLL1069.3). 3000 transformants were selected on synthetic medium without uracil and then assayed by drop tests for decreased sensitivity to phleomycin compared to *sae2*Δ cells.

Extraction of yeast genomic DNA (Teeny yeast DNA preps)

Around $5x10^8$ yeast cells from overnight exponentially growing cultures (or cultures treated to induce damage) are harvested by centrifugation and washed with 1 mL of a 0.9 M sorbitol, 0.1 M EDTA pH 7.5 solution. Dried pellet can eventually be stored -20°C or it can be resuspended in 400 µL of the previous solution supplemented with 14 mM β-mercaptoethanol. Yeast cells wall is digested by 1-hour incubation at 37°C with 0.4 mg/mL 20T zymolyase. Spheroplasts are harvested by 1 minute centrifugation and resuspended in 400

μL 1X TE (10 mM Tris-HCl pH 7.5, 1 mM EDTA pH 7.5). After addition of 90 μL of a solution containing 278 mM EDTA pH 8.5, 445 mM Tris-base and 2.2% SDS, spheroplasts are incubated 30 minutes at 65°C. Following the addition of 80 μL 5M potassium acetate, samples are kept on ice for 1 hour. Cell residues are eliminated by 30 minutes centrifugation at 4°C. DNA is then precipitated with chilled 100% ethanol, resuspended in 500 μL 1X TE and incubated 1 hour with 2,5 μL 1 mg/mL RNase to eliminate RNA. DNA is then precipitated with 500 μL isopropanol and resuspended in the appropriate volume of 1X TE solution.

Polymerase Chain Reaction (PCR)

PCR allows to obtain high copy number of a specific DNA fragment starting from a very low quantity of DNA. The reaction is directed to the DNA fragment of interest, by using a couple of oligonucleotides flanking the specific DNA sequence. These oligonucleotides work as primers for the DNA polymerase. The reaction consists of several polymerization cycles, based on 3 main temperature-dependent steps: denaturation of DNA (which occurs over 90°C), primer annealing to the DNA (it typically takes place at 45-60°C depending on primers features), synthesis of the sequence of interest by a thermophilic DNA polymerase (which usually works at 72°C). Different polymerases with different properties (processivity, fidelity, working temperature) are commercially available and suitable for different purposes.

Taq polymerase is generally used for analytical or mutagenic PCR. High-fidelity polymerases, like Phusion, VENT and Q5 polymerases, are generally employed when 100% accuracy is required. The typical 50 μL PCR mixture contains 1μL template DNA, 0.5 μM each primer, 200 μM dNTPs, 5 μL 10X

Reaction Buffer, 1 mM MgCl2, 1-2 U DNA polymerase and water to 50 μL. The typical cycle-program for a reaction is as follows: step 1, 2 minutes denaturation at 94- 95°C; step 2, 30 seconds denaturation at 94-95°C; step 3, 1 minute annealing at primers Tm (melting temperature); step 4, 1 minute synthesis per kb at 72°C; step 5, return to step 2 and repeat 30 times; step 6, 10 minutes at 72°C. The choice of primers sequences determines the working Tm, which depends on the length (L) and GC% content of the oligonucleotides and can be calculated as follows: Tm (°C) = 59.9 + 0.41(GC%) – 675/L.

Agarose gel electrophoresis

Agarose gel electrophoresis is the easiest and most common way to separate and analyze DNA molecules. This technique allows the separation of DNA fragments based on their different molecular weight (or length in kb). The purpose of this technique might be to visualize the DNA, to quantify it or to isolate a particular DNA fragment. The DNA is visualized by the addition in the gel of Ethidium Bromide (EtBr), a fluorescent dye that intercalates between the bases of nucleic acids. Ethidium Bromide absorbs UV light and emits the energy as visible orange light, revealing the DNA molecules to which it is bound. To pour a gel, agarose powder is mixed with 1X TAE (0.04 M TrisAcetate, 0.001 M EDTA) to the desired concentration, and the solution is heated until it is completely melted. Most gels are between 0.8% and 2% METHODS - 195 - agarose. A 0.8% gel displays good resolution of large DNA fragments (5-10 Kb), while a 2% gel shows good resolution of small fragments (0.2-1 Kb). Ethidium Bromide is added to the gel at a final

concentration of 1 μg/mL to facilitate visualization of the DNA after electrophoresis. After cooling the gel solution to about 60°C, it is poured into a casting tray containing a sample comb and it is allowed to solidify at RT or at 4°C. Then, the gel is placed into an electrophoresis chamber, it is covered with 1X TAE buffer, and the comb is removed. Samples containing DNA mixed with loading buffer are pipetted into the sample wells. The loading buffer contains 0.05% bromophenol blue and 5% glycerol, which give colour and density to the sample. A marker containing DNA fragments of known length and concentration is loaded in parallel to determine the size and the quantity of DNA fragments in the samples. Current is applied and DNA migrates toward the positive electrode. When adequate migration has occurred, DNA fragments are visualized by placing the gel under an UV transilluminator.

Spot assays

Cells grown overnight were diluted to $1x10^7$ cells/ml. 10-fold serial dilutions were spotted on YEPD with or without indicated concentrations of DNA damaging drugs. Plates were incubated for three days at 25°C or 30°C.

Yeast two-hybrid analysis

Yeast two-hybrid assays were performed by co-transforming GBD and GAD (Gal4-activating domain) plasmids (in the pGBKT7 and pGADT7 vectors) in various combinations in the PJ69-4A budding yeast strain (*MATa trp1-901 leu2-3,112 ura3-52 his3-200 gal4 gal80 LYS2::GAL1-HIS3 GAL2-ADE2*

met2::GAL7-lacZ). Transformants were screened for interaction by spotting 5-fold dilutions on minimal plates lacking tryptophan and leucine for selection of GBD and GAD plasmids, respectively. Interactions were assessed by analysis of the expression of the *HIS3* markers by plating on minimal medium lacking histidine. The plates were then incubated at 30 °C for 3 (SC-leu-trp) or 4 (selective plates) days.

Plasmid relegation assay

The centromeric pRS316 plasmid was digested with the *Bam*HI restriction enzyme before being transformed into the cells. Parallel transformation with undigested pRS316 DNA was used to determine the transformation efficiency. Efficiency of religation was determined by counting the number of colonies that were able to grow on medium selective for the plasmid marker and was normalized respect to the transformation efficiency for each sample. The religation efficiency in mutant cells was compared to that of wild-type cells that was set up to 100%.

Recombination assay

To measure recombination frequency, we used a strain carrying the lys2::I-*Sce*I recipient allele at the *LYS2* locus on chromosome II containing an I-*Sce*I cleavage site, the *lys2* donor allele (*lys2Δ3'*) at the *CAN1* locus on chromosome V and a galactose-inducible I-*Sce*I gene inserted at the *HIS3* locus on chromosome XV (*his3D::kanMX-pGAL*-I-*Sce*I) (Guo et al., 2017). I-*Sce*I expression was induced by adding galactose (1% final) to cells growing

exponentially in YEPR. Following galactose addition, cells were plated on YEPD and SC-lys media, incubated at 30°C and repair frequencies were calculated as the ratio of Lys^+ to total colonies. Data for each strain were based on at least three independent experiments, with 15 independent cultures per experiment.

Analysis of DSB resection at MAT locus (Southern blot method)

YEPR exponentially growing cell cultures of JKM139 derivative strains, carrying the HO cut site at the *MAT* locus, were transferred to YEPRG at time zero. Genomic DNA was extracted at different time points following the induction of the HO endonuclease. The *Sp*I-digested genomic DNA was precipitated by adding 0.3 M NaAc pH 5.2, 5 mM EDTA pH 8, and two volumes EtOH 100%. After chilling overnight, samples are centrifuged 30 minutes at 4°C and pellet is resuspended in alkaline gel loading buffer (50 mM NaOH, 1 mM EDTA pH 8, 2.5% Ficoll (type 400), and 0.025% bromophenol blue). Denatured DNA is loaded onto a 0.8% agarose gel, previously equilibrated in alkaline electrophoresis buffer (50 mM NaOH, 1 mM EDTA pH 8), and a glass plate is placed on the gel to prevent the dye diffusing from the agarose during the run. Denaturing gel is run slowly at low voltages (e.g., 30V overnight). After the DNA has migrated about 14 cm, the gel can be stained with 0.5 μg/mL Ethidium Bromide in 1X TAE buffer for 1 hour and DNA is visualized by placing the gel under an UV transilluminator. Gel is then soaked in 0.25 N HCl for 7 minutes with gentle agitation, rinsed with water for 10 minutes, soaked in 0.5 NaOH, 1.5 M NaCl for 30 minutes and rinsed

again with water for 10 minutes. DNA is blotted overnight by capillary transfer onto neutral nylon membrane using 10X SSC. Membrane is then neutralized in 0.5M Tris-HCl pH 7.5, 1 M NaCl, air dried and UV-crosslinked. Hybridization is carried out by incubating the membrane for 5 hours at 42°C with pre-hybridization buffer (5X SSPE, 50% formamide, 4X denhardt's solution +BSA, 6% destran sulphate, 100 µg/mL salmon sperm DNA, 200 µg/mL tRNA carrier), followed by overnight incubation at 42°C with the pre-hybridization buffer supplemented with the single-stranded RNA (ssRNA) probe, that anneals with the unresected strand at one side of the HO-induced DSB (Casari et al., 2021). This probe was obtained by *in vitro* transcription using Promega Riboprobe System-T7 and plasmid pML514 as a template. Plasmid pML514 was constructed by inserting in the pGEM7Zf *Eco*RI site a 900-bp fragment containing part of the *MAT* locus (coordinates 200870 to 201587 on chromosome III) and labelling it with [α-32P]-UTP. Following hybridization, membrane is washed twice with 5X SSPE (20X SSPE: 3 M NaCl, 200 mM NaH_2PO_4, 20mM EDTA, pH 7.4) at 42°C for 15 minutes; 30' with 1X SSPE 0.1%, SDS at 42°C; 30 minutes with 0.1X SSPE, 0.1% SDS at 42°C; twice with 0.2X SSPE 0.1%, SDS at 68°C for 15 minutes; and 5 minutes with 0.2X SSPE at RT. Finally, membrane is air dried and exposed to an autoradiography film. Quantitative analysis of DSB resection was performed by calculating the ratio of band intensities for ssDNA and total amount of DSB products. The resection efficiency was normalized with respect to the HO cleavage efficiency for each time point. The amount of ssDNA was normalized to cut efficiency by subtracting the value of the uncut band from the total amount of DSB products for each time point. Densitometric analysis of band intensities was performed using Scion Image Beta 4.0.2 software.

Southern blot analysis of telomere length

To determine the length of native telomeres, genomic DNA was extracted from YEPR exponentially growing cell cultures of W303 derivative strains. The *Xho*I-digested genomic DNA was precipitated by adding 0.3 M NaAc pH 5.2, 5 mM EDTA pH 8.0, and two volumes EtOH 100%. After chilling overnight, samples are centrifuged 30 minutes at 4°C and pellet is resuspended in a gel-loading buffer with 0.025% bromophenol blue. *Xho*I-digested genomic DNA was subjected to 0.8% agarose gel electrophoresis at low voltages (e.g., 60V overnight). After the DNA has migrated about 20 cm, the gel can be stained with 0.5 μg/mL Ethidium Bromide in 1X TAE buffer for 1 hour and DNA is visualized by placing the gel under an UV transilluminator. Gel is then soaked with gentle agitation in 0.2 M NaOH, 0.6 M NaCl solution for 45 minutes, rinsed with water for 10 minutes, soaked in 1.5 M NaCl, 1 M Tris pH 7.4 solution for 45 minutes and rinsed again with water for 10 minutes. DNA is blotted overnight by capillary transfer onto neutral nylon membrane using 10X SSC. Membrane is then air dried and UV-crosslinked. Hybridization is carried out by incubating the membrane for 5 hours at 55°C with pre-hybridization buffer (0.5 M $NaPO_4$ pH 7.2, 1 mM EDTA pH 7.5, SDS 7%, BSA 1%), followed by overnight incubation at 55°C with the pre-hybridization buffer supplemented with a ^{32}P-labeled poly(GT) probe. This probe anneals with telomeric DNA, and it was obtained by *in vitro* transcription using DECAprime II kit (Thermo Fisher Scientific) and labelling it with [α-^{32}P] ATP. Following hybridization, membrane is washed twice with 0.2 M $NaPO_4$ pH 7.2, SDS 1% solution at 55°C for two hours. Finally, membrane is air dried and exposed to an autoradiography film.

DSB repair by SSA

DSB repair by SSA in YMV45 strains were detected by Southern blot analysis using an Asp718-*Sal*I fragment containing part of the *LEU2* gene as a probe (Trovesi et al., 2011). To determine the efficiency of DSB repair by SSA, the normalized intensity of the SSA product band was divided by the total amount of SSA and cut products, and it was normalized to cut efficiency by subtracting the value of the uncut band from the total amount of DSB products for each time point.

DSB repair by ectopic recombination

DSB repair by ectopic recombination was detected by Southern blot method in tGI354 background (Trovesi et al., 2011). To determine the repair efficiency, the intensity of the uncut band at 2h after HO induction (maximum efficiency of DSB formation) was subtracted to the normalized values of NCO and CO bands at the subsequent time points after galactose addition. The obtained values were divided by the normalized intensity of the uncut *MATa* band at time zero before HO induction (100%).

Western blotting

Protein extracts for western blot analysis were prepared by trichloroacetic acid (TCA) precipitation. Total protein extracts are prepared from $1x10^8$ cells, collected from exponentially growing yeast cultures (or cultures treated to induce damage). Cells are harvested by centrifugation, washed with 1 mL 20% trichloracetic acid (TCA) to prevent proteolysis, and then resuspended in 100

or 200 µL 20% TCA. After the addition of acid-washed glass beads, the samples were vortexed for 10 min. The beads were washed with 200 µL of 5% TCA twice and the extract was collected in a new tube. The crude extract was precipitated by centrifugation at 850 xg for 10 min. TCA was discarded and samples were resuspended in 70 µL 6X Laemmli buffer (60 mM Tris, pH 6.8, 2% SDS, 10% glycerol, 100mM DTT, 0.2% bromophenol blue) and 30 µL 1M Tris pH 8.0. Prior to loading, samples were boiled at 100°C for 2 minutes and centrifuged at 850xg for 10 min. Supernatant containing the solubilized proteins were separated on 10% polyacrylamide gels. (10% Running gel: 375 mM Tris-HCl pH 8.8, 0,1% SDS, 10% Acrylamide, 0,13% Bisacrylamide, 0,1% APS, 0.001% Temed – Stacking gel: 125 mM Tris-HCl pH 6.8, 0,1% SDS, 5% Acrylamide, 0,14% Bisacrylamide, 0,1% APS, 0.001% Temed). Proteins are separated based on their molecular weight by polyacrylamide gel electrophoresis in the presence of sodium dodecyl sulphate (SDS-PAGE). When adequate migration has occurred, proteins are blotted onto nitrocellulose membrane. Membrane is usually saturated by 1-hour incubation in 1X TBS (150 mM NaCl, 50 mM Tris-HCl pH 8) supplemented with 4% milk and 0.2% triton X-100. Membranes are then incubated for 2 hours with primary antibodies (in 1X TBS + 4% milk + 0.2% triton) and washed three times for 10 minutes with 1X TBS. Subsequently membranes are incubated for 1 hour with secondary antibodies (in 1X TBS + 4% milk + 0,2% triton) and again washed three times with 1X TBS. Detection is performed with ECL (Enhanced ChemiLuminescence - Genespin) and autoradiography films according to the manufacturer. HA- or Myc- or Flag-tagged proteins were detected by using anti-HA (12CA5) (1:2000) or anti-Myc (9E10) (1:1000) or anti-Flag (F1804 by Sigma) (1:500) antibodies, respectively.

Coimmunoprecipitation (CoIP)

$2x10^9$ exponentially growing cells are collected by centrifugation, washed with water, and put on ice. Total protein extracts were prepared by breaking cells in 400 µl of buffer containing 50 mM HEPES pH 7.5, 300 mM NaCl, 20% glycerol, 1 mM sodium orthovanadate, 60 mM β- glycerophosphate, 1mM phenylmethylsulfonyl fluoride (PMSF) and protease inhibitor cocktail (Roche Diagnostics). 200 µL glass beads are added and cells are mechanically disrupted by 14 breakage cycles composed by 30 seconds vortexing and 30 seconds interval each. Glass beads are then washed with 200 µL cold breaking buffer and the resulting extracts, once separated from the beads, are centrifuged at 4°C at 14000 rpm for 20 minutes. Clarified and quantified protein extracts were incubated for 2 h at 4°C with 50 µl of Protein G-Dynabeads and 5 µg anti-MYC (9E10) or anti-HA (12CA5) antibodies. 15 µL normalized extracts are kept as "input". The resins were then washed twice with 1 ml of breaking buffer. IP samples are finally mixed with 30 µL of Laemmli buffer (15 µL for input samples) and boiled for 3 minutes. Bound proteins were visualized by western blotting with anti-HA (12CA5) (1:2000) or anti-Myc (9E10) (1:1000) antibodies after electrophoresis on a 10% or 15% SDS-polyacrylamide gel.

Chromatin immunoprecipitation (ChIP) and qPCR

YEPR exponentially growing cell cultures (50 mL at concentration of $8x10^6$ cells/mL) of JKM139 derivative strains, carrying the HO cut site at the *MAT* locus, were transferred to YEPRG at time zero. Crosslinking was done with 1% formaldehyde for 5 min (Mre11), 10 min (Rad9 and Exo1) or 15 min (Rif2, Tel1, H3 histone and H2A histone). The reaction was stopped by adding 0.125

M Glycine for 5 min. Treated cells are kept on ice until centrifugation at 3000 rpm for 5 minutes at 4°C. Cell pellet is washed with 30 mL HBS buffer (50 mM HEPES pH 7.5, 140 mM NaCl) and then with 25 mL ChIP lysis buffer (50 mM HEPES pH 7.5, 140 mM NaCl, 1 mM EDTA pH 8,1% IGEPAL CA-630, 0.1% Sodium deoxycholate). After centrifugation at 3000 rpm for 5 minutes, the supernatant is carefully and completely removed. Then 0.4 mL of ChIP lysis buffer, supplemented with complete anti-proteolitic tablets (Roche) and 1 mM phenylmethylsulfonyl fluoride (PMSF), is added and samples are resuspended and stored at -80°C. The following day, cells are broken at 4°C with glass beads by mechanical disruption. After breaking cells, the glass beads are eliminated. This passage is followed by centrifugation at 4°C at 14000 rpm for 30 minutes. Pellet is resuspended in 0.5 mL ChIP lysis buffer, supplemented with antiproteolitics and PMSF, and then sonicated (5 cycles of 25 seconds at 40% power output), to share DNA in fragments of 500-1000 bp. After centrifugation at 4°C at 10000 rpm for 5 minutes 460 µL supernatant are retained and further clarified by centrifugation at 4°C at 10000 rpm for 15 minutes. 400 µL of clarified supernatant are immunoprecipitated with Dynabeads coated with specific antibodies, while 5 µL supernatant are kept as "input DNA".

Immunoprecipitation was performed by incubating samples with Dynabeads Protein G (Thermo Fisher Scientific) for 3 h at 4°C in the presence of 5 µg anti-HA (12CA5) or anti-Myc antibodies (9E10). H2A and H3 histones were immunoprecipitated by using 5 µg anti-H2A (39945, Active Motif) and 4 µg anti-H3 (ab1791, Abcam) antibodies, respectively. After 3 hours incubation with the desired antibodies, dynabeads are washed RT as follow: twice with SDS buffer (50 mM HEPES pH 7.5, 1 mM EDTA pH 8, 140 mM NaCl,

0.025% SDS), once with High-Salt buffer (50 mM HEPES pH 7.5, 1 mM EDTA pH 8, 1 M NaCl), once with T/L buffer (20 mM Tris-HCl pH 7.5, 250 mM LiCl, 1 mM EDTA pH 8, 0.05% sodium deoxycholate, 0.5% IGEPAL CA630), and finally twice with T/E buffer (20 mM Tris-HCl pH 7.5, 0.1 mM EDTA pH 8). All the washes are done by pulling down Dynabeads and then nutating them for 5 minutes with the specific washing buffer. After the last wash, Dynabeads are resuspended in 145 µL 1X TE + 1% SDS, shaked on a vortex for 2 minutes, kept at 65°C for 10 minutes, shaked on vortex again and then pulled down. Then, 120 µL of the supernatant are put at 65°C overnight for reverse cross-linking. Also, the previously taken input DNA samples must be put at 65°C overnight after the addition of 115 µL of 1X TE + 1% SDS buffer. The next day DNA is purified by using QIAGEN QIAquick PCR purification kit. 600 µL PB buffer are added to each sample and, after vortexing, the sample is loaded onto spin columns, followed by centrifugation at 5000 rpm for 1 minute. 400 µL PE buffer are added to the columns, followed by centrifugation at 14000 rpm for 1 minute, then 300 µL PE buffer are added to the columns again and, after 5 minutes waiting, columns are centrifuged at 14000 rpm for 2 minutes. Finally, 25 µL EB buffer are added in the columns and, after 1-minute incubation, DNA is eluted by centrifuging at 14000 rpm for 1 minute. Elution is repeated a second time in the same way, then input DNA is diluted 1:50 in EB buffer. Quantification of immunoprecipitated DNA was achieved by qPCR on a Bio-Rad CFX Connect™ Real-Time System apparatus or on a Bio-Rad MiniOpticon apparatus and by using Bio-Rad CFX Maestro 1.1 software. Triplicate samples in 20 µl reaction mixture containing 10 ng of template DNA, 300 nM for each primer (located at different distances from the HO-induced DSB and at the

ARO1 locus of chromosome IV), 2× SsoFast™ EvaGreen® supermix (Bio-Rad #1725201) (2X reaction buffer with dNTPs, Sso7d-fusion polymerase, MgCl2, EvaGreen dye and stabilizers) were run in white 96-well PCR plates Multiplate (Bio-Rad #MLL9651) or 48-well PCR plates Multiplate (BioRad #MLL4851). The qPCR program was as follows: step 1, 98°C for 2 min; step 2, 90°C for 5 s; step 3, 60°C for 15 s; step 4, return repeat 40 times from step 2. At the end of the cycling program, a melting program (from 65°C to 95°C 23 with a 0.5°C increment every 5 s) was run to test the specificity of each qPCR. Data are expressed as fold enrichment at the HO-induced DSB over that at the non-cleaved *ARO1* locus, after normalization of the ChIP signals to the corresponding input for each time point. Fold enrichment was then normalized to the efficiency of DSB induction (cut efficiency). For histone loss, the fold enrichment from each sample after HO induction was divided by the fold enrichment from uninduced cells, and log2 of the resulting values was calculated.

Rad50 and Rif2 purification and ATPase assay

Rad50 and Mre11 were expressed in yeast cells and purified as previously described (Cassani et al., 2016). To assemble the Mre11-Rad50 complex, Rad50 and Mre11 were incubated together for 5 h on ice and separated from unassembled proteins in a Sephacryl S-400 gel filtration column. To express recombinant Rif2 and Rif2^{S6E}, *RIF2* and *rif2-S6E* genes were chemically synthetized (GenScript, Piscataway, NJ, USA), cloned in frame with a C-terminal 6xHis-Tag into the pET21a vector and introduced in *Escherichia coli*

BL21 (DE3) cells. To purify Rif2 and Rif2^{S6E}, the corresponding proteins were produced in ZYM-5052 medium supplemented with ampicillin (100 mg/L), extracted and purified as previously described (Cassani et al., 2016). Fractions containing the highest amount of protein were pooled and buffer-exchanged with 10 mM ammonium acetate pH 7.0 by gel filtration on PD-10 columns (GE Healthcare, Little Chalfont, UK). Samples were lyophilized in a freeze-dryer (Heto FD1.0, Gemini BV, Apeldoorn, the Netherlands) and stored at −20 °C. Protein concentration was determined with the Bradford assay (Bio-Rad, Hercules, USA), using bovine serum albumin as a standard. The ATPase assay was performed as previously described (34). Briefly, wild-type Mre11-Rad50 (100 nM), Rif2 (2 μM) and Rif2^{S6E} (2 μM) were used in the presence of 100-bp dsDNA (200 nM) and 50 μm [α-^{32}P]ATP. Radioactive ATP and ADP were separated by thin layer chromatography.

Recombinant production and purification of Ku heterodimers

The bicistronic constructs containing Ku70-Strep or Ku70^{C85Y}-Strep and Ku80-6xHis were designed as previously described (Hanakahi, 2007). In particular, the genes were chemically synthetized (GenScript, Piscataway, NJ, USA) and cloned into the pET21a vector. Ku heterodimers were recombinantly produced in *Escherichia coli* BL21 (DE3) cells and purified. Briefly, the Ku70–Ku80 and Ku70^{C85Y}–Ku80 heterodimers were produced in ZYM-5052 medium (Studier, 2005) supplemented with ampicillin (100 mg/L), extracted and purified by immobilized ion metal affinity chromatography

(ABT, Torrejon de Ardoz, Madrid, Spain), followed by Strep purification on Strep-Tactin resin (IBA Lifesciences, Gottingen, Germany). Fractions containing the highest amount of protein were pooled and buffer-exchanged with HEPES buffer (HEPES 25 mM, NaCl 100 mM, pH 7) by gel filtration on PD-10 columns (GE Healthcare, Little Chalfont, UK). Protein concentration was determined with the Bradford assay (Bio-Rad, Hercules, USA), using bovine serum albumin as a standard. SDS-PAGE was performed on 12% polyacrylamide gels and stained with Gel-Code Blue (Pierce, Rockford, USA) after electrophoresis. Broad-range, pre-stained molecular-mass markers (GeneSpin, Milan, Italy) were used as standards.

Size-exclusion chromatography (SEC) analysis

The quaternary structure of Ku70–Ku80 and Ku70^{C85Y}–Ku80 was determined by SEC with an NGC Quest 10 Plus Chromatography System (Bio-Rad, California, USA), equipped with a Superdex 200 10/30 column (GE Healthcare, Little Chalfont, UK) with a cutoff of 10–600 kDa. Chromatographic separations were carried out in HEPES buffer (HEPES 25 mM, NaCl 100 mM, pH 7) as the mobile phase, at a flow rate of 0.5 ml/min and a protein concentration of 0.5 mg/ml; chromatograms were recorded at 280 nm. The molecular weight was determined using a calibration curve made with the following standards: M-βGal (450.93 kDa), yeast alcohol dehydrogenase (150 kDa), BSA (66.5 kDa), Lipase B of *Candida antarctica* (34.7 kDa), green fluorescence protein (27.5 kDa), and cytochrome c (horse heart, 12.4 kDa). For each standard protein the distribution coefficient (K_d) was calculated using the following equation:

$$Kd = \frac{V_E - V_0}{V_T - V_0}$$

where V_E is the elution volume, V_0 is the void volume, which is determined with blue dextran (2000 kDa), and V_T is the total volume, determined with Uracil (0.112 kDa). The calibration curve Log(MW) versus K_d was built and the interpolated linear equation was used to calculate Ku70–Ku80 and Ku70^{C85Y}–Ku80 molecular weight from their K_d values. Experiments were performed in triplicate.

Electrophoretic mobility shift assay (EMSA)

EMSA was performed by incubating 13 nM of 21 bp ^{32}P-labeled dsDNA (5'-CCGCACACCCACACACCAGTG-3') with purified Ku70–Ku80 and Ku70^{C85Y}–Ku80 (0; 26; 39; 52; 78; 104 nM) in ice for 30 min in binding buffer (100 mM NaCl, 25 mM Tris/HCl pH 7.5, 2 mM MgCl2, 7% (v/v) glycerol and 1 mM DTT) to a final volume of 50 µl. Reactions were loaded on a non-denaturing 6% acrylamide/bisacrylamide gel and separated by running for 4 hours at 120 V at 4 °C using a low-ionic strength buffer (6.73 mM Tris–HCl pH 7.5, 3.3 mM NaOAc pH 5, 1 mM EDTA). The gel was soaked for 15 min in 10% methanol, 10% acetic acid solution and vacuum-dried, and exposed to an autoradiography film.

Molecular modeling

The structural models for Ku70^{C85Y} mutant protein within the Ku70–Ku80 heterodimer were prepared starting from the crystal structure (PDB ID:

5Y58). PDB file was processed with MAESTRO (Schrödinger Release 2022-2: Maestro, Schrödinger, LLC, New York, NY, 2021) using the Protein Preparation Wizard tool (Sastry et al., 2013) to add missing hydrogen atoms and assign proper bond orders, and with PRIME (Jacobson et al., 2004) to fill in missing loops and side chain atoms. The mutation was generated in MAESTRO replacing the original side chains with the mutated residue tool. The regions in a range of 10 Å from the mutation were minimized using MACROMODEL (Schrödinger Release 2022-2: MacroModel, Schrödinger, LLC, New York, NY, 2021). Minimizations were carried on using AMBER force field (Weiner et al., 1986) with implicit solvent, using PRCG method with maximum iteration of 2500 and a gradient convergence threshold of 0.05. In order to investigate the interaction of Ku70–Ku80 and Ku70^{C85Y}–Ku80 heterodimer with DNA, the structure of a Ku-bound DNA (sequence 5'-TAAACTAAAAAC-3') was extracted from the crystal of the human Ku complex (PDB ID: 1JEY). The DNA end was blunted by removal of the protruding end and submitted as a binding partner to HADDOCK2.4 server (Jacobson et al., 2004) together with Ku70–Ku80 or Ku70^{C85Y}–Ku80 heterodimer. The interface was defined by a constraint for active residues comprising the conserved positive residues facing the β-barrel in each heterodimer, such as R73, R265, R298 and K333 for Ku70 and R41, R210, R258, K401 and K402 for Ku80. The best position for DNA within the Ku–DNA complex was obtained with the Ku70^{C85Y}–Ku80 complex and adopted for the wild-type complex as well. The HADDOCK2.4 refinement protocol (Neijenhuis et al., 2022) was used to refine the models of wild-type Ku70–Ku80 and Ku70^{C85Y}–Ku80 heterodimers with the DNA molecule described above, with the minimized energy protocol with standard parameters

(https://wenmr.science.
uu.nl/haddock2.4/settings#refinement). This minimization protocol performs a series of short molecular dynamics (MD) simulations with explicit solvent after a solvent shell is built around the complex with position restraint on the α backbone of the protein, thus allowing the amino acids chains to move. Next, 1250 MD steps are performed at 300 K with position restraints for residues not involved in intermolecular contacts within 5 Å. Finally, the system is cooled down (1000 MD steps at 300, 200 and 100 K) with position restraints on the heavy atoms of the protein complex, excluding the interface atoms. The protocol output is the energetically lowest conformation for the complex and the corresponding HADDOCK score, which is an indicator of the interaction strength (HADDOCK-score$_{itw}$ = 1.0*E_{vdw} + 0.2*E_{elec} + 1.0*E_{desolv} + 0.1*E_{air}, where E_{vdw} is the van der Waals energy, E_{elec} is the electrostatic energy, E_{desolv} is the desolvation energy and E_{air} is the restraint violation energy, which is not added in refinement since no ambiguous interaction restraints are imposed).

Computational structural models for the complex between the 1-36 aa region of *S. cerevisiae* Rif2 and Rad50 monomer were built by AlphaFold-Multimer v3 on Colab Pro (https://colab.research.google.com/github/sokrypton/ColabFold/blob/main/AlphaFold2.ipynb) with pb100 template mode. The confidence of the models was assessed by the LDDT parameter and multimer metric, with the following final parameters for the top rank model: pLDDT=85.8, pTM=0.832, ipTM=0.768. Visual inspection was performed to assess that the amino acids previously identified as directly involved in the interaction were part of the predicted interface, in detail F8 for Rif2 and K6,

K81, and I93 for Rad50. Structures were visualized with UCSF Chimera 1.17 (https://www.cgl.ucsf.edu/chimera/). Structural superposition was also achieved with UCSF Chimera.

Quantification and statistical analysis

Quantification and statistical analysis were performed using Microsoft Excel Professional 365 software or PRISM (GraphPad). Data are expressed as mean values ± standard deviation (s.d). P-values were determined by using unpaired two-tailed t-test. No statistical methods or criteria were used to estimate size or to include or exclude samples.

REFERENCES

Adkins, N. L., Niu, H., Sung, P., & Peterson, C. L. (2013). NUCLEOSOME DYNAMICS REGULATE DNA PROCESSING. *Nature Structural & Molecular Biology*, *20*(7), 836. https://doi.org/10.1038/nsmb.2585

Aguilera, A., & García-Muse, T. (2013). Causes of genome instability. *Annual Review of Genetics*, *47*, 1–32. https://doi.org/10.1146/annurev-genet-111212-133232

Aguilera, A., & Gómez-González, B. (2008). Genome instability: A mechanistic view of its causes and consequences. *Nature Reviews. Genetics*, *9*(3), 204–217. https://doi.org/10.1038/nrg2268

Ahnesorg, P., Smith, P., & Jackson, S. P. (2006). XLF interacts with the XRCC4-DNA ligase IV complex to promote nonhomologous end-joining. *Cell*, *124*, 301–313.

Alani, E., Padmore, R., & Kleckner, N. (1990). Analysis of wild-type and rad50 mutants of yeast suggests an intimate relationship between meiotic chromosome synapsis and recombination. *Cell*, *61*(3), 419–436. https://doi.org/10.1016/0092-8674(90)90524-I

Al-Tassan, N., Chmiel, N. H., Maynard, J., Fleming, N., Livingston, A. L., Williams, G. T., Hodges, A. K., Davies, D. R., David, S. S., Sampson, J. R., & Cheadle, J. P. (2002). Inherited variants of MYH associated with somatic G:C-->T:A mutations in colorectal tumors. *Nature Genetics*, *30*(2), 227–232. https://doi.org/10.1038/ng828

Anand, R., Ranjha, L., Cannavo, E., & Cejka, P. (2016). Phosphorylated CtIP functions as a co-factor of the MRE11-RAD50-NBS1 endonuclease in DNA end resection. *Mol. Cell*, *64*, 940–950.

Aparicio, T., Baer, R., & Gautier, J. (2014). DNA double-strand break repair pathway choice and cancer. *DNA Repair*, *19*, 169–175. https://doi.org/10.1016/j.dnarep.2014.03.014

Aravind, L., & Koonin, E. V. (2001). Prokaryotic homologs of the eukaryotic DNA-end-binding protein Ku, novel domains in the Ku protein and prediction of a prokaryotic double-strand break repair system. *Genome Res*, *11*, 1365–1374.

Aylon, Y., Liefshitz, B., & Kupiec, M. (2004). The CDK regulates repair of double-strand breaks by homologous recombination during the cell cycle. *EMBO J*, *23*, 4868–4875.

Azad, G., & Tomar, R. (2016). The multifunctional transcription factor Rap1: A regulator of yeast physiology. *Frontiers in Bioscience*, *21*. https://doi.org/10.2741/4429

Bacal, J., Moriel-Carretero, M., Pardo, B., Barthe, A., Sharma, S., Chabes, A., Lengronne, A., & Pasero, P. (2018). Mrc1 and Rad9 cooperate to regulate initiation and elongation of DNA replication in response to DNA damage. *EMBO J*, *37*, 99319.

Bae, S. H., Choi, E., Lee, K. H., Park, J. S., Lee, S. H., & Seo, Y. S. (1998). Dna2 of *Saccharomyces cerevisiae* possesses a single-stranded DNA-specific endonuclease activity that is able to act on double-stranded DNA in the presence of ATP. *The Journal of Biological Chemistry*, *273*(41), 26880–26890. https://doi.org/10.1074/jbc.273.41.26880

Baldo, V., Testoni, V., Lucchini, G., & Longhese, M. P. (2008). Dominant TEL1-hy mutations compensate for Mec1 lack of functions in the DNA damage response. *Molecular and Cellular Biology*, *28*(1), 358–375. https://doi.org/10.1128/MCB.01214-07

Balestrini, A., Ristic, D., Dionne, I., Liu, X. Z., Wyman, C., Wellinger, R. J., & Petrini, J. H. J. (2013). The Ku heterodimer and the metabolism of single-ended DNA double-strand breaks. *Cell Reports*, *3*(6), 2033–2045. https://doi.org/10.1016/j.celrep.2013.05.026

Bass, T. E., Luzwick, J. W., Kavanaugh, G., Carroll, C., Dungrawala, H., Glick, G. G., Feldkamp, M. D., Putney, R., Chazin, W. J., & Cortez, D. (2016). ETAA1 acts at stalled replication forks to maintain genome integrity. *Nature Cell Biology*, *18*(11), 1185–1195. https://doi.org/10.1038/ncb3415

Berens, T. J., & Toczyski, D. P. (2012). Keeping it together in times of stress: Checkpoint function at stalled replication forks. *Molecular Cell*, *45*(5), 585–586. https://doi.org/10.1016/j.molcel.2012.02.011

Berkovich, E., RJ, M., Jr, & Kastan, M. B. (2007). Roles of ATM and NBS1 in chromatin structure modulation and DNA double-strand break repair. *Nat Cell Biol*, *9*, 683–690.

Bertocci, B., Smet, A., Weill, J. C., & Reynaud, C. A. (2006). Nonoverlapping functions of DNA polymerases mu, lambda, and terminal deoxynucleotidyltransferase during immunoglobulin V(D)J recombination *in vivo*. *Immunity*, *25*, 31–41.

Bertuch, A. A., & Lundblad, V. (2003). The Ku heterodimer performs separable activities at double-strand breaks and chromosome termini. *Mol Cell Biol*, *23*, 8202–8215.

Bizard, A. H., & Hickson, I. D. (2014). The dissolution of double Holliday junctions. *Cold Spring Harbor Perspectives in Biology*, *6*(7), a016477. https://doi.org/10.1101/cshperspect.a016477

Blier, P. R., Griffith, A. J., Craft, J., & Hardin, J. A. (1993). Binding of Ku protein to DNA. Measurement of affinity for ends and demonstration of binding to nicks. *J. Biol. Chem*, *268*, 7594–7601.

Bonetti, D., Clerici, M., Anbalagan, S., Martina, M., Lucchini, G., & Longhese, M. P. (2010). Shelterin-Like Proteins and Yku Inhibit Nucleolytic Processing of *Saccharomyces cerevisiae* Telomeres. *PLOS Genetics*, *6*(5), e1000966. https://doi.org/10.1371/journal.pgen.1000966

Bonetti, D., Clerici, M., Manfrini, N., Lucchini, G., & Longhese, M. P. (2010). The MRX complex plays multiple functions in resection of Yku- and Rif2-protected DNA ends. *PLoS One*, *5*, 14142.

Bonetti, D., Rinaldi, C., Vertemara, J., Notaro, M., Pizzul, P., Tisi, R., Zampella, G., & Longhese, M. P. (2020). DNA binding modes influence Rap1 activity in the regulation of telomere length and MRX functions at DNA ends. *Nucleic Acids Research*, *48*(5), 2424–2441. https://doi.org/10.1093/nar/gkz1203

Bonetti, D., Villa, M., Gobbini, E., Cassani, C., Tedeschi, G., & Longhese, M. P. (2015a). *Escape of Sgs1 from Rad9 inhibition reduces the requirement for Sae2 and functional MRX in DNA end.*

Bonetti, D., Villa, M., Gobbini, E., Cassani, C., Tedeschi, G., & Longhese, M. P. (2015b). Escape of Sgs1 from Rad9 inhibition reduces the requirement for Sae2 and functional MRX in DNA end resection. *EMBO Reports*, *16*(3), 351–361. https://doi.org/10.15252/embr.201439764

Bosotti, R., Isacchi, A., & Sonnhammer, E. L. (2000). FAT, a novel domain in PIK-related kinases. *Trends Biochem Sci*, *25*, 225–227.

Britton, S., Chanut, P., Delteil, C., Barboule, N., Frit, P., & Calsou, P. (2020). ATM antagonizes NHEJ proteins assembly and DNA-ends synapsis at single-ended DNA double strand breaks. *Nucleic Acids Res*, *48*, 9710–9723.

Britton, S., Coates, J., & Jackson, S. P. (2013). A new method for high-resolution imaging of Ku foci to decipher mechanisms of DNA double-strand break repair. *J Cell Biol*, *202*, 579–595.

Cannavo, E., & Cejka, P. (2014). Sae2 promotes dsDNA endonuclease activity within Mre11-Rad50-Xrs2 to resect DNA breaks. *Nature*, *514*, 122–125.

Cannavo, E., Johnson, D., Andres, S. N., Kissling, V. M., Reinert, J. K., Garcia, V., Erie, D. A., Hess, D., Thomä, N. H., Enchev, R. I., Peter, M., Williams, R. S., Neale, M. J., & Cejka, P. (2018). Regulatory control of DNA end resection by Sae2 phosphorylation. *Nature Communications*, *9*(1), Article 1. https://doi.org/10.1038/s41467-018-06417-5

Cannavo, E., Reginato, G., & Cejka, P. (2019). Stepwise 5' DNA end-specific resection of DNA breaks by the Mre11-Rad50-Xrs2 and Sae2 nuclease ensemble. *Proceedings of the National Academy of Sciences*, *116*(12), 5505–5513. https://doi.org/10.1073/pnas.1820157116

Cary, R. B., Peterson, W., SR, J, B., DG, B., EM, C., & D.J. (1997). DNA looping by Ku and the DNA-dependent protein kinase. *Proc Natl Acad Sci USA*, *94*, 4267–4272.

Casari, E., Gnugnoli, M., Rinaldi, C., Pizzul, P., Colombo, C. V., Bonetti, D., & Longhese, M. P. (2022). To Fix or not to fix: Maintenance of chromosome ends versus repair of DNA double-strand breaks. *Cells*, *11*, 3224.

Casari, E., Gobbini, E., Clerici, M., & Longhese, M. P. (2021). Resection of a DNA double-strand break by alkaline gel electrophoresis and southern blotting. *Methods Mol Biol*, *2153*, 33–45.

Casari, E., Gobbini, E., Gnugnoli, M., Mangiagalli, M., Clerici, M., & Longhese, M. P. (2021). Dpb4 promotes resection of DNA double-strand breaks and checkpoint activation by acting in two different protein complexes. *Nat Commun*, *12*, 4750.

Cassani, C., Gobbini, E., Vertemara, J., Wang, W., Marsella, A., Sung, P., Tisi, R., Zampella, G., & Longhese, M. P. (2018). Structurally distinct Mre11 domains mediate MRX functions in resection, end-tethering and DNA damage resistance. *Nucleic Acids Res*, *46*, 2990–3008.

Cassani, C., Gobbini, E., Wang, W., Niu, H., Clerici, M., Sung, P., & Longhese, M. P. (2016). Tel1 and Rif2 Regulate MRX Functions in End-Tethering and Repair of DNA Double-Strand Breaks. *PLOS Biology*, *14*(2), e1002387. https://doi.org/10.1371/journal.pbio.1002387

Cassani, C., Vertemara, J., Bassani, M., Marsella, A., Tisi, R., Zampella, G., & Longhese, M. P. (2019). The ATP-bound conformation of the Mre11-Rad50 complex is essential for Tel1/ATM activation. *Nucleic Acids Research*, *47*(7), 3550–3567. https://doi.org/10.1093/nar/gkz038

Cejka, P. (2015). DNA End Resection: Nucleases Team Up with the Right Partners to Initiate Homologous Recombination. *The Journal of Biological Chemistry*, *290*(38), 22931–22938. https://doi.org/10.1074/jbc.R115.675942

Cejka, P., Cannavo, E., Polaczek, P., Masuda-Sasa, T., Pokharel, S., Campbell, J. L., & Kowalczykowski, S. C. (2010). DNA end resection by Dna2-Sgs1-RPA and its stimulation by Top3-Rmi1 and Mre11-Rad50-Xrs2. *Nature*, *467*, 112–116.

Chan, S. W., Boule, J. B., & Zakian, V. A. (2008). Two pathways recruit telomerase to *Saccharomyces cerevisiae* telomeres. *PLoS Genet*, *4*, 1000236.

Chang, H. H. Y., Pannunzio, N. R., Adachi, N., & Lieber, M. R. (2017). Non-homologous DNA end joining and alternative pathways to double-strand break repair. *Nat Rev Mol Cell Biol*, *18*, 495–506.

Chang, H. H. Y., Watanabe, G., Gerodimos, C. A., Ochi, T., Blundell, T. L., Jackson, S. P., & Lieber, M. R. (2016). Different DNA end configurations dictate which NHEJ components are most important for joining efficiency. *J Biol Chem*, *291*, 24377–24389.

Chanut, P., Britton, S., Coates, J., Jackson, S. P., & Calsou, P. (2016). Coordinated nuclease activities counteract Ku at single-ended DNA double-strand breaks. *Nature Communications*, *7*, 12889. https://doi.org/10.1038/ncomms12889

Chaplin, A. K., & Blundell, T. L. (2020). Structural biology of multicomponent assemblies in DNA double-strand-break repair through non-homologous end joining. *Curr. Opin. Struct. Biol*, *61*.

Chaplin, A. K., Hardwick, S. W., Stavridi, A. K., Buehl, C. J., Goff, N. J., Ropars, V., Liang, S., Oliveira, T. M., Chirgadze, D. Y., Meek, K., Charbonnier, J. B., & Blundell, T. L. (2021). *Cryo-EM of NHEJ supercomplexes provides insights into DNA repair Mol Cell 81* (pp. 3400–3409).

Chapman, J. R., Taylor, M. R. G., & Boulton, S. J. (2012). Playing the end game: DNA double-strand break repair pathway choice. *Molecular Cell*, *47*(4), 497–510. https://doi.org/10.1016/j.molcel.2012.07.029

Chen, H., Donnianni, R. A., Handa, N., Deng, S. K., Oh, J., Timashev, L. A., Kowalczykowski, S. C., & Symington, L. S. (2015). Sae2 promotes DNA damage resistance by removing the Mre11-Rad50-Xrs2 complex from DNA and attenuating Rad53 signaling. *Proceedings of the National Academy of Sciences of the United States of America*, *112*(15), E1880-1887. https://doi.org/10.1073/pnas.1503331112

Chen, S., Lee, L., Naila, T., Fishbain, S., Wang, A., Tomkinson, A. E., Lees-Miller, S. P., & He, Y. (2021). Structural basis of long-range to short-range synaptic transition in NHEJ. *Nature*, *593*, 294–298.

Chen, Y. C., Teng, S. C., & Wu, K. J. (2009). Phosphorylation of telomeric repeat binding factor 1 (TRF1) by Akt causes telomere shortening. *Cancer Invest*, *27*, 24–28.

Chen, Y., Rai, R., Zhou, Z. R., Kanoh, J., Ribeyre, C., Yang, Y., Zheng, H., Damay, P., Wang, F., Tsujii, H., Hiraoka, Y., Shore, D., Hu, H. Y., Chang, S., & Lei, M. (2011). A conserved motif within RAP1 has diversified roles in telomere protection and regulation in different organisms. *Nat Struct Mol Biol*, *18*, 213–221.

Churikov, D., Corda, Y., Luciano, P., & Geli, V. (2013). Cdc13 at a crossroads of telomerase action. *Front Oncol*, *3*, 39.

Ciccia, A., & Elledge, S. J. (2010). The DNA Damage Response: Making it safe to play with knives. *Molecular Cell*, *40*(2), 179–204. https://doi.org/10.1016/j.molcel.2010.09.019

Clerici, M., Mantiero, D., Guerini, I., Lucchini, G., & Longhese, M. P. (2008). The Yku70-Yku80 complex contributes to regulate double-strand break processing and checkpoint activation during the cell cycle. *EMBO Reports*, *9*(8), 810–818. https://doi.org/10.1038/embor.2008.121

Clerici, M., Mantiero, D., Lucchini, G., & Longhese, M. P. (2005). The *Saccharomyces cerevisiae* Sae2 protein promotes resection and bridging of double strand break ends. *J. Biol. Chem*, *280*, 38631–38638.

Clerici, M., Mantiero, D., Lucchini, G., & Longhese, M. P. (2006). The *Saccharomyces cerevisiae* Sae2 protein negatively regulates DNA damage checkpoint signalling. *EMBO Rep*, *7*, 212–218.

Clerici, M., Paciotti, V., Baldo, V., Romano, M., Lucchini, G., & Longhese, M. P. (2001). Hyperactivation of the yeast DNA damage checkpoint by TEL1 and DDC2 overexpression. *The EMBO Journal*, *20*(22), 6485–6498. https://doi.org/10.1093/emboj/20.22.6485

Clerici, M., Trovesi, C., Galbiati, A., Lucchini, G., & Longhese, M. P. (2014). Mec1/ATR regulates the generation of single-stranded DNA that attenuates Tel1/ATM signaling at DNA ends. *The EMBO Journal*, *33*(3), 198–216. https://doi.org/10.1002/embj.201386041

Colombo, C. V., Menin, L., Ranieri, R., Bonetti, D., Clerici, M., & Longhese, M. P. (2019). Uncoupling Sae2 Functions in Downregulation of Tel1 and Rad53 Signaling Activities. *Genetics*, *211*(2), 515–530. https://doi.org/10.1534/genetics.118.301830

Conrad, M. N., Wright, J. H., Wolf, A. J., & Zakian, V. A. (1990). RAP1 protein interacts with yeast telomeres *in vivo*: Overproduction alters telomere structure and decreases chromosome stability. *Cell*, *63*(4), 739–750. https://doi.org/10.1016/0092-8674(90)90140-a

Critchlow, S. E., Bowater, R. P., & Jackson, S. P. (1997). Mammalian DNA double-strand break repair protein XRCC4 interacts with DNA ligase IV. *Current Biology: CB*, *7*(8), 588–598. https://doi.org/10.1016/s0960-9822(06)00258-2

Daley, J. M., & Wilson, T. E. (2005). Rejoining of DNA double-strand breaks as a function of overhang length. *Mol Cell Biol*, *25*, 896–906.

D'Amours, D., & Jackson, S. P. (2001). The yeast Xrs2 complex functions in S phase checkpoint regulation. *Genes & Development*, *15*(17), 2238–2249. https://doi.org/10.1101/gad.208701

de Lange, T. (2018). Shelterin-Mediated Telomere Protection. *Annual Review of Genetics*, *52*, 223–247. https://doi.org/10.1146/annurev-genet-032918-021921

de Vries, E., van Driel, W., Bergsma, W. G., Arnberg, A. C., & van der Vliet, P. C. (1989). HeLa nuclear protein recognizing DNA termini and translocating on DNA forming a regular DNA-multimeric protein complex. *Journal of Molecular Biology*, *208*(1), 65–78. https://doi.org/10.1016/0022-2836(89)90088-0

DeFazio, L. G., Stansel, R. M., Griffith, J. D., & Chu, G. (2002). Synapsis of DNA ends by DNA dependent protein kinase. *EMBO J*, *21*, 3192–3200.

de Lange, T. (2018). Shelterin-mediated telomere protection. *Annu. Rev. Genet.*, 52, 223-247

Deshpande, R. A., Lee, J.-H., Arora, S., & Paull, T. T. (2016). Nbs1 Converts the Human Mre11/Rad50 Nuclease Complex into an Endo/Exonuclease Machine Specific for Protein-DNA Adducts. *Molecular Cell*, *64*(3), 593–606. https://doi.org/10.1016/j.molcel.2016.10.010

Deshpande, R. A., Williams, G. J., Limbo, O., Williams, R. S., Kuhnlein, J., Lee, J.-H., Classen, S., Guenther, G., Russell, P., Tainer, J. A., & Paull, T. T. (2014). ATP-driven Rad50 conformations regulate DNA tethering, end resection, and ATM

checkpoint signaling. *The EMBO Journal*, *33*(5), 482–500. https://doi.org/10.1002/embj.201386100

Downs, J. A., & Jackson, S. P. (2004a). A means to a DNA end: The many roles of Ku. *Nat Rev Mol Cell Biol*, *5*, 367–378.

Downs, J. A., & Jackson, S. P. (2004b). A means to a DNA end: The many roles of Ku. *Nat. Rev. Mol. Cell. Biol*, *5*, 367–378.

Downs, J. A., Lowndes, N. F., & Jackson, S. P. (2000). A role for *Saccharomyces cerevisiae* histone H2A in DNA repair. *Nature*, *408*, 1001–1004.

Dudášová, Z., Dudáš, A., & Chovanec, M. (2004). Non-homologous end-joining factors of *Saccharomyces cerevisiae*. *FEMS Microbiol Rev*, *28*, 581–601.

Errami, A., Finnie, N. J., Morolli, B., Jackson, S. P., Lohman, P. H., & Zdzienicka, M. Z. (1998). Molecular and biochemical characterization of new X-ray-sensitive hamster cell mutants defective in Ku80. *Nucleic Acids Res*, *26*, 4332–4338.

Falck, J., Coates, J., & Jackson, S. P. (2005). Conserved modes of recruitment of ATM, ATR and DNA-pkcs to sites of DNA damage. *Nature*, *434*, 605–611.

Ferrari, M., Dibitetto, D., De Gregorio, G., Eapen, V. V., Rawal, C. C., Lazzaro, F., Tsabar, M., Marini, F., Haber, J. E., & Pellicioli, A. (2015). Functional interplay between the 53BP1-ortholog Rad9 and the Mre11 complex regulates resection, end-tethering and repair of a double-strand break. *PLoS Genetics*, *11*(1), e1004928. https://doi.org/10.1371/journal.pgen.1004928

Finn, K., Lowndes, N. F., & Grenon, M. (2012). Eukaryotic DNA damage checkpoint activation in response to double-strand breaks. *Cellular and Molecular Life Sciences: CMLS*, *69*(9), 1447–1473. https://doi.org/10.1007/s00018-011-0875-3

Fishel, R., Lescoe, M. K., Rao, M. R., Copeland, N. G., Jenkins, N. A., Garber, J., Kane, M., & Kolodner, R. (1993). The human mutator gene homolog MSH2 and its association with hereditary nonpolyposis colon cancer. *Cell*, *75*(5), 1027–1038. https://doi.org/10.1016/0092-8674(93)90546-3

Fisher, T. S., Taggart, A. K. P., & Zakian, V. A. (2004). Cell cycle-dependent regulation of yeast telomerase by Ku. *Nature Structural & Molecular Biology*, *11*(12), 1198–1205. https://doi.org/10.1038/nsmb854

Fisher, T. S., & Zakian, V. A. (2005). Ku: A multifunctional protein involved in telomere maintenance. *DNA Repair*, *4*(11), 1215–1226. https://doi.org/10.1016/j.dnarep.2005.04.021

Fishman-Lobell, J., Rudin, N., & Haber, J. E. (1992). Two alternative pathways of double-strand break repair that are kinetically separable and independently modulated. *Molecular and Cellular Biology*, *12*(3), 1292–1303. https://doi.org/10.1128/mcb.12.3.1292-1303.1992

Foster, S. S., Balestrini, A., & Petrini, J. H. (2011). Functional interplay of the Mre11 nuclease and Ku in the response to replication-associated DNA damage. *Mol. Cell. Biol*, *31*, 4379–4389.

Frank-Vaillant, M., & Marcand, S. (2001). NHEJ regulation by mating type is exercised through a novel protein, Lif2p, essential to the ligase IV pathway. *Genes Dev*, *15*, 3005–3012.

Frigerio, C., Di Nisio, E., Galli, M., Colombo, C. V., Negri, R., & Clerici, M. (2023). The Chromatin Landscape around DNA Double-Strand Breaks in Yeast and Its Influence on DNA Repair Pathway Choice. *International Journal of Molecular Sciences*, *24*(4), 3248. https://doi.org/10.3390/ijms24043248

Furuse, M., Nagase, Y., Tsubouchi, H., Murakami-Murofushi, K., Shibata, T., & Ohta, K. (1998). Distinct roles of two separable *in vitro* activities of yeast Mre11 in mitotic and meiotic recombination. *The EMBO Journal*, *17*(21), 6412–6425. https://doi.org/10.1093/emboj/17.21.6412

Gallardo, F., Laterreur, N., Cusanelli, E., Querido, E., Wellinger, R. J., & Chartrand, P. (2011). Live cell imaging of telomerase RNA dynamics reveals cell cycle-dependent clustering of telomerase at elongating telomeres. *Mol Cell*, *44*, 819–827.

Gallardo, F., Olivier, C., Dandjinou, A. T., Wellinger, R. J., & Chartrand, P. (2008). TLC1 RNA nucleo-cytoplasmic trafficking links telomerase biogenesis to its recruitment to telomeres. *The EMBO Journal*, *27*(5), 748–757. https://doi.org/10.1038/emboj.2008.21

Garcia, V., Phelps, S. E., Gray, S., & Neale, M. J. (2011). Bidirectional resection of DNA double-strand breaks by Mre11 and Exo1. *Nature*, *479*, 241–244.

Gerald, J. N. F., Benjamin, J. M., & Kron, S. J. (2002). Robust G1 checkpoint arrest in budding yeast: Dependence on DNA damage signaling and repair. *Journal of Cell Science*, *115*(Pt 8), 1749–1757. https://doi.org/10.1242/jcs.115.8.1749

Giannattasio, M., Lazzaro, F., Plevani, P., & Muzi-Falconi, M. (2005). The DNA damage checkpoint response requires histone H2B ubiquitination by Rad6-Bre1 and H3 methylation by Dot1. *J Biol Chem*, *280*, 9879–9886.

Gilbert, C. S., Green, C. M., & Lowndes, N. F. (2001). Budding yeast Rad9 is an ATP-dependent Rad53 activating machine. *Mol Cell*, *8*, 129–136.

Gobbini, E., Cesena, D., Galbiati, A., Lockhart, A., & Longhese, M. P. (2013). Interplays between ATM/Tel1 and ATR/Mec1 in sensing and signaling DNA double-strand breaks. *DNA Repair*, *12*(10), 791–799. https://doi.org/10.1016/j.dnarep.2013.07.009

Gobbini, E., Trovesi, C., Cassani, C., & Longhese, M. P. (2014). Telomere uncapping at the crossroad between cell cycle arrest and carcinogenesis. *Molecular & Cellular Oncology*, *1*(1), e29901. https://doi.org/10.4161/mco.29901

Gobbini, E., Villa, M., Gnugnoli, M., Menin, L., Clerici, M., & Longhese, M. P. (2015). Sae2 function at DNA double-strand breaks is bypassed by dampening Tel1 or Rad53 activity. *PLoS Genet*, *11*, 1005685.

Goodarzi, A. A., Yu, Y., Riballo, E., Douglas, P., Walker, S. A., Ye, R., Härer, C., Marchetti, C., Morrice, N., Jeggo, P. A., & Lees-Miller, S. P. (2006). DNA-PK autophosphorylation facilitates Artemis endonuclease activity. *EMBO J*, *25*, 3880–3889.

Graham, T. G., Walter, J. C., & Loparo, J. J. (2016). Two-stage synapsis of DNA ends during nonhomologous end joining. *Mol Cell*, *61*, 850–858.

Granata, M., Lazzaro, F., Novarina, D., Panigada, D., Puddu, F., Abreu, C. M., Kumar, R., Grenon, M., Lowndes, N. F., Plevani, P., & Muzi-Falconi, M. (2010). Dynamics of Rad9 chromatin binding and checkpoint function are mediated by its dimerization and are cell cycle-regulated by CDK1 activity. *PLoS Genet*, *6*, 1001047.

Gravel, S., Chapman, J. R., Magill, C., & Jackson, S. P. (2008). DNA helicases Sgs1 and BLM promote DNA double-strand break resection. *Genes & Development*, *22*(20), 2767–2772. https://doi.org/10.1101/gad.503108

Grawunder, U., Wilm, M., Wu, X., Kulesza, P., Wilson, T. E., Mann, M., & Lieber, M. R. (1997). Activity of DNA ligase IV stimulated by complex formation with XRCC4 protein in mammalian cells. *Nature*, *388*, 492–495.

Greenwell, P. W., Kronmal, S. L., Porter, S. E., Gassenhuber, J., Obermaier, B., & Petes, T. D. (1995). TEL1, a gene involved in controlling telomere length in *S. cerevisiae*, is homologous to the human ataxia telangiectasia gene. *Cell*, *82*(5), 823–829. https://doi.org/10.1016/0092-8674(95)90479-4

Greider, C. W., & Blackburn, E. H. (1985). Identification of a specific telomere terminal transferase activity in Tetrahymena extracts. *Cell*, *43*(2 Pt 1), 405–413. https://doi.org/10.1016/0092-8674(85)90170-9

Grenon, M., Costelloe, T., Jimeno, S., O'Shaughnessy, A., Fitzgerald, J., Zgheib, O., Degerth, L., & Lowndes, N. F. (2007). Docking onto chromatin via the *Saccharomyces cerevisiae* Rad9 Tudor domain. *Yeast*, *24*, 105–119.

Griffith, A. J., Blier, P. R., Mimori, T., & Hardin, J. A. (1992). Ku polypeptides synthesized *in vitro* assemble into complexes which recognize ends of double-stranded DNA. *J. Biol. Chem*, *267*.

Gu, J., Li, S., Zhang, X., Wang, L. C., Niewolik, D., Schwarz, K., Legerski, R. J., Zandi, E., & Lieber, M. R. (2010). DNA-PKcs regulates a single-stranded DNA endonuclease activity of Artemis. *DNA Repair*, *9*, 429–437.

Guo, X., Hum, Y. F., Lehner, K., & Jinks-Robertson, S. (2017). Regulation of hetDNA Length during Mitotic Double-Strand Break Repair in Yeast. *Molecular Cell*, *67*(4), 539-549.e4. https://doi.org/10.1016/j.molcel.2017.07.009

Haahr, P., Hoffmann, S., Tollenaere, M. A. X., Ho, T., Toledo, L. I., Mann, M., Bekker-Jensen, S., Räschle, M., & Mailand, N. (2016). Activation of the ATR kinase by the RPA-binding protein ETAA1. *Nature Cell Biology*, *18*(11), 1196–1207. https://doi.org/10.1038/ncb3422

Hailemariam, S., Bona, P., Galletto, R., Hohl, M., Petrini, J. H., & Burgers, P. M. (2019). The telomere-binding protein Rif2 and ATP-bound Rad50 have opposing roles in the activation of yeast Tel1ATM kinase. *J Biol Chem*, *294*, 18846–18852.

Hammel, M., Yu, Y., Mahaney, B. L., Cai, B., Ye, R., Phipps, B. M., Rambo, R. P., Hura, G. L., Pelikan, M., So, S., Abolfath, R. M., Chen, D. J., Lees-Miller, S. P., & Tainer, J. A. (2010). Ku and DNA-dependent protein kinase dynamic conformations and assembly regulate DNA binding and the initial non-homologous end joining complex. *The Journal of Biological Chemistry*, *285*(2), 1414–1423. https://doi.org/10.1074/jbc.M109.065615

Hammet, A., Magill, C., Heierhorst, J., & Jackson, S. P. (2007). Rad9 BRCT domain interaction with phosphorylated H2AX regulates the G1 checkpoint in budding yeast. *EMBO Rep*, *8*, 851–857.

Hanahan, D., & Weinberg, R. A. (2000). The hallmarks of cancer. *Cell*, *100*(1), 57–70. https://doi.org/10.1016/s0092-8674(00)81683-9

Hanahan, D., & Weinberg, R. A. (2011). Hallmarks of cancer: The next generation. *Cell*, *144*(5), 646–674. https://doi.org/10.1016/j.cell.2011.02.013

Hanakahi, L. A. (2007). 2-Step purification of the Ku DNA repair protein expressed in *Escherichia coli*. *Protein Expression and Purification*, *52*(1), 139–145. https://doi.org/10.1016/j.pep.2006.10.002

Hardy, C. F., Sussel, L., & Shore, D. (1992). A RAP1-interacting protein involved in transcriptional silencing and telomere length regulation. *Genes & Development*, *6*(5), 801–814. https://doi.org/10.1101/gad.6.5.801

Harrington, J. J., & Lieber, M. R. (1994). Functional domains within FEN-1 and RAD2 define a family of structure-specific endonucleases: Implications for nucleotide excision repair. *Gene Develop*, *8*, 1344–1355.

Hartlerode, A. J., & Scully, R. (2009). Mechanisms of double-strand break repair in somatic mammalian cells. *The Biochemical Journal*, *423*(2), 157–168. https://doi.org/10.1042/BJ20090942

Hefferin, M. L., & Tomkinson, A. E. (2005). Mechanism of DNA double-strand break repair by non-homologous end joining. *DNA Repair*, *4*, 639–648.

Helena, J. M., Joubert, A. M., Grobbelaar, S., Nolte, E. M., Nel, M., Pepper, M. S., Coetzee, M., & Mercier, A. E. (2018). Deoxyribonucleic Acid Damage and Repair: Capitalizing on Our Understanding of the Mechanisms of Maintaining Genomic Integrity for Therapeutic Purposes. *International Journal of Molecular Sciences*, *19*(4), 1148. https://doi.org/10.3390/ijms19041148

Hirano, Y., Fukunaga, K., & Sugimoto, K. (2009). Rif1 and rif2 inhibit localization of tel1 to DNA ends. *Molecular Cell*, *33*(3), 312–322. https://doi.org/10.1016/j.molcel.2008.12.027

Holloman, W. K. (2011). Unraveling the mechanism of BRCA2 in homologous recombination. *Nature Structural & Molecular Biology*, *18*(7), 748–754. https://doi.org/10.1038/nsmb.2096

Hopfner, K. P., Karcher, A., Craig, L., Woo, T. T., Carney, J. P., & Tainer, J. A. (2001). Structural biochemistry and interaction architecture of the DNA double-strand break repair Mre11 nuclease and Rad50-ATPase. *Cell*, *105*(4), 473–485. https://doi.org/10.1016/s0092-8674(01)00335-x

Hopfner, K.-P., Craig, L., Moncalian, G., Zinkel, R. A., Usui, T., Owen, B. A. L., Karcher, A., Henderson, B., Bodmer, J.-L., McMurray, C. T., Carney, J. P., Petrini, J. H. J., & Tainer, J. A. (2002). The Rad50 zinc-hook is a structure

joining Mre11 complexes in DNA recombination and repair. *Nature*, *418*(6897), Article 6897. https://doi.org/10.1038/nature00922

Hopfner, K.-P., Karcher, A., Shin, D. S., Craig, L., Arthur, L. M., Carney, J. P., & Tainer, J. A. (2000). Structural Biology of Rad50 ATPase: ATP-Driven Conformational Control in DNA Double-Strand Break Repair and the ABC-ATPase Superfamily. *Cell*, *101*(7), 789–800. https://doi.org/10.1016/S0092-8674(00)80890-9

Huertas, P., Cortés-Ledesma, F., Sartori, A. A., Aguilera, A., & Jackson, S. P. (2008). CDK targets Sae2 to control DNA-end resection and homologous recombination. *Nature*, *455*(7213), 689–692. https://doi.org/10.1038/nature07215

Huertas, P., & Jackson, S. P. (2009). Human CtIP mediates cell cycle control of DNA end resection and double strand break repair. *The Journal of Biological Chemistry*, *284*(14), 9558–9565. https://doi.org/10.1074/jbc.M808906200

Ira, G., Pellicioli, A., Balijja, A., Wang, X., Fiorani, S., Carotenuto, W., Liberi, G., Bressan, D., Wan, L., Hollingsworth, N. M., Haber, J. E., & Foiani, M. (2004). DNA end resection, homologous recombination and DNA damage checkpoint activation require CDK1. *Nature*, *431*, 1011–1017.

Ittisoponpisan, S., Islam, S. A., Khanna, T., Alhuzimi, E., David, A., & Sternberg, M. J. E. (2019). Can Predicted Protein 3D Structures Provide Reliable Insights into whether Missense Variants Are Disease Associated? *Journal of Molecular Biology*, *431*(11), 2197–2212. https://doi.org/10.1016/j.jmb.2019.04.009

Iwasaki, D., Hayashihara, K., Shima, H., Higashide, M., Terasawa, M., Gasser, S. M., & Shinohara, M. (2016). The MRX complex ensures NHEJ fidelity through multiple pathways including Xrs2-FHA-dependent Tel1 activation. *PLoS Genet*, *12*, 1005942.

Jacobson, M. P., Pincus, D. L., Rapp, C. S., Day, T. J., Honig, B., Shaw, D. E., & Friesner, R. A. (2004). A hierarchical approach to all-atom protein loop prediction. *Proteins*, *55*, 351–367.

Jain, D., & Cooper, J. P. (2010). Telomeric Strategies: Means to an End. *Annual Review of Genetics*, *44*(1), 243–269. https://doi.org/10.1146/annurev-genet-102108-134841

Javaheri, A., Wysocki, R., Jobin-Robitaille, O., Altaf, M., Côté, J., & Kron, S. J. (2006). Yeast G1 DNA damage checkpoint regulation by H2A phosphorylation is

independent of chromatin remodeling. *Proc Natl Acad Sci USA*, *103*, 13771–13776.

Kabir, S., Sfeir, A., & Lange, T. (2010). Taking apart Rap1: An adaptor protein with telomeric and non-telomeric functions. *Cell Cycle*, *9*, 4061–4067.

Kaizer, H., Connelly, C. J., Bettridge, K., Viggiani, C., & Greider, C. W. (2015). Regulation of Telomere Length Requires a Conserved N-Terminal Domain of Rif2 in *Saccharomyces cerevisiae*. *Genetics*, *201*(2), 573–586. https://doi.org/10.1534/genetics.115.177899

Käshammer, L., Saathoff, J.-H., Lammens, K., Gut, F., Bartho, J., Alt, A., Kessler, B., & Hopfner, K.-P. (2019). Mechanism of DNA End Sensing and Processing by the Mre11-Rad50 Complex. *Molecular Cell*, *76*(3), 382-394.e6. https://doi.org/10.1016/j.molcel.2019.07.035

Kaye, J. A., Melo, J. A., Cheung, S. K., Vaze, M. B., Haber, J. E., & Toczyski, D. P. (2004). DNA Breaks Promote Genomic Instability by Impeding Proper Chromosome Segregation. *Current Biology*, *14*(23), 2096–2106. https://doi.org/10.1016/j.cub.2004.10.051

Keener, R., Connelly, C. J., & Greider, C. W. (2019). Tel1 Activation by the MRX Complex Is Sufficient for Telomere Length Regulation but Not for the DNA Damage Response in *Saccharomyces cerevisiae*. *Genetics*, *213*(4), 1271–1288. https://doi.org/10.1534/genetics.119.302713

Keeney, S., Giroux, C. N., & Kleckner, N. (1997). Meiosis-specific DNA double-strand breaks are catalyzed by Spo11, a member of a widely conserved protein family. *Cell*, *88*(3), 375–384. https://doi.org/10.1016/s0092-8674(00)81876-0

Keeney, S., & Kleckner, N. (1995). Covalent protein-DNA complexes at the 5' strand termini of meiosis-specific double-strand breaks in yeast. *Proceedings of the National Academy of Sciences of the United States of America*, *92*(24), 11274–11278. https://doi.org/10.1073/pnas.92.24.11274

Kegel, A., Sjöstrand, J. O., & Aström, S. U. (2001). Nej1p, a cell type-specific regulator of nonhomologous end joining in yeast. *Curr Biol*, *11*, 1611–1617.

Khayat, F., Cannavo, E., Alshmery, M., Foster, W. R., Chahwan, C., Maddalena, M., Smith, C., Oliver, A. W., Watson, A. T., Carr, A. M., Cejka, P., & Bianchi, A. (2021). Inhibition of MRN activity by a telomere protein motif. *Nature Communications*, *12*(1). Scopus. https://doi.org/10.1038/s41467-021-24047-2

Kim, J. A., Kruhlak, M., Dotiwala, F., Nussenzweig, A., & Haber, J. E. (2007). Heterochromatin is refractory to gamma-H2AX modification in yeast and mammals. *J Cell Biol*, *178*, 209–218.

Kinoshita, E., van der Linden, E., Sanchez, H., & Wyman, C. (2009). RAD50, an SMC family member with multiple roles in DNA break repair: How does ATP affect function? *Chromosome Research : An International Journal on the Molecular, Supramolecular and Evolutionary Aspects of Chromosome Biology*, *17*(2), 277–288. https://doi.org/10.1007/s10577-008-9018-6

Kondo, T., Wakayama, T., Naiki, T., Matsumoto, K., & Sugimoto, K. (2001). Recruitment of Mec1 and Ddc1 checkpoint proteins to double-strand breaks through distinct mechanisms. *Science*, *294*, 867–870.

Kowalczykowski, S. C. (2015). An overview of the molecular mechanisms of recombinational DNA repair. *Cold Spring Harb Perspect Biol*, *7*, 016410.

Krejci, L., Altmannova, V., Spirek, M., & Zhao, X. (2012). Homologous recombination and its regulation. *Nucleic Acids Research*, *40*(13), 5795–5818. https://doi.org/10.1093/nar/gks270

Krogh, B. O., & Symington, L. S. (2004). Recombination Proteins in Yeast. *Annual Review of Genetics*, *38*(1), 233–271. https://doi.org/10.1146/annurev.genet.38.072902.091500

Kumar, S., & Burgers, P. M. (2013). Lagging strand maturation factor Dna2 is a component of the replication checkpoint initiation machinery. *Genes & Development*, *27*(3), 313–321. https://doi.org/10.1101/gad.204750.112

Kurtz, S., & Shore, D. (1991). RAP1 protein activates and silences transcription of mating-type genes in yeast. *Genes Dev*, *5*, 616–628.

Kyrion, G., Boakye, K. A., & Lustig, A. J. (1992). C-terminal truncation of RAP1 results in the deregulation of telomere size, stability, and function in *Saccharomyces cerevisiae*. *Molecular and Cellular Biology*, *12*(11), 5159–5173.

Lammens, K., Bemeleit, D. J., Möckel, C., Clausing, E., Schele, A., Hartung, S., Schiller, C. B., Lucas, M., Angermüller, C., Söding, J., Sträßer, K., & Hopfner, K.-P. (2011). The Mre11:Rad50 Structure Shows an ATP-Dependent Molecular Clamp in DNA Double-Strand Break Repair. *Cell*, *145*(1), 54–66. https://doi.org/10.1016/j.cell.2011.02.038

Langerak, P., Mejia-Ramirez, E., Limbo, O., & Russell, P. (2011). Release of Ku and MRN from DNA ends by Mre11 nuclease activity and Ctp1 is required for

homologous recombination repair of double-strand breaks. *PLoS Genet*, *7*, 1002271.

Lazzaro, F., Sapountzi, V., Granata, M., Pellicioli, A., Vaze, M., Haber, J. E., Plevani, P., Lydall, D., & Muzi-Falconi, M. (2008). Histone methyltransferase Dot1 and Rad9 inhibit single-stranded DNA accumulation at DSBs and uncapped telomeres. *EMBO J*, *27*, 1502–1512.

Leach, F. S., Nicolaides, N. C., Papadopoulos, N., Liu, B., Jen, J., Parsons, R., Peltomäki, P., Sistonen, P., Aaltonen, L. A., & Nyström-Lahti, M. (1993). Mutations of a mutS homolog in hereditary nonpolyposis colorectal cancer. *Cell*, *75*(6), 1215–1225. https://doi.org/10.1016/0092-8674(93)90330-s

Lee, J. H., & Paull, T. T. (2005). ATM activation by DNA double-strand breaks through the Mre11-Rad50-Nbs1 complex. *Science*, *308*, 551–554.

Lee, J.-H., Mand, M. R., Deshpande, R. A., Kinoshita, E., Yang, S.-H., Wyman, C., & Paull, T. T. (2013). Ataxia telangiectasia-mutated (ATM) kinase activity is regulated by ATP-driven conformational changes in the Mre11/Rad50/Nbs1 (MRN) complex. *The Journal of Biological Chemistry*, *288*(18), 12840–12851. https://doi.org/10.1074/jbc.M113.460378

Lee, J.-H., & Paull, T. T. (2004). Direct activation of the ATM protein kinase by the Mre11/Rad50/Nbs1 complex. *Science (New York, N.Y.)*, *304*(5667), 93–96. https://doi.org/10.1126/science.1091496

Lee, K., Zhang, Y., & Lee, S. E. (2008). *Saccharomyces cerevisiae* ATM orthologue suppresses break-induced chromosome translocations. *Nature*, *454*, 543–546.

Lee, S. E., Moore, J. K., Holmes, A., Umezu, K., Kolodner, R. D., & Haber, J. E. (1998a). Saccharomyces Ku70, Mre11/Rad50 and RPA proteins regulate adaptation to G2/M arrest after DNA damage. *Cell*, *94*, 399–409.

Lee, S. E., Moore, J. K., Holmes, A., Umezu, K., Kolodner, R. D., & Haber, J. E. (1998b). Saccharomyces Ku70, Mre11/Rad50, and RPA Proteins Regulate Adaptation to G2/M Arrest after DNA Damage. *Cell*, *94*(3), 399–409. https://doi.org/10.1016/S0092-8674(00)81482-8

Lee, Y.-C., Zhou, Q., Chen, J., & Yuan, J. (2016). RPA-Binding Protein ETAA1 Is an ATR Activator Involved in DNA Replication Stress Response. *Current Biology: CB*, *26*(24), 3257–3268. https://doi.org/10.1016/j.cub.2016.10.030

Lempiäinen, H., & Halazonetis, T. D. (2009). Emerging common themes in regulation of PIKKs and PI3Ks. *EMBO J*, *28*, 3067–3073.

Levikova, M., Klaue, D., Seidel, R., & Cejka, P. (2013). Nuclease activity of *Saccharomyces cerevisiae* Dna2 inhibits its potent DNA helicase activity. *Proceedings of the National Academy of Sciences of the United States of America*, *110*(22), E1992-2001. https://doi.org/10.1073/pnas.1300390110

Levikova, M., Pinto, C., & Cejka, P. (2017). The motor activity of DNA2 functions as an ssDNA translocase to promote DNA end resection. *Genes & Development*, *31*(5), 493–502. https://doi.org/10.1101/gad.295196.116

Levy, D. L., & Blackburn, E. H. (2004). Counting of Rif1p and Rif2p on *Saccharomyces cerevisiae* Telomeres Regulates Telomere Length. *Molecular and Cellular Biology*, *24*(24), 10857–10867. https://doi.org/10.1128/MCB.24.24.10857-10867.2004

Lewis, L. K., & Resnick, M. A. (2000). Tying up loose ends: Nonhomologous end-joining in *Saccharomyces cerevisiae*. *Mutation Research*, *451*(1–2), 71–89. https://doi.org/10.1016/s0027-5107(00)00041-5

Li, X., & Tyler, J. K. (2016). Nucleosome disassembly during human non-homologous end joining followed by concerted HIRA- and CAF-1-dependent reassembly. *eLife*, *5*, 15129.

Lieber, M. R. (2010). The mechanism of double-strand DNA break repair by the non-homologous DNA end-joining pathway. *Annu Rev Biochem*, *79*, 181–211.

Lilley, D. M. J. (2017). Holliday junction-resolving enzymes-structures and mechanisms. *FEBS Letters*, *591*(8), 1073–1082. https://doi.org/10.1002/1873-3468.12529

Lim, H. S., Kim, J. S., Park, Y. B., Gwon, G. H., & Cho, Y. (2011). Crystal structure of the Mre11-Rad50-ATPγS complex: Understanding the interplay between Mre11 and Rad50. *Genes Dev*, *25*, 1091–1104.

Limbo, O., Chahwan, C., Yamada, Y., de Bruin, R. A. M., Wittenberg, C., & Russell, P. (2007). Ctp1 Is a Cell-Cycle-Regulated Protein that Functions with Mre11 Complex to Control Double-Strand Break Repair by Homologous Recombination. *Molecular Cell*, *28*(1), 134–146. https://doi.org/10.1016/j.molcel.2007.09.009

Lisby, M., Barlow, J. H., Burgess, R. C., & Rothstein, R. (2004). Choreography of the DNA damage response: Spatiotemporal relationships among checkpoint and repair proteins. *Cell*, *118*(6), 699–713. https://doi.org/10.1016/j.cell.2004.08.015

Liu, Y., Sung, S., Kim, Y., Li, F., Gwon, G., Jo, A., Kim, A. K., Kim, T., Song, O. K., Lee, S. E., & Cho, Y. (2016). ATP-dependent DNA binding, unwinding, and resection by the Mre11/Rad50 complex. *EMBO J*, *35*, 743–758.

Llorente, B., & Symington, L. S. (2004). The Mre11 nuclease is not required for 5' to 3' resection at multiple HO-induced double-strand breaks. *Molecular and Cellular Biology*, *24*(21), 9682–9694. https://doi.org/10.1128/MCB.24.21.9682-9694.2004

Lloyd, J., Chapman, J. R., Clapperton, J. A., Haire, L. F., Hartsuiker, E., Li, J., Carr, A. M., Jackson, S. P., & Smerdon, S. J. (2009). A Supramodular FHA/BRCT-Repeat Architecture Mediates Nbs1 Adaptor Function in Response to DNA Damage. *Cell*, *139*(1), 100–111. https://doi.org/10.1016/j.cell.2009.07.043

Lobachev, K. S., Gordenin, D. A., & Resnick, M. A. (2002a). The Mre11 complex is required for repair of hairpin-capped double-strand breaks and prevention of chromosome rearrangements. *Cell*, *108*(2), 183–193. https://doi.org/10.1016/s0092-8674(02)00614-1

Lobachev, K. S., Gordenin, D. A., & Resnick, M. A. (2002b). The Mre11 complex is required for repair of hairpin-capped double-strand breaks and prevention of chromosome rearrangements. *Cell*, *108*(2), 183–193. https://doi.org/10.1016/s0092-8674(02)00614-1

Lobachev, K., Vitriol, E., Stemple, J., Resnick, M. A., & Bloom, K. (2004). Chromosome Fragmentation after Induction of a Double-Strand Break Is an Active Process Prevented by the RMX Repair Complex. *Current Biology*, *14*(23), 2107–2112. https://doi.org/10.1016/j.cub.2004.11.051

Longhese, M. P., Paciotti, V., Neecke, H., & Lucchini, G. (2000). Checkpoint proteins influence telomeric silencing and length maintenance in budding yeast. *Genetics*, *155*, 1577–1591.

Lustig, A. J., Kurtz, S., & Shore, D. (1990). Involvement of the silencer and UAS binding protein RAP1 in regulation of telomere length. *Science*, *250*(4980), 549–553. https://doi.org/10.1126/science.2237406

Majka, J., Niedziela-Majka, A., & Burgers, P. M. (2006). The checkpoint clamp activates Mec1 kinase during initiation of the DNA damage checkpoint. *Mol Cell*, *24*, 891–901.

Mallory, J. C., & Petes, T. D. (2000). Protein kinase activity of Tel1p and Mec1p, two *Saccharomyces cerevisiae* proteins related to the human ATM protein kinase. *Proc Natl Acad Sci USA*, *97*, 13749–13754.

Marcand, S., Pardo, B., Gratias, A., Cahun, S., & Callebaut, I. (2008). Multiple pathways inhibit NHEJ at telomeres. *Genes & Development*, *22*(9), 1153–1158. https://doi.org/10.1101/gad.455108

Marsella, A., Gobbini, E., Cassani, C., Tisi, R., Cannavo, E., Reginato, G., Cejka, P., & Longhese, M. P. (2021). Sae2 and Rif2 regulate MRX endonuclease activity at DNA double-strand breaks in opposite manners. *Cell Rep*, *34*, 108906.

Martina, M., Clerici, M., Baldo, V., Bonetti, D., Lucchini, G., & Longhese, M. P. (2012). A balance between Tel1 and Rif2 activities regulates nucleolytic processing and elongation at telomeres. *Mol Cell Biol*, *32*, 1604–1617.

McGee, J. S., Phillips, J. A., Chan, A., Sabourin, M., Paeschke, K., & Zakian, V. A. (2010). Reduced Rif2 and lack of Mec1 target short telomeres for elongation rather than double-strand break repair. *Nature Structural & Molecular Biology*, *17*(12), 1438–1445. https://doi.org/10.1038/nsmb.1947

McKee, A. H. Z., & Kleckner, N. (1997). A General Method for Identifying Recessive Diploid-Specific Mutations in *Saccharomyces cerevisiae*, Its Application to the Isolation of Mutants Blocked at Intermediate Stages of Meiotic Prophase and Characterization of a New Gene SAE2. *Genetics*, *146*(3), 797–816. https://doi.org/10.1093/genetics/146.3.797

McVey, M., & Lee, S. E. (2008). MMEJ repair of double-strand breaks (director's cut): Deleted sequences and alternative endings. *Trends in Genetics: TIG*, *24*(11), 529–538. https://doi.org/10.1016/j.tig.2008.08.007

Meek, K., Dang, V., & Lees-Miller, S. P. (2008). DNA-PK: the means to justify the end? *Adv Immunonol*, *99*, 33–58.

Mehta, A., & Haber, J. E. (2014). Sources of DNA double-strand breaks and models of recombinational DNA repair. *Cold Spring Harbor Perspectives in Biology*, *6*(9), a016428. https://doi.org/10.1101/cshperspect.a016428

Melo, J. A., Cohen, J., & Toczyski, D. P. (2001). Two checkpoint complexes are independently recruited to sites of DNA damage *in vivo*. *Genes Dev*, *15*, 2809–2821.

Miller, A. S., Daley, J. M., Pham, N. T., Niu, H., Xue, X., Ira, G., & Sung, P. (2017). A novel role of the Dna2 translocase function in DNA break resection. *Genes & Development*, *31*(5), 503–510. https://doi.org/10.1101/gad.295659.116

Mimitou, E. P., & Symington, L. S. (2008). Sae2, Exo1 and Sgs1 collaborate in DNA double-strand break processing. *Nature*, *455*(7214), Article 7214. https://doi.org/10.1038/nature07312

Mimitou, E. P., & Symington, L. S. (2010). Ku prevents Exo1 and Sgs1-dependent resection of DNA ends in the absence of a functional MRX complex or Sae2. *EMBO J*, *29*, 3358–3369.

Mimitou, E. P., Yamada, S., & Keeney, S. (2017). A global view of meiotic double-strand break end resection. *Science (New York, N.Y.)*, *355*(6320), 40–45. https://doi.org/10.1126/science.aak9704

Mimori, T., & Hardin, J. A. (1986). Mechanism of interaction between Ku protein and DNA. *J. Biol. Chem*, *261*, 10375–10379.

Miyake, Y., Nakamura, M., Nabetani, A., Shimamura, S., Tamura, M., Yonehara, S., Saito, M., & Ishikawa, F. (2009). RPA-like mammalian Ctc1-Stn1-Ten1 complex binds to single-stranded DNA and protects telomeres independently of the Pot1 pathway. *Mol Cell*, *36*, 193–206.

Möckel, C., Lammens, K., Schele, A., & Hopfner, K.-P. (2012). ATP driven structural changes of the bacterial Mre11:Rad50 catalytic head complex. *Nucleic Acids Research*, *40*(2), 914–927. https://doi.org/10.1093/nar/gkr749

Moretti, P., & Shore, D. (2001). Multiple Interactions in Sir Protein Recruitment by Rap1p at Silencers and Telomeres in Yeast. *Molecular and Cellular Biology*, *21*(23), 8082–8094. https://doi.org/10.1128/MCB.21.23.8082-8094.2001

Morin, I., Ngo, H. P., Greenall, A., Zubko, M. K., Morrice, N., & Lydall, D. (2008). Checkpoint-dependent phosphorylation of Exo1 modulates the DNA damage response. *EMBO J*, *27*, 2400–2410.

Morrow, D. M., Tagle, D. A., Shiloh, Y., Collins, F. S., & Hieter, P. (1995). TEL1, an *S. cerevisiae* homolog of the human gene mutated in ataxia telangiectasia, is functionally related to the yeast checkpoint gene MEC1. *Cell*, *82*(5), 831–840. https://doi.org/10.1016/0092-8674(95)90480-8

Myler, L. R., Gallardo, I. F., Soniat, M. M., Deshpande, R. A., Gonzalez, X. B., Kim, Y., Paull, T. T., & Finkelstein, I. J. (2017). Single-Molecule Imaging Reveals How Mre11-Rad50-Nbs1 Initiates DNA Break Repair. *Molecular Cell*, *67*(5), 891-898.e4. https://doi.org/10.1016/j.molcel.2017.08.002

Myler, L. R., Toia, B., Vaughan, C. K., Takai, K., Matei, A. M., Wu, P., Paull, T. T., de Lange, T., & Lottersberger, F. (2023). DNA-PK and the TRF2 iDDR inhibit

MRN-initiated resection at leading-end telomeres. *Nature Structural & Molecular Biology*, *30*(9), 1346–1356. https://doi.org/10.1038/s41594-023-01072-x

Nakada, D., Matsumoto, K., & Sugimoto, K. (2003). ATM-related Tel1 associates with double-strand breaks through an Xrs2-dependent mechanism. *Genes Dev*, *17*, 1957–1962.

Nakai, W., Westmoreland, J., Yeh, E., Bloom, K., & Resnick, M. A. (2011). Chromosome integrity at a double-strand break requires exonuclease 1 and MRX. *DNA Repair*, *10*, 102–110.

Navadgi-Patil, V. M., & Burgers, P. M. (2009). A tale of two tails: Activation of DNA damage checkpoint kinase Mec1/ATR by the 9-1-1 clamp and by Dpb11/TopBP1. *DNA Repair (Amst*, *8*, 996–1003.

Navadgi-Patil, V. M., & Burgers, P. M. (2011). Cell-cycle-specific activators of the Mec1/ATR checkpoint kinase. *Biochemical Society Transactions*, *39*(2), 600–605. https://doi.org/10.1042/BST0390600

Neale, M. J., Pan, J., & Keeney, S. (2005). Endonucleolytic processing of covalent protein linked DNA double-strand breaks. *Nature*, *436*, 1053–1057.

Negrini, S., Gorgoulis, V. G., & Halazonetis, T. D. (2010). Genomic instability-an evolving hallmark of cancer. *Nat Rev Mol Cell Biol*, *11*, 220–228.

Neijenhuis, T., van Keulen, S. C., & Bonvin, A. M. J. J. (2022). Interface refinement of low- to medium-resolution Cryo-EM complexes using HADDOCK2.4. *Structure (London, England: 1993)*, *30*(4), 476-484.e3. https://doi.org/10.1016/j.str.2022.02.001

Nicolette, M. L., Lee, K., Guo, Z., Rani, M., Chow, J. M., Lee, S. E., & Paull, T. T. (2010). Mre11-Rad50-Xrs2 and Sae2 promote 5' strand resection of DNA double-strand breaks. *Nature Structural & Molecular Biology*, *17*(12), 1478–1485. https://doi.org/10.1038/nsmb.1957

Nimonkar, A. V., Genschel, J., Kinoshita, E., Polaczek, P., Campbell, J. L., Wyman, C., Modrich, P., & Kowalczykowski, S. C. (2011). BLM-DNA2-RPA-MRN and EXO1-BLM-RPA-MRN constitute two DNA end resection machineries for human DNA break repair. *Genes Dev*, *25*, 350–362.

Niu, H., Chung, W. H., Zhu, Z., Kwon, Y., Zhao, W., Chi, P., Prakash, R., Seong, C., Liu, D., Lu, L., Ira, G., & Sung, P. (2010). Mechanism of the ATP-dependent DNA end-resection machinery from *Saccharomyces cerevisiae*. *Nature*, *467*, 108–111.

Nugent, C. I., Hughes, T. R., Lue, N. F., & Lundblad, V. (1996). Cdc13p: A single-strand telomeric DNA-binding protein with a dual role in yeast telomere maintenance. *Science*, *274*, 249–252.

Nyberg, K. A., Michelson, R. J., Putnam, C. W., & Weinert, T. A. (2002). Toward maintaining the genome: DNA damage and replication checkpoints. *Annual Review of Genetics*, *36*, 617–656. https://doi.org/10.1146/annurev.genet.36.060402.113540

O'Driscoll, M., Ruiz-Perez, V. L., Woods, C. G., Jeggo, P. A., & Goodship, J. A. (2003). A splicing mutation affecting expression of ataxia-telangiectasia and Rad3-related protein (ATR) results in Seckel syndrome. *Nat Genet*, *33*, 497–501.

Ogawa, H., Johzuka, K., Nakagawa, T., Leem, S. H., & Hagihara, A. H. (1995). Functions of the yeast meiotic recombination genes, MRE11 and MRE2. *Advances in Biophysics*, *31*, 67–76. https://doi.org/10.1016/0065-227x(95)99383-z

Oh, J., Al-Zain, A., Cannavo, E., Cejka, P., & Symington, L. S. (2016). Xrs2 Dependent and Independent Functions of the Mre11-Rad50 Complex. *Molecular Cell*, *64*(2), 405–415. https://doi.org/10.1016/j.molcel.2016.09.011

Oh, J., Lee, S. J., Rothstein, R., & Symington, L. S. (2018). Xrs2 and Tel1 independently contribute to MR-mediated DNA tethering and replisome stability. *Cell Rep*, *25*, 1681–1692.

Ono, M., Tucker, P. W., & Capra, J. D. (1994). Production and characterization of recombinant human Ku antigen. *Nucleic Acids Res*, *22*, 3918–3924.

Orthwein, A., Noordermeer, S. M., Wilson, M. D., Landry, S., Enchev, R. I., Sherker, A., Munro, M., Pinder, J., Salsman, J., Dellaire, G., Xia, B., Peter, M., & Durocher, D. (2015). A mechanism for the suppression of homologous recombination in G1 cells. *Nature*, *528*(7582), 422–426. https://doi.org/10.1038/nature16142

Öz, R., Wang, J. L., Guerois, R., Goyal, G., Sriram, K. K., Ropars, V., Sharma, R., Koca, F., Charbonnier, J. B., Modesti, M., Strick, T. R., & Westerlund, F. (2021). Dynamics of Ku and bacterial non-homologous end-joining characterized using single DNA molecule analysis. *Nucleic Acids Res*, *49*, 2629–2641.

Pannunzio, N. R., Watanabe, G., & Lieber, M. R. (2018). Nonhomologous DNA end-joining for repair of DNA double-strand breaks. *J Biol Chem*, *293*, 10512–10523.

Pardo, B., & Marcand, S. (2005). Rap1 prevents telomere fusions by non-homologous end joining. *EMBO J*, *24*, 3117–3127.

Park, Y. B., Hohl, M., Padjasek, M., Jeong, E., Jin, K. S., Krężel, A., Petrini, J. H. J., & Cho, Y. (2017). Eukaryotic Rad50 functions as a rod-shaped dimer. *Nature Structural & Molecular Biology*, *24*(3), Article 3. https://doi.org/10.1038/nsmb.3369

Paull, T. T., & Gellert, M. (1998). The 3' to 5' exonuclease activity of Mre11 facilitates repair of DNA double-strand breaks. *Mol Cell*, *1*, 969–979.

Paull, T. T., & Gellert, M. (1999). Nbs1 potentiates ATP-driven DNA unwinding and endonuclease cleavage by the Mre11/Rad50 complex. *Genes & Development*, *13*(10), 1276–1288.

Pellicioli, A., Lee, S. E., Lucca, C., Foiani, M., & Haber, J. E. (2001). Regulation of Saccharomyces Rad53 checkpoint kinase during adaptation from DNA damage-induced G2/M arrest. *Molecular Cell*, *7*(2), 293–300. https://doi.org/10.1016/s1097-2765(01)00177-0

Peterson, S. E., Stellwagen, A. E., Diede, S. J., Singer, M. S., Haimberger, Z. W., Johnson, C. O., Tzoneva, M., & Gottschling, D. E. (2001). The function of a stem-loop in telomerase RNA is linked to the DNA repair protein Ku. *Nat Genet*, *27*, 64–67.

Pfander, B., & Diffley, J. F. (2011). Dpb11 coordinates Mec1 kinase activation with cell cycle-regulated Rad9 recruitment. *EMBO J*, *30*, 4897–4907.

Pham, N., Yan, Z., Yu, Y., Faria Afreen, M., Malkova, A., Haber, J. E., & Ira, G. (2021). Mechanisms restraining break-induced replication at two-ended DNA double-strand breaks. *The EMBO Journal*, *40*(10), e104847. https://doi.org/10.15252/embj.2020104847

Pinto, C., Kasaciunaite, K., Seidel, R., & Cejka, P. (2016). Human DNA2 possesses a cryptic DNA unwinding activity that functionally integrates with BLM or WRN helicases. *eLife*, *5*, e18574. https://doi.org/10.7554/eLife.18574

Pizzul, P., Casari, E., Gnugnoli, M., Rinaldi, C., Corallo, F., & Longhese, M. P. (2022). The DNA damage checkpoint: A tale from budding yeast. *Frontiers in Genetics*, *13*. https://www.frontiersin.org/articles/10.3389/fgene.2022.995163

Poinsignon, C., Moshous, D., Callebaut, I., Chasseval, R., Villey, I., & Villartay, J. P. (2004). The metallo-beta-lactamase/beta-CASP domain of Artemis constitutes the catalytic core for V(D)J recombination. *J Exp Med*, *199*, 315–321.

Porter, S. E., Greenwell, P. W., Ritchie, K. B., & Petes, T. D. (1996). The DNA-binding protein Hdf1p (a putative Ku homologue) is required for maintaining normal telomere length in *Saccharomyces cerevisiae*. *Nucleic Acids Res*, *24*, 582–585.

Prinz, S., Amon, A., & Klein, F. (1997). Isolation of COM1, a New Gene Required to Complete Meiotic Double-Strand Break-Induced Recombination in *Saccharomyces cerevisiae*. *Genetics*, *146*(3), 781–795. https://doi.org/10.1093/genetics/146.3.781

Puddu, F., Oelschlaegel, T., Guerini, I., Geisler, N. J., Niu, H., Herzog, M., Salguero, I., Ochoa-Montaño, B., Viré, E., Sung, P., Adams, D. J., Keane, T. M., & Jackson, S. P. (2015). Synthetic viability genomic screening defines Sae2 function in DNA repair. *The EMBO Journal*, *34*(11), 1509–1522. https://doi.org/10.15252/embj.201590973

Ramsden, D. A., & Gellert, M. (1998). Ku protein stimulates DNA end joining by mammalian DNA ligases: A direct role for Ku in repair of DNA double-strand breaks. *EMBO J*, *17*, 609–614.

Ranjha, L., Howard, S. M., & Cejka, P. (2018). Main steps in DNA double-strand break repair: An introduction to homologous recombination and related processes. *Chromosoma*, *127*(2), 187–214. https://doi.org/10.1007/s00412-017-0658-1

Reginato, G., Cannavo, E., & Cejka, P. (2017). Physiological protein blocks direct the Mre11-Rad50-Xrs2 and Sae2 nuclease complex to initiate DNA end resection. *Genes Dev*, *31*, 2325–2330.

Reid, D. A., Keegan, S., Leo-Macias, A., Watanabe, G., Strande, N. T., Chang, H. H., Oksuz, B. A., Fenyo, D., Lieber, M. R., Ramsden, D. A., & Rothenberg, E. (2015). Organization and dynamics of the nonhomologous end-joining machinery during DNA double-strand break repair. *Proc Natl Acad Sci USA*, *112*, 2575–2584.

Ribes-Zamora, A., Indiviglio, S. M., Mihalek, I., Williams, C. L., & Bertuch, A. A. (2013). TRF2 interaction with Ku heterotetramerization interface gives insight into c-NHEJ prevention at human telomeres. *Cell Rep*, *5*, 194–206.

Ribes-Zamora, A., Mihalek, I., Lichtarge, O., & Bertuch, A. A. (2007). Distinct faces of the Ku heterodimer mediate DNA repair and telomeric functions. *Nat. Struct. Mol. Biol*, *14*, 301–307.

Ribeyre, C., & Shore, D. (2012). Anticheckpoint pathways at telomeres in yeast. *Nature Structural & Molecular Biology*, *19*(3), 307–313. https://doi.org/10.1038/nsmb.2225

Ritchie, K. B., & Petes, T. D. (2000). The Mre11p/Rad50p/Xrs2p complex and the Tel1p function in a single pathway for telomere maintenance in yeast. *Genetics*, *155*, 475–479.

Rivera-Calzada, A., Spagnolo, L., Pearl, L. H., & Llorca, O. (2007). Structural model of full-length human Ku70-Ku80 heterodimer and its recognition of DNA and DNA-PKcs. *EMBO Rep*, *8*, 56–62.

Roberts, S. A., & Ramsden, D. A. (2007). Loading of the nonhomologous end joining factor, Ku, on protein-occluded DNA ends. *J Biol Chem*, *282*, 10605–10613.

Roisné-Hamelin, F., Pobiega, S., Jézéquel, K., Miron, S., Dépagne, J., Veaute, X., Busso, D., Du, M.-H. L., Callebaut, I., Charbonnier, J.-B., Cuniasse, P., Zinn-Justin, S., & Marcand, S. (2021). Mechanism of MRX inhibition by Rif2 at telomeres. *Nature Communications*, *12*(1). Scopus. https://doi.org/10.1038/s41467-021-23035-w

Roos, W. P., Thomas, A. D., & Kaina, B. (2016). DNA damage and the balance between survival and death in cancer biology. *Nature Reviews. Cancer*, *16*(1), 20–33. https://doi.org/10.1038/nrc.2015.2

Rass, E., Willaume, S., & Bertrand, P. (2022). 53BP1: Keeping It under Control, Even at a Distance from DNA Damage. *Genes. 13*(12):2390. https://doi:10.3390/genes13122390

Saldivar, J. C., Cortez, D., & Cimprich, K. A. (2017). The essential kinase ATR: Ensuring faithful duplication of a challenging genome. *Nature Reviews. Molecular Cell Biology*, *18*(10), 622–636. https://doi.org/10.1038/nrm.2017.67

San Filippo, J., Sung, P., & Klein, H. (2008). Mechanism of eukaryotic homologous recombination. *Annual Review of Biochemistry*, *77*, 229–257. https://doi.org/10.1146/annurev.biochem.77.061306.125255

Sanchez, Y., Bachant, J., Wang, H., Hu, F., Liu, D., Tetzlaff, M., & Elledge, S. J. (1999). Control of the DNA damage checkpoint by Chk1 and Rad53 protein kinases through distinct mechanisms. *Science*, *286*, 1166–1171.

Saponaro, M., Callahan, D., Zheng, X., Krejci, L., Haber, J. E., Klein, H. L., & Liberi, G. (2010). Cdk1 targets Srs2 to complete synthesis-dependent strand annealing and to promote recombinational repair. *PLoS Genetics*, *6*(2), e1000858. https://doi.org/10.1371/journal.pgen.1000858

Sartori, A. A., Lukas, C., Coates, J., Mistrik, M., Fu, S., Bartek, J., Baer, R., Lukas, J., & Jackson, S. P. (2007). Human CtIP promotes DNA end resection. *Nature*, *450*, 509–514.

Sastry, G. M., Adzhigirey, M., Day, T., Annabhimoju, R., & Sherman, W. J. (2013). Protein and ligand preparation: Parameters, protocols, and influence on virtual screening enrichments. *Comput Aided Mol Des*, *27*, 221–234.

Savitsky, K., Sfez, S., Tagle, D. A., Ziv, Y., Sartiel, A., Collins, F. S., Shiloh, Y., & Rotman, G. (1995). The complete sequence of the coding region of the ATM gene reveals similarity to cell cycle regulators in different species. *Hum Mol Genet*, *4*, 2025-.

Sebesta, M., & Krejci, L. (2016). Mechanism of Homologous Recombination. In F. Hanaoka & K. Sugasawa (Eds.), *DNA Replication, Recombination, and Repair: Molecular Mechanisms and Pathology* (pp. 73–109). Springer Japan. https://doi.org/10.1007/978-4-431-55873-6_4

Seifert, F. U., Lammens, K., Stoehr, G., Kessler, B., & Hopfner, K. P. (2016). Structural mechanism of ATP-dependent DNA binding and DNA end bridging by eukaryotic Rad50. *EMBO J*, *35*, 759–772.

Seol, J.-H., Shim, E. Y., & Lee, S. E. (2018). Microhomology-mediated end joining: Good, bad and ugly. *Mutation Research*, *809*, 81–87. https://doi.org/10.1016/j.mrfmmm.2017.07.002

Sharif, H., Li, Y., Dong, Y., Dong, L., Wang, W. L., Mao, Y., & Wu, H. (2017). Cryo-EM structure of the DNA-PK holoenzyme. *Proc Natl Acad Sci USA*, *114*, 7367–7372.

Sharples, G. J., & Leach, D. R. (1995). Structural and functional similarities between the SbcCD proteins of *Escherichia coli* and the RAD50 and MRE11 (RAD32) recombination and repair proteins of yeast. *Molecular Microbiology*, *17*(6), 1215–1217. https://doi.org/10.1111/j.1365-2958.1995.mmi_17061215_1.x

Shi, T., Bunker, R. D., Mattarocci, S., Ribeyre, C., Faty, M., Gut, H., Scrima, A., Rass, U., Rubin, S. M., Shore, D., & Thomä, N. H. (2013). Rif1 and Rif2 shape telomere function and architecture through multivalent Rap1 interactions. *Cell*, *153*(6), 1340–1353. https://doi.org/10.1016/j.cell.2013.05.007

Shibata, A. (2017). Regulation of repair pathway choice at two-ended DNA double-strand breaks. *Mutation Research*, *803–805*, 51–55. https://doi.org/10.1016/j.mrfmmm.2017.07.011

Shibata, A., Moiani, D., Arvai, A. S., Perry, J., Harding, S. M., Genois, M. M., Maity, R., Rossum-Fikkert, S., Kertokalio, A., & Romoli, F. (2014). DNA double-strand break repair pathway choice is directed by distinct MRE11 nuclease activities. *Mol. Cell*, *53*, 7–18.

Shim, E. Y., Chung, W. H., Nicolette, M. L., Zhang, Y., Davis, M., Zhu, Z., Paull, T. T., Ira, G., & Lee, S. E. (2010). *Saccharomyces cerevisiae* Mre11/Rad50/Xrs2 and Ku proteins regulate association of Exo1 and Dna2 with DNA breaks. *EMBO J*, *29*, 3370–3380.

Shimada, K., Pasero, P., & Gasser, S. M. (2002). ORC and the intra-S-phase checkpoint: A threshold regulates Rad53p activation in S phase. *Genes Dev*, *16*, 3236–3252.

Shroff, R., Arbel-Eden, A., Pilch, D., Ira, G., Bonner, W. M., Petrini, J. H., Haber, J. E., & Lichten, M. (2004). Distribution and dynamics of chromatin modification induced by a defined DNA double-strand break. *Curr Biol*, *14*, 1703–1711.

Sleigh, MJ. (1976). The mechanism of DNA breakage by phleomycin *in vitro*. *Nucleic Acids Res.*, 3(4):891-901.

So, A., Le Guen, T., Lopez, B. S., & Guirouilh-Barbat, J. (2017). Genomic rearrangements induced by unscheduled DNA double strand breaks in somatic mammalian cells. *The FEBS Journal*, *284*(15), 2324–2344. https://doi.org/10.1111/febs.14053

Spagnolo, L., Rivera-Calzada, A., Pearl, L. H., & Llorca, O. (2006). Three-dimensional structure of the human DNA-PKcs/Ku70/Ku80 complex assembled on DNA and its implications for DNA DSB repair. *Mol Cell*, *22*, 511–519.

Stellwagen, A. E., Haimberger, Z. W., Veatch, J. R., & Gottschling, D. E. (2003). Ku interacts with telomerase RNA to promote telomere addition at native and broken chromosome ends. *Genes & Development*, *17*(19), 2384–2395. https://doi.org/10.1101/gad.1125903

Stracker, T. H., & Petrini, J. H. J. (2011). The MRE11 complex: Starting from the ends. *Nature Reviews Molecular Cell Biology*, *12*(2), Article 2. https://doi.org/10.1038/nrm3047

Studier, F. W. (2005). Protein production by auto-induction in high density shaking cultures. *Protein Expression and Purification*, *41*(1), 207–234. https://doi.org/10.1016/j.pep.2005.01.016

Sturzenegger, A., Burdova, K., Kanagaraj, R., Levikova, M., Pinto, C., Cejka, P., & Janscak, P. (2014). DNA2 cooperates with the WRN and BLM RecQ helicases to mediate long-range DNA end resection in human cells. *J Biol Chem*, *289*, 27314–27326.

Sussel, L., & Shore, D. (1991). Separation of transcriptional activation and silencing functions of the RAP1-encoded repressor/activator protein 1: Isolation of viable mutants affecting both silencing and telomere length. *Proceedings of the National Academy of Sciences of the United States of America*, *88*(17), 7749–7753. https://doi.org/10.1073/pnas.88.17.7749

Syed, A., & Tainer, J. A. (2018). The MRE11-RAD50-NBS1 Complex Conducts the Orchestration of Damage Signaling and Outcomes to Stress in DNA Replication and Repair. *Annual Review of Biochemistry*, *87*, 263–294. https://doi.org/10.1146/annurev-biochem-062917-012415

Symington, L. S. (2014). End resection at double-strand breaks: Mechanism and regulation. *Cold Spring Harbor Perspectives in Biology*, *6*(8), a016436. https://doi.org/10.1101/cshperspect.a016436

Symington, L. S., & Gautier, J. (2011). Double-strand break end resection and repair pathway choice. *Annu Rev Genet*, *45*, 247–271.

Tercero, J. A., Longhese, M. P., & Diffley, J. F. (2003). A central role for DNA replication forks in checkpoint activation and response. *Mol Cell*, *11*, 1323–1336.

Toczyski, D. P., Galgoczy, D. J., & Hartwell, L. H. (1997). CDC5 and CKII control adaptation to the yeast DNA damage checkpoint. *Cell*, *90*(6), 1097–1106. https://doi.org/10.1016/s0092-8674(00)80375-x

Toh, G. W., O'Shaughnessy, A. M., Jimeno, S., Dobbie, I. M., Grenon, M., Maffini, S., O'Rorke, A., & Lowndes, N. F. (2006). Histone H2A phosphorylation and H3 methylation are required for a novel Rad9 DSB repair function following checkpoint activation. *DNA Repair*, *5*, 693–703.

Tran, P. T., Erdeniz, N., Dudley, S., & Liskay, R. M. (2002). Characterization of nuclease-dependent functions of Exo1p in *Saccharomyces cerevisiae*. *DNA Repair*, *1*(11), 895–912. https://doi.org/10.1016/S1568-7864(02)00114-3

Trovesi, C., Falcettoni, M., Lucchini, G., Clerici, M., & Longhese, M. P. (2011). Distinct Cdk1 requirements during single-strand annealing, noncrossover, and crossover recombination. *PLoS Genetics*, *7*(8), e1002263. https://doi.org/10.1371/journal.pgen.1002263

Trujillo, K. M., Yuan, S. S., Lee, E. Y., & Sung, P. (1998). Nuclease activities in a complex of human recombination and DNA repair factors Rad50, Mre11, and p95. *J Biol Chem*, *273*, 21447–21450.

Tseng, H. M., & Tomkinson, A. E. (2002). A physical and functional interaction between yeast Pol4 and Dnl4-Lif1 links DNA synthesis and ligation in nonhomologous end joining. *J Biol Chem*, *277*, 45630–45637.

Tsukuda, T., Fleming, A. B., Nickoloff, J. A., & Osley, M. A. (2005). Chromatin remodelling at a DNA double-strand break site in *Saccharomyces cerevisiae*. *Nature*, *438*, 379–383.

Usui, T., Ogawa, H., & Petrini, J. H. (2001). A DNA damage response pathway controlled by Tel1 and the Mre11 complex. *Mol. Cell*, *7*, 1255–1266.

Usui, T., Ohta, T., Oshiumi, H., Tomizawa, J., Ogawa, H., & Ogawa, T. (1998). Complex Formation and Functional Versatility of Mre11 of Budding Yeast in Recombination. *Cell*, *95*(5), 705–716. https://doi.org/10.1016/S0092-8674(00)81640-2

Vaze, M. B., Pellicioli, A., Lee, S. E., Ira, G., Liberi, G., Arbel-Eden, A., Foiani, M., & Haber, J. E. (2002). Recovery from checkpoint-mediated arrest after repair of a double-strand break requires Srs2 helicase. *Molecular Cell*, *10*(2), 373–385. https://doi.org/10.1016/s1097-2765(02)00593-2

Viscardi, V., Baroni, E., Romano, M., Lucchini, G., & Longhese, M. P. (2003). Sudden telomere lengthening triggers a Rad53-dependent checkpoint in *Saccharomyces cerevisiae*. *Molecular Biology of the Cell*, *14*(8), 3126–3143. https://doi.org/10.1091/mbc.e02-11-0719

Viscardi, V., Bonetti, D., Cartagena-Lirola, H., Lucchini, G., & Longhese, M. P. (2007). MRX-dependent DNA damage response to short telomeres. *Molecular Biology of the Cell*, *18*(8), 3047–3058. https://doi.org/10.1091/mbc.e07-03-0285

Vodenicharov, M. D., Laterreur, N., & Wellinger, R. J. (2010). Telomere capping in non-dividing yeast cells requires Yku and Rap1. *EMBO J*, *29*, 3007–3019.

Walker, J. R., Corpina, R. A., & Goldberg, J. (2001). Structure of the Ku heterodimer bound to DNA and its implications for double-strand break repair. *Nature*, *412*(6847), Article 6847. https://doi.org/10.1038/35088000

Wang, H., & Xu, X. (2017). Microhomology-mediated end joining: New players join the team. *Cell & Bioscience*, *7*, 6. https://doi.org/10.1186/s13578-017-0136-8

Wang, J. L., Duboc, C., Wu, Q., Ochi, T., Liang, S., Tsutakawa, S. E., Lees-Miller, S. P., Nadal, M., Tainer, J. A., Blundell, T. L., & Strick, T. R. (2018). Dissection of DNA double-strand-break repair using novel single-molecule forceps. *Nat Struct Mol Biol*, *25*, 482–487.

Wang, W., Daley, J. M., Kwon, Y., Krasner, D. S., & Sung, P. (2017). Plasticity of the Mre11-Rad50-Xrs2-Sae2 nuclease ensemble in the processing of DNA-bound obstacles. *Genes Dev*, *31*, 2331–2336.

Wanrooij, P. H., & Burgers, P. M. (2015). Yet another job for Dna2: Checkpoint activation. *DNA Repair*, *32*, 17–23. https://doi.org/10.1016/j.dnarep.2015.04.009

Waterman, D. P., Haber, J. E., & Smolka, M. B. (2020a). CHECKPOINT RESPONSES TO DNA DOUBLE-STRAND BREAKS. *Annual Review of Biochemistry*, *89*, 103–133. https://doi.org/10.1146/annurev-biochem-011520-104722

Waterman, D. P., Haber, J. E., & Smolka, M. B. (2020b). Checkpoint Responses to DNA Double-Strand Breaks. *Annual Review of Biochemistry*, *89*, 103–133. https://doi.org/10.1146/annurev-biochem-011520-104722

Weiner, S. J., Kollman, P. A., Nguyen, D. T., & Case, D. A. (1986). An all atom force field for simulations of proteins and nucleic acids. *J Comput Chem*, *7*, 230–252.

Wellinger, R. J., & Zakian, V. A. (2012). Everything You Ever Wanted to Know About *Saccharomyces cerevisiae* Telomeres: Beginning to End. *Genetics*, *191*(4), 1073–1105. https://doi.org/10.1534/genetics.111.137851

Westmoreland, J. W., & Resnick, M. A. (2013). Coincident resection at both ends of random, γ-induced double-strand breaks requires MRX (MRN), Sae2 (Ctp1), and Mre11-nuclease. *PLoS Genetics*, *9*(3), e1003420. https://doi.org/10.1371/journal.pgen.1003420

Weterings, E., Verkaik, N. S., Brüggenwirth, H. T., Hoeijmakers, J. H., & Gent, D. C. (2003). The role of DNA dependent protein kinase in synapsis of DNA ends. *Nucleic Acids Res*, *31*, 7238–7246.

Williams, G. J., Lees-Miller, S. P., & Tainer, J. A. (2010). Mre11–Rad50–Nbs1 conformations and the control of sensing, signaling, and effector responses at DNA double-strand breaks. *DNA Repair*, *9*(12), 1299–1306. https://doi.org/10.1016/j.dnarep.2010.10.001

Williams, G. J., Williams, R. S., Williams, J. S., Moncalian, G., Arvai, A. S., Limbo, O., Guenther, G., SilDas, S., Hammel, M., Russell, P., & Tainer, J. A. (2011). ABC ATPase signature helices in Rad50 link nucleotide state to Mre11 interface for DNA repair. *Nat Struct Mol Biol*, *18*, 423–431.

Williams, J. M., Ouenzar, F., Lemon, L. D., Chartrand, P., & Bertuch, A. A. (2014). The principal role of Ku in telomere length maintenance is promotion of Est1 association with telomeres. *Genetics*, *197*, 1123–1136.

Williams, R. S., Dodson, G. E., Limbo, O., Yamada, Y., Williams, J. S., Guenther, G., Classen, S., Glover, J. N. M., Iwasaki, H., Russell, P., & Tainer, J. A. (2009). Nbs1 Flexibly Tethers Ctp1 and Mre11-Rad50 to Coordinate DNA Double-Strand Break Processing and Repair. *Cell*, *139*(1), 87–99. https://doi.org/10.1016/j.cell.2009.07.033

Williams, R. S., Moncalian, G., Williams, J. S., Yamada, Y., Limbo, O., Shin, D. S., Groocock, L. M., Cahill, D., Hitomi, C., Guenther, G., Moiani, D., Carney, J. P., Russell, P., & Tainer, J. A. (2008). Mre11 Dimers Coordinate DNA End Bridging and Nuclease Processing in Double-Strand-Break Repair. *Cell*, *135*(1), 97–109. https://doi.org/10.1016/j.cell.2008.08.017

Wiltzius, J. J. W., Hohl, M., Fleming, J. C., & Petrini, J. H. J. (2005). The Rad50 hook domain is a critical determinant of Mre11 complex functions. *Nature Structural & Molecular Biology*, *12*(5), Article 5. https://doi.org/10.1038/nsmb928

Wold, M. S. (1997). Replication protein A: A heterotrimeric, single-stranded DNA-binding protein required for eukaryotic DNA metabolism. *Annual Review of Biochemistry*, *66*, 61–92. https://doi.org/10.1146/annurev.biochem.66.1.61

Wotton, D., & Shore, D. (1997). A novel Rap1p-interacting factor, Rif2p, cooperates with Rif1p to regulate telomere length in *Saccharomyces cerevisiae*. *Genes & Development*, *11*(6), 748–760. https://doi.org/10.1101/gad.11.6.748

Wright, W. D., Shah, S. S., & Heyer, W.-D. (2018). Homologous recombination and the repair of DNA double-strand breaks. *The Journal of Biological Chemistry*, *293*(27), 10524–10535. https://doi.org/10.1074/jbc.TM118.000372

Wu, P., Takai, H., & Lange, T. (2012). Telomeric 3' overhangs derive from resection by Exo1 and Apollo and fill-in by POT1b-associated CST. *Cell*, *150*, 39–52.

Wysocki, R., Javaheri, A., Allard, S., Sha, F., Coté, J., & Kron, S. J. (2005). Role of Dot1- dependent histone H3 methylation in G1 and S phase DNA damage checkpoint functions of Rad9. *Mol Cell Biol*, *25*, 8430–8443.

Yaneva, M., Kowalewski, T., & Lieber, M. R. (1997). Interaction of DNA-dependent protein kinase with DNA and with Ku: Biochemical and atomic-force microscopy studies. *EMBO J*, *16*, 5098–50112.

You, Z., Chahwan, C., Bailis, J., Hunter, T., & Russell, P. (2005). ATM activation and its recruitment to damaged DNA require binding tothe C terminus of Nbs1. Mol. *Cell. Biol*, *25*, 5363–5379.

Yu, T. Y., Kimble, M. T., & Symington, L. S. (2018). Sae2 antagonizes Rad9 accumulation at DNA double-strand breaks to attenuate checkpoint signaling and facilitate end resection. *Proc. Natl. Acad.*

Zahid, S., Seif El Dahan, M., Iehl, F., Fernandez-Varela, P., Le Du, M. H., Ropars, V., & Charbonnier, J. B. (2021). The multifaceted roles of Ku70/80. *Int. J. Mol. Sci*, *22*, 4134.

Zhao, B., Watanabe, G., Morten, M. J., Reid, D., Rothenberg, E., & Lieber, M. R. (2019). The essential elements for the noncovalent association of two DNA ends during NHEJ synapsis. *Nat Commun*, *10*, 3588.

Zhu, M., Zhao, H., Limbo, O., & Russell, P. (2018). Mre11 complex links sister chromatids to promote repair of a collapsed replication fork. *Proceedings of the National Academy of Sciences of the United States of America*, *115*(35), 8793–8798. https://doi.org/10.1073/pnas.1808189115

Zhu, Z., Chung, W. H., Shim, E. Y., Lee, S. E., & Ira, G. (2008a). Sgs1 helicase and two nucleases Dna2 and Exo1 resect DNA double-strand break ends. *Cell*, *134*, 981–994.

Zhu, Z., Chung, W.-H., Shim, E. Y., Lee, S. E., & Ira, G. (2008b). Sgs1 Helicase and Two Nucleases Dna2 and Exo1 Resect DNA Double-Strand Break Ends. *Cell*, *134*(6), 981–994. https://doi.org/10.1016/j.cell.2008.08.037

Zou, L., & Elledge, S. J. (2003). Sensing DNA damage through ATRIP recognition of RPA-ssDNA complexes. *Science*, *300*, 1542–1548.

APPENDIX

Cell Reports
2023 Oct 28; 42:11:113360
Doi: 10.1016/j.celrep.2023.113360

The PP2A phosphatase counteracts the functions of the 9-1-1 axis in checkpoint activation

Erika Casari[1], **Paolo Pizzul**[1], Carlo Rinaldi[1], Marco Gnugnoli[1], Michela Clerici[1], Maria Pia Longhese[1*]

[*] Corresponding Author

[1] Dipartimento di Biotecnologie e Bioscienze, Università degli Studi di Milano-Bicocca, Milano, 20126, Italy

Frontiers in
Cell and Developmental Biology
2023 Sep 13; 11:1250264
doi: 10.3389/fcell.2023.1250264

frontiers in Cell and Developmental Biology

The multistep path to replicative senescence onset: zooming on triggering and inhibitory events at telomeric DNA

Paolo Pizzul[1†], Carlo Rinaldi[1†], Diego Bonetti[1 *]

[*] Corresponding Author

† These authors contributed equally to this work and share first authorship

[1] Dipartimento di Biotecnologie e Bioscienze, Università degli Studi di Milano-Bicocca, Milano, 20126, Italy

Cells
2022 Oct 14; 11(20) 3224
doi: 10.3390/cells11203224

To fix or not to fix: maintenance of chromosome ends versus repair of DNA double-strand breaks

Erika Casari[1], Marco Gnugnoli[1], Carlo Rinaldi[1], **Paolo Pizzul**[1], Chiara Vittoria Colombo[1], Diego Bonetti[1], Maria Pia Longhese[1*]

[*] Corresponding Author

[1] Dipartimento di Biotecnologie e Bioscienze, Università degli Studi di Milano-Bicocca, Milano, 20126, Italy

Frontiers in Genetics
2022 Sep 15; 8:618157
doi: 10.3389//fgene.2022.995163

The DNA damage checkpoint: a tale from budding yeast

Paolo Pizzul[1†], Erika Casari[1†], Marco Gnugnoli[1], Carlo Rinaldi[1], Flavio Corallo[1], Maria Pia Longhese[1*]

[*] Corresponding Author

† These authors contributed equally to this work and share first authorship

[1] Dipartimento di Biotecnologie e Bioscienze, Università degli Studi di Milano-Bicocca, Milano, 20126, Italy

Frontiers in
Cell and Developmental Biology
2021 Jan 11; 8:618157
doi: 10.3389/fcell.2020.618157

Sensing R-loop-associated DNA damage to safeguard genome stability

Carlo Rinaldi[1], **Paolo Pizzul**[1], Maria Pia Longhese[1], Diego Bonetti[1*]

* Corresponding Author

[1] Dipartimento di Biotecnologie e Bioscienze, Università degli Studi di Milano- Bicocca, Milano, 20126, Italy

CONTRIBUTIONS

Binding of Rif2 to Rad50 inhibits Tel1 functions at DNA double-strand breaks by limiting MRX-Tel1 interaction.

MPL conceived the study, and supervised and coordinated the work. PP and MPL designed the experiments. PP performed drop tests shown in Figs. 11 and 15, the telomere length analysis shown in Fig. 11, DSB resection and relative analysis shown in Fig. 13, the ChIP analysis and western blot shown in Figs. 12, 13, 15, and 16; the end-tethering experiments shown in Figs. 18 and 20, and the coimmunoprecipitation shown in Figs. 12 and 17. EC performed drop tests shown in Fig. 15, the tetrad dissection; she contributed to perform coimmunoprecipitation shown in Figs. 12 and 17. CR contributed to perform end-tethering experiments shown in Figs. 18 and 20. MG helped to performed the recombination assay shown in Fig. 13 and the southern blot shown in Fig. 19. MM helped to perform the ATPase assay. RT performed computational analyses and performed the construction of structural models shown in shown in Figs. 9 and 10. PP and MPL analyzed the data, wrote the manuscript, and realized the working model shown in Fig D1. CR, PP, EC, MG, and MPL revised the text.

The PP2A phosphatase counteracts the functions of the 9-1-1 axis in checkpoint activation.

Conceptualization, E.C., M.C., and M.P.L.; investigation, E.C., P.P., C.R., and M.G.; writing original draft, M.P.L.; review & editing, E.C., M.C., and M.P.L.; supervision, M.P.L.; funding acquisition, M.P.L.

The multistep path to replicative senescence onset: zooming on triggering and inhibitory events at telomeric DNA.

DB conceived the idea. CR, PP, and DB wrote, revised, and edited the manuscript. PP created figures.

The Ku complex promotes DNA end-bridging and this function is antagonized by Tel1/ATM kinase.

MPL conceived the study, and supervised and coordinated the work. CR and MPL designed the experiments. CR performed the screen and identified the five *ku70* alleles including *ku70-C85Y*; he also performed drop tests shown in Figs. 21 and 24, the telomere length analysis shown in Fig. 22, DSB resection and relative analysis shown in Fig. 23, the ChIP analysis and western blot, end-tethering experiments, and the coimmunoprecipitation. PP performed drop tests shown in Figs. 22 and 25; he contributed to perform telomere length analysis shown in Fig. 22 and DSB resection shown in Fig. 23. EC contributed to perform coimmunoprecipitation shown in Fig. 25. RT performed computational analyses and interpretation, she also performed the construction of structural models shown in Figs. 21 and 31. CR, PP and MPL analyzed the data, wrote the manuscript, and realized the working model shown in Fig D2. CR, PP, EC, and MPL revised the text.

To fix or not to fix: maintenance of chromosome ends versus repair of DNA double-strand breaks.

MPL conceived the idea. MPL, EC, and MG wrote the original draft. CR, PP, CVC, and DB revised and edited the manuscript.

The DNA damage checkpoint: a tale from budding yeast.

MPL conceived the idea. PP, EC, and MPL wrote the manuscript. MG, CR, and FC revised and edited the manuscript.

Sensing R-loop-associated DNA damage to safeguard genome stability.

DB and MPL conceived the idea. CR and DB wrote the manuscript. DB, CR, and MPL revised and edited the manuscript. CR and PP created the figures.